SYSTEMATIC EVALUATION OF ALTERNATIVE ACID SYSTEM FOR HIGH-TEMPERATURE CARBONATE FORMATION

A Thesis

by

RITEN PRAFULBHAI GAJIPARA

Submitted to the Graduate and Professional School of
Texas A&M University
in partial fulfillment of the requirements for the degree of

MASTER OF SCIENCE

Chair of Committee,	Ding Zhu
Co-Chair of Committee,	A. Daniel Hill
Committee Members,	Marcelo Sanchez
Head of Department,	Akhil Datta-Gupta

August 2023

Major Subject: Petroleum Engineering

ABSTRACT

The dissolution pattern created by injecting acid into carbonate formation for well stimulation can be characterized as one of three types: compact dissolution, wormholing, and uniform dissolution. The dissolution pattern depends on interstitial velocity of acid, which is related to injection rate. Compact dissolution is created at low injection rates, wormholing at intermediate rates, and uniform dissolution at high injection rates. Out of these dissolution patterns, wormholing is considered the most desirable for efficient stimulation of carbonate formation. In a typical wormhole efficiency curve, there exists an optimal interstitial velocity that requires the minimum amount of acid to propagate wormhole to a certain distance. The wormhole structures change from large-diameter at low interstitial velocity (compact dissolution), to well-controlled diameter at optimal interstitial velocity (wormholing), and to more branched pattern at high interstitial velocity (uniform dissolution).

Conventionally, hydrochloric acid (HCl) has been used as the preferred acid system for carbonate acidizing treatment. Alternative acid systems have been developed to overcome some of the weaknesses of HCl and to improve stimulation efficiency. Such acid systems are of particular interest for high-temperature carbonate reservoirs because HCl shows very high reactivity and corrosiveness at high temperatures. Some of the advantages of alternative acid systems are better wormhole efficiency at lower injection rates and less corrosiveness to protect tubulars and surface equipment. The performance of alternative acid needs to be evaluated at high temperatures for the feasibility of being and effective stimulation fluid. The purpose of this study is to experimentally evaluate the performance of an alternative acid system over a wide range of

temperatures up to 300°F. The goal is to confirm the applicability of the acid system and identify the optimal conditions for field operations.

Core flood experiments are conducted using Indiana Limestone and Silurian Dolomite cores of 1.5-inch diameter and varying length in this study. Porosity and permeability are measured before acid flooding. The temperature range for experiments is from 125°F to 300°F. Wormhole efficiency curves are generated by running 3-5 experiments at different interstitial velocities for each temperature. Optimal conditions at each temperature are determined from experimental results. The cores are CT scanned after each test to visualize the wormhole structure created.

The alternative acid system exhibits very efficient performance with a dominant wormhole created at each test condition. This indicated that the alternative acid system can be used as a stimulation fluid for carbonate reservoirs over a broad range of temperatures up to 300°F. Many studies have observed that wormhole efficiency decreases with increasing temperature for HCl. This is because of the increased reactivity of acid at high temperatures, which results in high optimal interstitial velocity. Similar behavior is observed with alternative acid systems in this study. The performance of alternative acid is also compared with that of 15% HCl at a particular interstitial velocity. The results show better stimulation efficiency for alternative acid systems as compared to HCl.

DEDICATION

To my loving parents and my brother, Akhil.

ACKNOWLEDGEMENTS

I would like to thank my committee chair, Dr. Ding Zhu, and committee co-chair, Dr. A. Daniel Hill, for giving me the opportunity to work on this project, and their guidance and support throughout the course of this research. I would also like to thank my committee member, Dr. Marcelo Sanchez, for his support during this research. Thanks to Fluid Energy Group for supporting this research and providing feedback along the way.

Thanks to lab safety coordinator, John Maldonado for all assistance related to the facilities and equipment that made this research possible. Thanks to Greyson Betterncourt for training me to get familiar with matrix acidizing experiments. Special thanks to my colleagues and friends at Texas A&M University for all their support throughout.

CONTRIBUTORS AND FUNDING SOURCES

Contributors

This research was supported by my committee chair, Dr. Ding Zhu, co-chair, Dr. A. Daniel Hill, of the Harold Vance Department of Petroleum Engineering and committee member, Dr. Marcelo Sanchez of the Zachry Department of Civil and Environmental Engineering.

Funding Sources

This research was supported by a graduate research assistantship funded by Fluid Energy Group.

TABLE OF CONTENTS

LIST OF FIGURES

LIST OF TABLES

1. INTRODUCTION

1.1 Background and Literature Review

Matrix acidizing is a widely used stimulation technique for carbonate reservoirs. It is an effective and relatively low-cost technique to stimulate carbonate formations. In this technique, the well performance is enhanced by injecting acid into the wellbore below formation fracture pressure. There two important phenomena in acidizing: surface reaction rate and mass transfer rate. Surface reaction rates are very high in carbonates, so mass transfer limits the overall reaction rate (Economides et al., 2013). This leads to nonuniform dissolution patterns, forming highly conductive channels called wormholes. Hydrochloric acid (HCl) is the most commonly used acid in the oil and gas industry for carbonate acidizing.

The efficiency of an acidizing treatment strongly depends on the structure of created wormholes. Numerous studies on wormhole behavior have shown that there exists an optimal condition for acid injection resulting in the highest efficiency (Hoefner and Fogler, 1989; Wang et al., 1993). At this optimal flow rate, the minimum amount of acid is required to propagate a wormhole to a certain distance. The optimal condition is described by two parameters: the optimal interstitial velocity ($v_{i,opt}$) and the optimal pore volume to breakthrough ($PV_{BT,opt}$). McDuff et al. (2010) studied wormhole behavior by conducting coreflooding experiments at various interstitial velocities as shown in **Figure 1**. It can be noticed that large conical-shaped wormholes are created at low rates, much narrower wormholes with few branching at intermediate rates, and highly branched wormholes at higher rates.

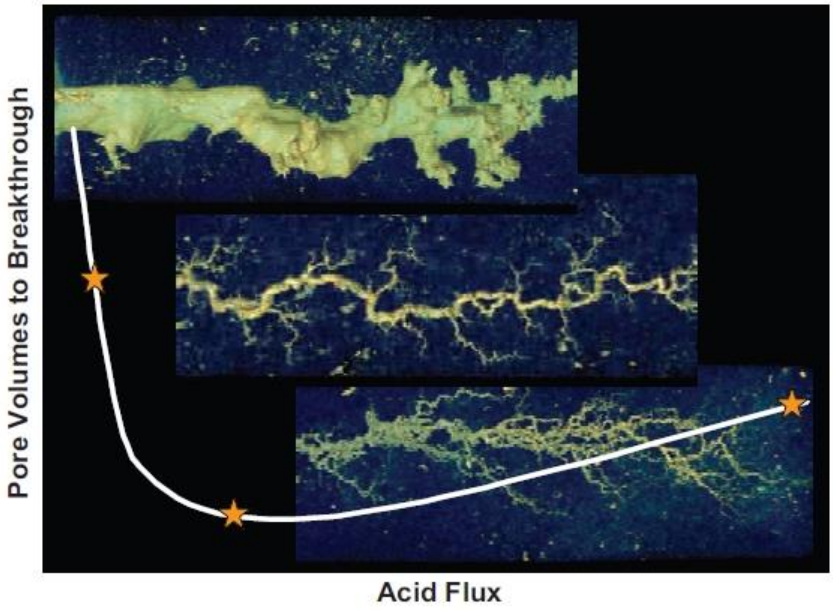

Figure 1 - Wormhole efficiency theory showing the relationship between injection rate and PV_{BT} (McDuff et al., 2010)

The behavior of the wormholes with changing interstitial velocity is studied by conducting acid coreflooding experiments at the lab scale. The experimental data can be curve-fitted using a correlation model developed by Buijse and Glasbergen (2005) to generate a wormhole efficiency curve for the given acid/rock system. **Figure 2** shows the typical wormholing behavior for various rock/acid systems. It can be noticed that when the interstitial velocity is below optimum the acid volume required to propagate the wormhole increases rapidly with decreasing flow rate. On the other hand, when the interstitial velocity is above the optimal, the PV_{BT} increases only gradually with increasing flow rate.

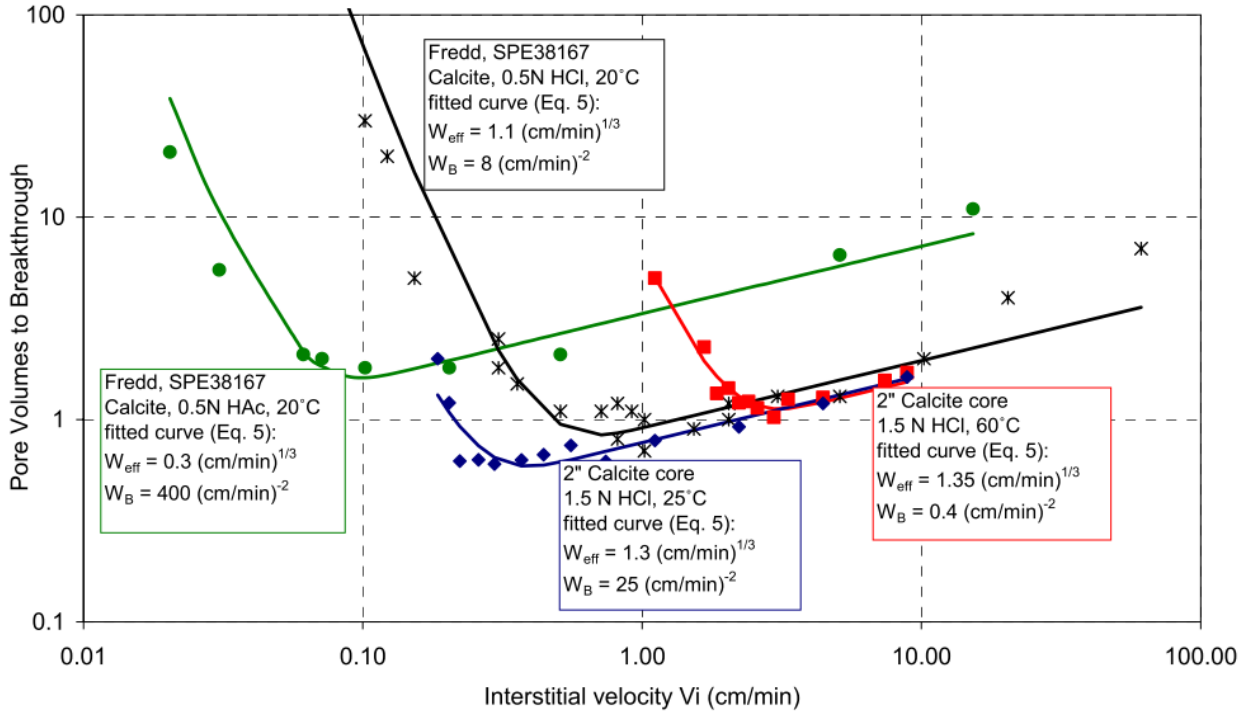

Figure 2 – Typical wormhole efficiency curves generated by curve-fitting experimental data (Buijse and Glasbergen, 2005)

The reaction rate between HCl and calcium carbonate is high which limits the acid transport deep into the formation. If the reaction rate could be controlled by some means, the acid would not be spent rapidly by contact with the rock and stay active longer (Sohn, 2018). This would result in high acid treatment efficiency.

The reactivity of acid can be reduced either by physical means or by chemical means. One way is to physically limit the reactivity by denying protons from HCl to reach the rock surface. This can be achieved by increasing the viscosity of the acid solution. The viscosity of acid solution can be increased by adding commonly used viscosifiers, like guar gum and synthetic polymers, to lower the reactivity (Hoefner and Fogler, 1987). The reactivity is reduced because the high viscosity limits the fluid movement. However, this method is not suitable to be used in high-temperature reservoir (above 150°F) stimulation applications (Knox et al., 1965). Another way to

reduce the reactivity of acid by physical means is with emulsions. This type of reduction in reactivity is achieved by the micro-emulsion of acid droplets in oil. Emulsified acids can be used in high-temperature reservoirs because of their thermodynamic stability as compared to gelled acids (Hoefner and Fogler, 1987). However, these acids also have higher apparent viscosity. So, higher pumping rates and pressure are required in the field which might not be economically feasible. Also, they cannot be used with many common chemical additives because the nature of emulsion limits the options for production engineers (Knox et al., 1965).

Reduction in reactivity by chemical means can be achieved by chemically limiting the protons from touching the carbonate surface. The main benefit of chemical retardation is that it does not increase the viscosity of acid as in gelled or emulsified acids. The level of chemical retardation can be controlled by changing the molar ratio of acid to the chemical retarder. This type of retardation is especially useful in high-temperature applications because of the possibility of controlling the rate of retardation (Sohn, 2018). Furthermore, retarded acids reduce corrosion of the tubings in the well and have lower safety and environmental risks. One of the challenges with retarded acids is high cost and side reactions that may cause formation damage (Knox et al., 1965). Another challenge of using retarded acids is achieving the optimal injection rate (Zhu et al., 2022). As wormhole penetrates into the reservoir, the wormhole tip velocity decreases. Hence, optimal injection rate may be difficult to achieve in the field, which causes the stimulation efficiency to decrease. Thus, the acid systems having low optimal interstitial velocities are preferred (Zhu et al., 2022).

The alternative acid system used in this study is formed by a Lewis-acid base reaction leading to an adduct or complex. It leads to an increase in activation energy. The reaction rate of such single-phase alternative acid system can be tailored for the particular reservoir rock

depending on the Lewis-base utilized (Zhu et al., 2022). This results in controlled reaction rates of the hydrogen proton with regulated mass transfer. This unique property of alternative acid system leads to a higher wormholing efficiency, compared to conventionally used HCl systems.

Numerous studies have shown that as temperature increases, wormhole efficiency decreases for hydrochloric acid. Several authors have studied the effect of temperature on wormhole efficiency by conducting coreflood experimental studies with HCl. Wang et al. (1993) studied the effect of temperature by conducting experiments with 3.6wt% HCl and Indiana limestone. The study found that the increase in temperature results in an increase in optimal interstitial velocity, thus suggesting a decrease in wormhole efficiency. The same effect was noticed by other researchers. Fredd and Fogler (1999) conducted coreflood experiments using 1.8wt% HCl with Indiana limestone for temperature up to 176°F. Bazin (2001) studied the effect of temperature on acidizing efficiency using Lavoux limestone with 7wt% HCl, and noticed an increase in $v_{i,opt}$ with temperature. Furui et al. (2010) conducted the experiments with Kansas Chalk using 15wt% HCl at higher temperatures (150°F and 200°F), and noticed the same trend of decreasing wormhole efficiency with temperature. Dong (2015) model quantified the effect of temperature on optimal conditions. Thus, the behavior of wormholes created by alternating acid also needs to be studied for a wide range of temperatures.

1.2 Objective

This study presents a systematic evaluation of wormhole behavior with various alternative acid systems at different temperatures up to 300°F. This study is done by conducting coreflood experiments at various temperatures. The wormhole efficiency of various alternative

acid systems is evaluated using Indiana limestone and Silurian dolomite cores of 1.5-inch diameter and varying lengths. The objectives of this study are defined as following:

1. Study the wormhole efficiency behavior using alternative acid systems by conducting coreflood experiments at various temperatures.
2. Evaluate acid stimulation efficiency from experimental results including differential pressure data, wormhole breakthrough behavior, and CT scan images of the wormholes.
3. Compare the stimulation efficiency of alternative systems to that of hydrochloric acid at similar testing conditions.

2. EXPERIMENTAL APPARATUS

The acid core flooding experiments were conducted using the experimental setup shown in **Figure 3**. This experimental setup was originally designed and assembled by Grabski (2012). The apparatus consists of a core holder, a water accumulator, an acid accumulator, a refill chamber, a hydraulic pump, a syringe pump, a back-pressure regulator, a nitrogen tank, heating tapes, and a data acquisition system connected to a computer.

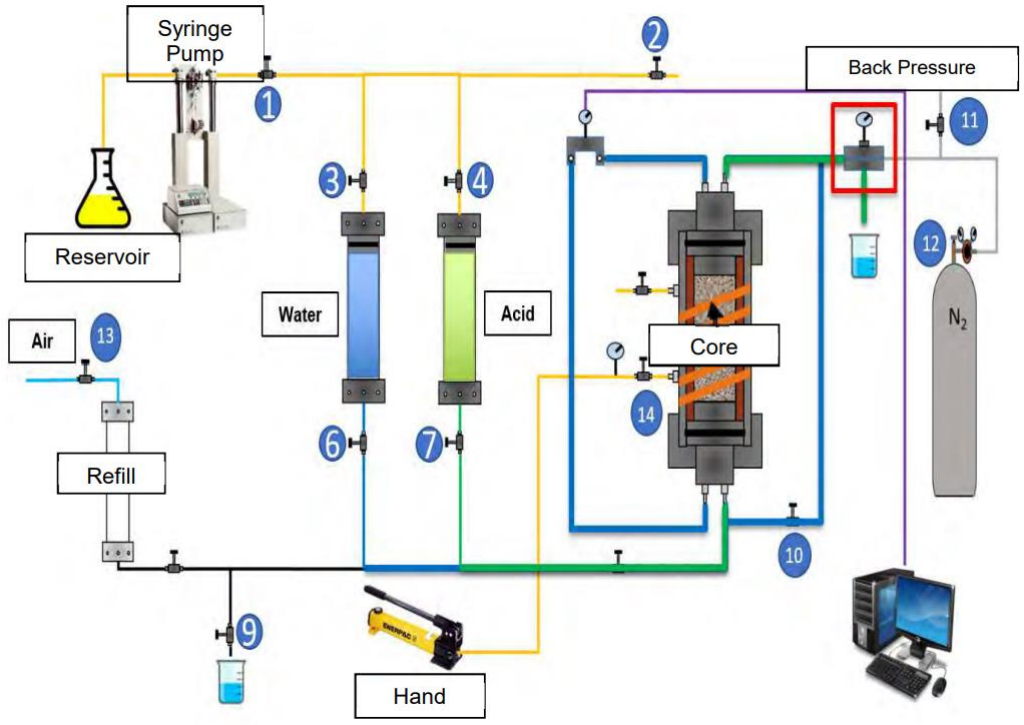

Figure 3 – Schematic of core flood experimental setup (Sohn, 2018)

2.1 Core Holder

The core holder is a cylindrical cell in which the core is placed, confining pressure is applied, and the fluids are allowed to pass through it. The core holder used to conduct the acid core

flood experiments is a Hassler-type core holder rated for 3000 psi pressure and 300°F temperature. It is designed for cores of 1.5-inch diameter and up to 20 inches in length. The core holder along with the plugs is shown in **Figure 4**.

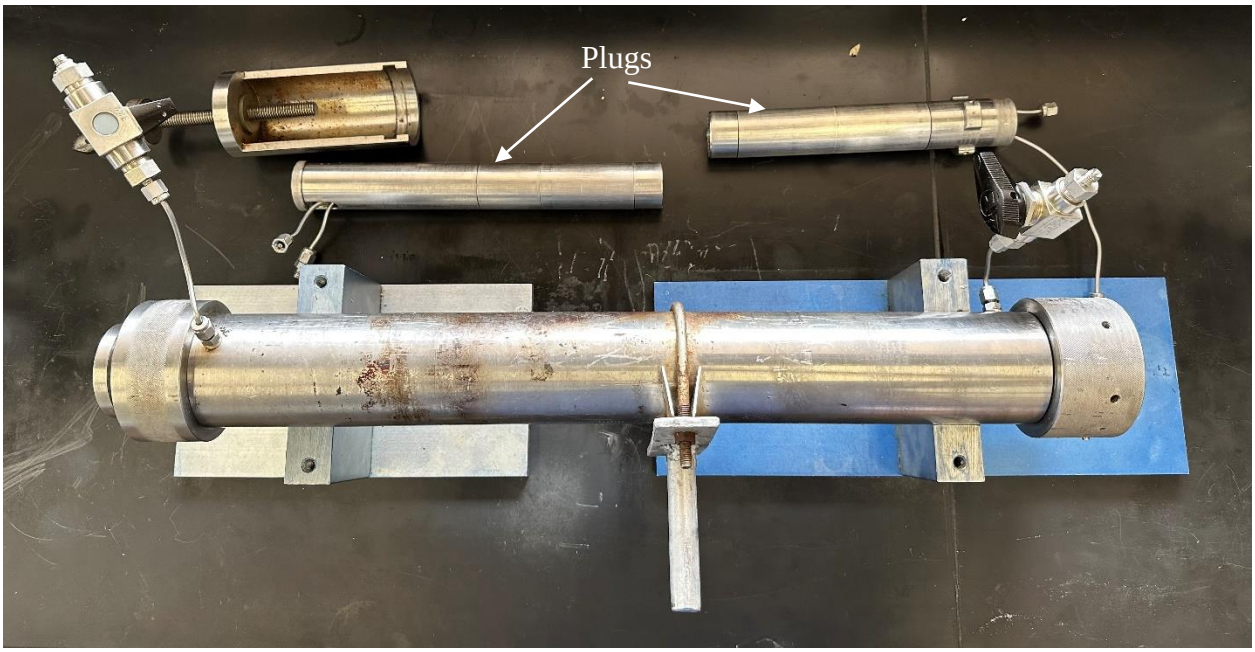

Figure 4 – Core holder with plugs and metal cap

The core holder mainly consists of the outer body, rubber sleeve, and plugs. The outer body and the plugs are made of Hastelloy C276. The inlet and outlet plug has two 1/8-inch tubing lines. During the experiment, one tubing from each plug is connected to a pressure transducer to measure the pressure drop between the inlet and outlet side. The other tubing in each plug is used to inject fluid. The sleeve is made of Viton rubber, which can tolerate high temperatures and pressure. It is assembled with the outer body along with 2 ferrules, 2 O-rings, and 2 end caps, and remains assembled unless repairs are needed. During the experiment, hydraulic oil is pumped into the space between the sleeve and the outer body to pressurize the sleeve. This ensures a seal around the core which prevents the fluid from bypassing the core. After putting the core into the core holder, the

bottom plug is inserted and turned to seal. The top plug is inserted from the other side and screwed in with a metal cap to seal.

2.2 Accumulators and Refill Chamber

Two hydraulic accumulators are used during an experiment: one for water, and the other for acid. The two accumulators along with the refill chamber are shown in **Figure 5**.

Figure 5 – Water accumulator (left), refill chamber (middle), and acid accumulator (right)

The accumulators have a piston on the inside which separates the injection fluid from the hydraulic oil on top. The hydraulic system in the accumulators prevents any flow back of fluid and absorbs any accidental pressure surges. The water accumulator is made of Stainless Steel 316, and

the acid accumulator is made of Hastelloy C276. Both the accumulators have a pressure rating of 5000 psi and a temperature rating of 300°F.

The refill chamber is a cylindrical pipe made of PVC and is resistant to acid corrosion. It has a removable screw on the top, which is removed to fill up the chamber with water or acid using a funnel. A hose from the laboratory air supply is connected to the top end of this refill chamber. To refill any of the accumulators, the refill chamber is first filled with the desired fluid and then the fluid is injected into the accumulator with the pressured air. This causes the piston in the accumulator to move up and the hydraulic oil from the top is dumped back into the reservoir flask connected to the injection pump for refill purposes.

2.3 Hydraulic Pump

An ENERPAC-392 hand pump (**Figure 6**) is used to apply confining pressure to the core during the experiment. The hand pump has a maximum pressure rating of 10,000 psi. The pump is connected to the outer body of the core holder. The hydraulic oil from the pump is injected into the space between the rubber sleeve and the outer body of the core holder. The pump pressure (confining pressure) is measured with a pressure gauge connected to the inlet. This pressure is kept at least 500 psi above the fluid injection pressure during the experiment to prevent the fluid from bypassing the core.

Figure 6 – ENERPAC-392 hydraulic hand pump (Grabski, 2012)

2.4 Syringe Pump

A high-precision – high-pressure syringe pump (**Figure 7**) is used to inject the fluid into the core holder at a constant rate. It is a Dual-pump Continuous Flow 260D Teledyne ISCO Syringe Pump with a 7,500 psi maximum pressure rating (Grabski, 2012). It can pump the fluid at a minimum flow rate of 0.001 mL/min and up to a maximum flow rate of 107 mL/min. It has two 260 mL pumps from which one pump can refill while the other pump is running creating a continuous fluid flow. The digital control panel can set the run mode to either a constant flow rate or constant pressure. Constant flow rate mode was used in conducting experiments in this study. The digital panel can control the injection flow rate, which also shows the injection pressure.

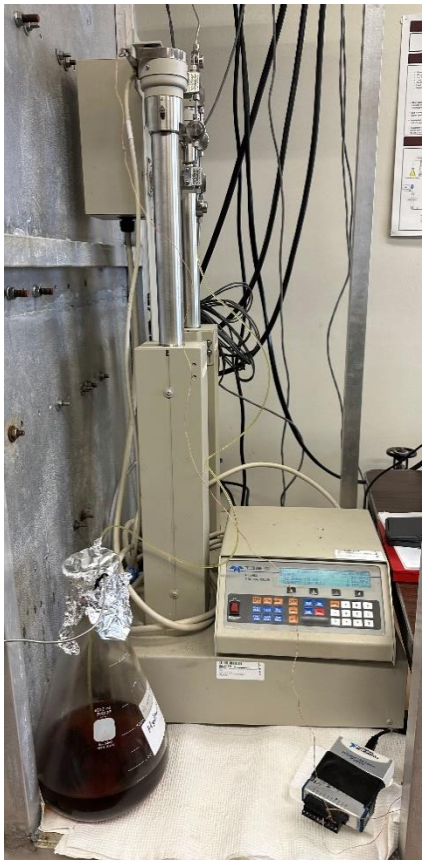

Figure 7 – Teledyne ISCO syringe pump and hydraulic oil reservoir flask

2.5 Back Pressure System

A back pressure regulator (**Figure 8**) applies back pressure at the outlet side of the core to keep the system pressurized during the experiment. The back pressure regulator ensures that this minimum pressure is maintained throughout the system and that CO_2 remains within the effluent solution. This back pressure regulator is connected to a nitrogen tank (**Figure 9**) to apply and control the back pressure. The regulator has a diaphragm that is pressed at a desired pressure by the nitrogen from the tank. This diaphragm lets the fluid pass only when the pressure exceeds the back pressure to lift it.

Figure 8 – Back pressure regulator with the diaphragm in the middle

Figure 9 – Nitrogen tank

2.6 Heating System

The experiments in this study were conducted at elevated temperatures ranging from 125°F to 300°F. Two heating tapes were used to heat up the system. One heating tape was wrapped around the core holder to heat up the core holder (**Figure 10**). This heating tape was controlled by LabView software and temperature was continuously measured using a thermocouple probe attached to the core holder. Another heating tape was wrapped around the tubing that connects to the inlet side of the core holder to heat up the fluid entering the core holder (**Figure 11**). This heating tape was controlled by a manual controller. A thermocouple probe was attached to the tubing near the inlet side of the core holder to measure the actual temperature of the fluid entering the core holder. These thermocouple probes were connected to the PC through a collection module shown in **Figure 12**.

Figure 10 – Core holder with heating tape

Figure 11 – Heating tape wrapped around the tubing to heat up the fluid

Figure 12 – Data acquisition module

3. EXPERIMENTAL PROCEDURE

This section includes a detailed description of the experimental procedure followed to conduct matrix acidizing core flood tests. The experiments were conducted with novel acid systems as well as 15% HCl at various temperatures. This matrix acidizing experimental procedure was designed by Grabski (2012). A few modifications in the procedure were adopted from Sohn (2018) and Bettencourt (2022).

3.1 Core Preparation

All the experiments were run with cores of 1.5-inch diameter and 20 inches length, unless otherwise mentioned. After the cores are cut into desired dimensions, the following procedure is used for core preparation before the actual experiment (Sohn, 2018):

1. Label the cores.
2. Dry the cores overnight in the oven, at least for 12 hours at 135°C temperature.
3. Weigh the cry cores and record the dry weight.
4. Saturate the cores with water for at least 12 hours.
5. Weigh the saturated cores and record the saturated weight.
6. Calculate the porosity and store the cores in water until the experiment.

To dry the cores, a tabletop oven was used. The cores were saturated in a PVC chamber connected to a vacuum pump. The cores were submerged in water and all the air within the pores was extracted with the vacuum pump. The porosity of core samples was calculated from the measured dry and saturated weights.

$$\phi = \frac{V_{pore}}{V_{bulk}} \times 100(\%) \quad (1)$$

$$V_{pore} = \frac{W_{sat} - W_{dry}}{\rho_{water}} \quad (2)$$

$$V_{bulk} = \frac{1}{4} \times \pi \times d^2 \times L \quad (3)$$

3.2 Acid Preparation

For the experiments with hydrochloric acid, 36wt% HCl was diluted to 15wt% by adding a calculated amount of water. The novel acid systems, HCR-6000, HCR-6000-MTX, HCR-9000 Ver-1 and Ver-2 were received from the manufacturer ready–to–use. A corrosion inhibitor (0.3vol%) was added to all the acids before the experiment.

3.3 Experiment Operating Procedure

The experimental apparatus schematic is shown in Figure 3. The valves mentioned in the following procedures can be referred to in Figure 3. The experimental procedure is subdivided into three sections: system preparation, running experiment, and disassembly.

3.3.1 System Preparation

The entire system must be depressurized before running any experiment. All the pressure gauges should read 0 psi. After ensuring the system is depressurized, fill the water and acid accumulators.

Acid Accumulator Preparation Steps:

1. Make sure the refill chamber is empty.
2. Remove the top screw and place a funnel on the refill chamber.
3. Fill the refill chamber with prepared acid.
4. Remove the funnel and seal the top with the screw.

5. Open the oil recycle valve #2 and make sure #6 and #9 are closed.
6. Open the acid accumulator valve #7.
7. Turn on the air supply valve to allow refill.
8. Make sure the acid accumulator is being filled by checking the oil flow into the reservoir flask.
9. Close the acid accumulator valve #7 when the liquid level in the refill chamber is low (usually about 1 inch from the bottom) to avoid the air entering the acid accumulator.
10. Turn off the air supply valve #13.
11. Close the oil recycle valve #2.
12. Empty the remaining acid in the refill chamber through valve #9.

After this step, the refill chamber should be cleaned at least twice by refilling it with water and emptying it to make sure no acid is left in the refill chamber. The next step is to fill the water accumulator.

Water Accumulator Preparation Steps:

1. Remove the top screw and place the funnel on the refill chamber.
2. Fill the refill chamber with water.
3. Remove the funnel and seal the top with the screw.
4. Open oil recycle valve #2.
5. Open water accumulator valve #6, and make sure valves #7 and #9 are closed.
6. Turn on air supply valve #6 to allow refill.
7. Make sure the water accumulator is being refilled by checking the oil flow into the reservoir flask.

8. Close the water accumulator valve #6 when either the water level in the tank is low or there is no more oil flow in the reservoir flask.
9. Turn off air supply valve #13.
10. Close the oil recycle valve #2.
11. Empty the refill chamber using valve #9.

After both the accumulators are filled and ready for the experiment, the core holder can be assembled.

Core Holder Assembly:

1. Clean the core holder and all the components by rinsing them with water.
2. Mark the flow direction on the core and take pictures of the inlet and outlet sides.
3. Insert the core into the core holder according to the flow direction.
4. Insert the bottom plug and twist right to secure.
5. Insert top plug until snug fit.
6. Place and screw in the top cap.
7. Mount the core holder properly onto the rig.
8. Wrap the heating tape around the core holder and place the thermocouple between the heating tape and the core holder.
9. Make all the tubing connections with the inlet and the outlet plugs properly.
10. Connect the confining pump tubing to the core holder and open valve #14.
11. Apply 500 psi confining pressure by pumping oil with the hand pump.
12. Close bypass valve #11 and open nitrogen tank valve #12 to apply 1200 psi backpressure.

3.3.2 Conducting Experiment

After the system is ready to start, the water accumulator valve is opened and syringe pump is turned on to allow the flow of water through the system. The injection pressure will start to increase after some time because of the back pressure. The confining pressure is kept at least 500 psi above the injection pressure. After the system is pressurized, it is checked for leaks and LabView is started. The next step is to measure the permeability of the core.

Steps for measuring permeability:

1. Adjust the injection rate to the desired rate from the pump.
2. Record baseline differential pressure while water is flowing through the bypass line.
3. Close bypass valve #10.
4. This will cause the injection pressure to increase. Make sure to maintain the confining pressure at least 500 psi above the injection pressure.
5. Let the differential pressure across the core stabilize and record it once constant.
6. Subtract the baseline pressure drop from the recorded pressure drop across the core to get the actual differential pressure.

From this differential pressure, the permeability of the core is calculated using a modified form of Darcy's law of permeability:

$$k = \frac{122.63 \times q \times L \times \mu}{\Delta P \times d^2} \quad (4)$$

where q is the injection rate in mL/min, L is the length of the core in inches, μ is the fluid viscosity in cp, ΔP is the actual differential pressure in psi, and d is the core diameter in inches.

After the permeability is calculated, both the heating tapes are connected to the power source, and the fume hood is turned on. The core heating tape is controlled from LabView and the fluid heating tape is controlled from a manual controller. The temperature is increased in steps of

25-30°F to avoid any overload on the heating tape and let it stabilize. The fluid and the core holder temperatures are monitored in LabView. During the heating process, the confining oil in the core holder expands due to increasing temperature. This cause the confining pressure to rise. Therefore, it needs to be decreased to the desired level through a needle valve in the confining pump. Once the desired temperature is reached and the system is stabilized, the acid injection can be started.

Acid Injection:

1. Make sure both the core holder and the injecting fluid reach desired temperature for the experiment.
2. Simultaneously open the acid accumulator valve #7 to inject acid and close water accumulator valve #6. Start the timer at the same time.
3. Observe the differential pressure and the pump pressure, and adjust the confining pressure if necessary.
4. Make sure the fluid temperature is at the desired level. Adjust the controller if necessary.
5. Put the end of the effluent tubing under the surface of the water in the effluent vessel to avoid any hazardous acidic vapor escaping the lab, especially during high-temperature experiments.
6. Once the pressure drop across the core reaches the baseline level, simultaneously close the acid accumulator valve #7 and open the water accumulator valve #6. Stop the timer at the same time and record the total injection time.
7. Turn off the heating tapes and stop LabView.
8. Allow water to flow through the system for a while to rinse the entire system. Check the pH of the outlet fluid to make sure no acid is left in the system.

After this, the system can be disassembled and the core can be analyzed.

3.3.3 Disassembly and Core Analysis

Steps for disassembly:

1. Decrease back pressure by releasing the backpressure valve #12 in steps to depressurize the system. Decrease the confining pressure by releasing the hand pump valve #14 in each step accordingly.
2. Stop the syringe pump.
3. Open oil recycle valve #2.
4. Check to see that all pressure gauges read 0 psi or lower pressure.
5. Unwrap the core heating tape using proper PPE due to high temperature and remove the thermocouple.
6. Disconnect in the same order in which the connections were made during assembly.
7. Remove the core holder.
8. Remove top and bottom plugs, and the core out carefully.
9. Drain the remaining water and acid from respective accumulators into a bucket.
10. Rinse the acid accumulator with water at least twice and measure the pH to make sure no acid is left in the accumulator.
11. Empty the bucket into the chemical waste disposal container.

Now the core flood experiment is finished. The core is placed in a tabletop oven to dry overnight. After that the core is scanned using a CT scanner. The CT scan file is processed following the workflow mentioned in Sohn (2018) thesis. The wormhole structures from the processed scans are analyzed.

4. RESULTS AND DISCUSSION[1]

4.1 Experimental Data Analysis

The experimental data analysis followed a general workflow as mentioned in Sohn, 2018 thesis. A general worksheet containing the basic calculation functions for interstitial velocity and pore volume to breakthrough was utilized for each experiment (**Figure 13**).

Coreflooding Data Sheet

Core#	6-225-3	□	Date	July 28, 2022	
Core diameter	1.5 inch				
Core length	20 inch	□	Acid Coreflooding		
			Temperature	220 °F	
Porosity Measurement					
Dry Mass	1241				
Saturated Mass	1340				
Porosity	17.094%				
Pore Volume	99 cm^3	□	Acid Injection Rate	6 cc/min	
		□	Interstitial Velocity	3.08 cm/min	
			Volume of Pipe between Core and Acid tank	3.33 cm^3	
Permeability Measurement					
Injection Rate	6 cc/min				
Pressure Differential	354.5 psi				
Permeability	18.47 md		Time for Acid to Get the Core	33.3 seconds	
			Time injected (m)	17 min	
Acid Formulation	15 wt% HCl	□	Time Injected (s)	12 sec	
Water	465 cm^3				
HCl (37 wt%)	285 cm^3	□	Total Time for Acid Injection	1032 seconds	
			Total Acid Volume	103.2 cm^3	
			Pore Volume Break Through	**1.008787879**	

Figure 13 – General worksheet for basic calculations during the experiment

Two important parameters for experimental data analysis are the interstitial velocity and the pore volume to breakthrough. The interstitial velocity is the actual velocity of the fluid going through the pore space of the core. It is calculated with dividing the injection rate by surface area and porosity of the core. Note that the interstitial velocity is calculated with the porosity of the core measured before the experiment. The pore volume to breakthrough is the volume of acid required, in terms of the pore volume of the core, for the wormhole to break through the core length. These parameters are calculated using the following equations:

[1] Some of the results are previously published in Gajipara et al., 2023.

$$v_i = \frac{q}{A \times \emptyset} \tag{5}$$

$$PV_{BT} = \frac{V_{acid}}{V_{pore}} \tag{6}$$

where v_i is the interstitial velocity, q is the injection rate, A is the surface area, Φ is the porosity of the core, V_{acid} is the volume of the acid required for a breakthrough, and V_{pore} is the pore volume of the core.

The interstitial velocity and the corresponding pore volume to breakthrough are plotted on a log-log plot for each test. Each set of data points is then curve-fitted using the Buijse-Glasbergen model, for which the below equations are used.

$$PV_{BT} = \frac{{v_i}^{1/3}}{W_{eff} \times B(v_i)} \tag{7}$$

$$W_{eff} = \frac{{v_{i,opt}}^{1/3}}{PV_{BT,opt}} \tag{8}$$

$$B(v_i) = \left(1 - e^{\left(-W_B \times {v_i}^2\right)^2}\right) \tag{9}$$

$$W_B = \frac{4}{{v_{i,opt}}^2} \tag{10}$$

where W_{eff} is the wormhole efficiency factor and W_B is the wormhole B-factor. These parameters are used to calculate the optimal conditions. The optimal pore volumes to breakthrough and interstitial velocity are determined by minimalizing a residue function. This is done by the solver function in Excel. The calculated data is then fitted into the graph as a curve reflecting the optimal conditions from the experimental data.

4.2 Effect of Temperature on Wormhole Efficiency Using HCR-6000 and HCl

A systematic experimental study has been carried out to evaluate HCR-6000 alternative acid at elevated temperatures. The experimental results are also compared with 15% HCl at the

same temperature levels. The HCR-6000 system results and evaluation are wormhole efficiency based, and each wormhole efficiency curve contains 3-5 core flood tests. The HCl results are only presented at a single injection rate that is close to the optimal condition at the same temperature for HCR-6000. The temperature used in the study is 125°F, 150°F, 225°F and 300°F. All experiments were run with Indiana Limestone quarried core samples, and the core dimensions are 1.5-inch diameter with a 20-inch length unless otherwise mentioned. The experimental conditions are listed in **Table 1**.

Table 1 - Experimental Conditions for HCR-6000 Alternative Acid Evaluation Study (Reprinted from Gajipara et al., 2023)

Temperature (°F)	Number of tests	Sample No.	Injection rate (mL/min)
125	4	6-125-4	1
		6-125-2	2
		6-125-1	4
		6-125-3	6.5
150	3	6-150-1	1
		6-150-2	2
		6-150-5	6
225	5	6-225-2	1.61
		6-225-4	4
		6-225-3	6
		6-225-5	8
		6-225-1	13
300	5	6-300-5	5.5
		6-300-1	8
		6-300-2	12
		6-300-4	16
		6-300-6	19

For most experiments, acid injection was stopped when wormholes break through the core, and acid injection time was recorded for breakthrough pore volume calculation. Some experiments did not reach breakthrough after a long injection time, and pressure started increasing. In such a

case, the acid injection was shut down, and wormhole lengths from the CT images were used to calculate pore volume to breakthrough.

4.2.1 Core Flood Tests with HCR-6000 at 125°F

Four tests are conducted at 125°F temperature. The tests use 90% HCR-6000 supplied by Fluid Energy Group (Purdy et al., 2019) with 0.3 vol% common commercial corrosion inhibitor. The core properties, such as permeability and porosity, are listed in **Table 2**. Test 6-125-4 is an added test to confirm wormhole efficiency, and it used a short core of 8 in (notice the lower dry weight compared with other tests).

The pore volume to breakthrough is calculated for each test (PV_{BT}). **Table 3** summarizes the experimental conditions in terms of injection rate and interstitial velocity, and calculated PV_{BT} for each test. From the table, it shows that the optimal condition is around an injection rate of 4 mL/min, giving the lowest pore volume to breakthrough of 0.65. The results with a fitted curve of the Buijse and Glasbergen (2005) correlation are plotted in **Figure 14**. This set of tests is trouble-less, and with four tests the optimal condition was identified.

Note that the lowest flux provided the lowest PV_{BT}, suggesting that even lower injection rates could provide optimum wormholing. Additionally, little change in wormhole geometry demonstrates the lower sensitivity of injection rate to wormhole propagation.

Table 2 - Core Properties for Tests Conducted at 125°F
(Reprinted from Gajipara et al., 2023)

Core #	Dry weight (g)	Saturated Weight (g)	Porosity (%)	Permeability (mD)
6-125-4	502	542	17	12
6-125-2	1263	1362	17	11
6-125-1	1274	1368	16	6
6-125-3	1233	1342	19	12

Table 3 - Experimental Results for Tests Conducted at 125°F (Reprinted from Gajipara et al., 2023)

Core #	Acid injection rate (mL/min)	Interstitial Velocity (cm/min)	Pore volume to breakthrough
6-125-4	1	0.51	0.47
6-125-2	2	1.03	0.81
6-125-1	4	2.16	0.65
6-125-3	6.5	3.03	0.69

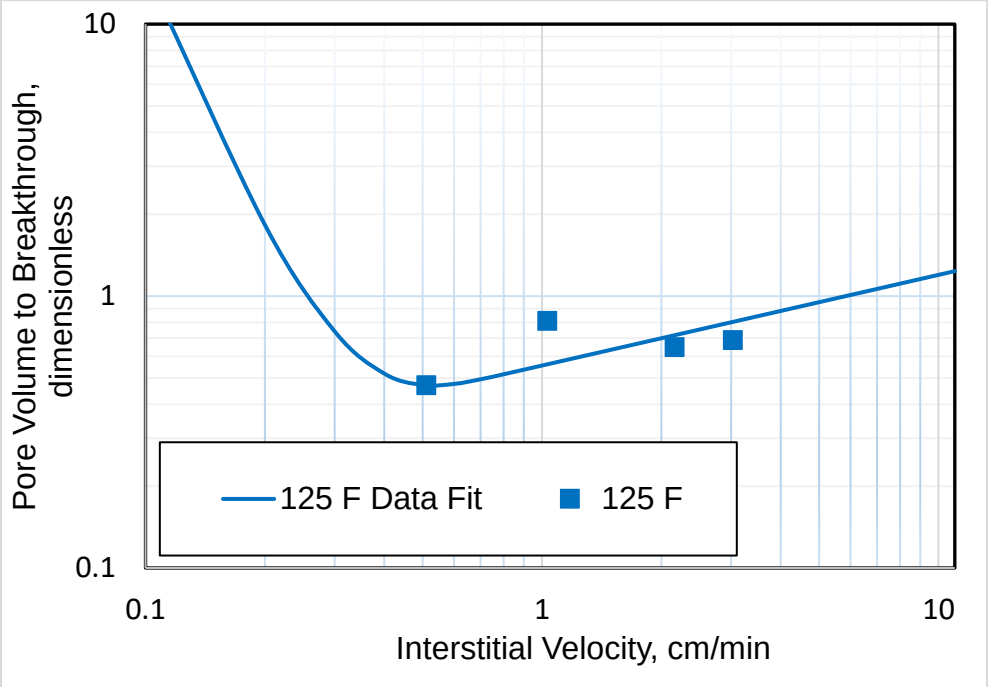

Figure 14 - Experimental results for 125°F tests (Reprinted from Gajipara et al., 2023)

The pressure history during the test and the CT scan image of the wormhole are shown in **Figures 15-18** at different injection rates respectively.

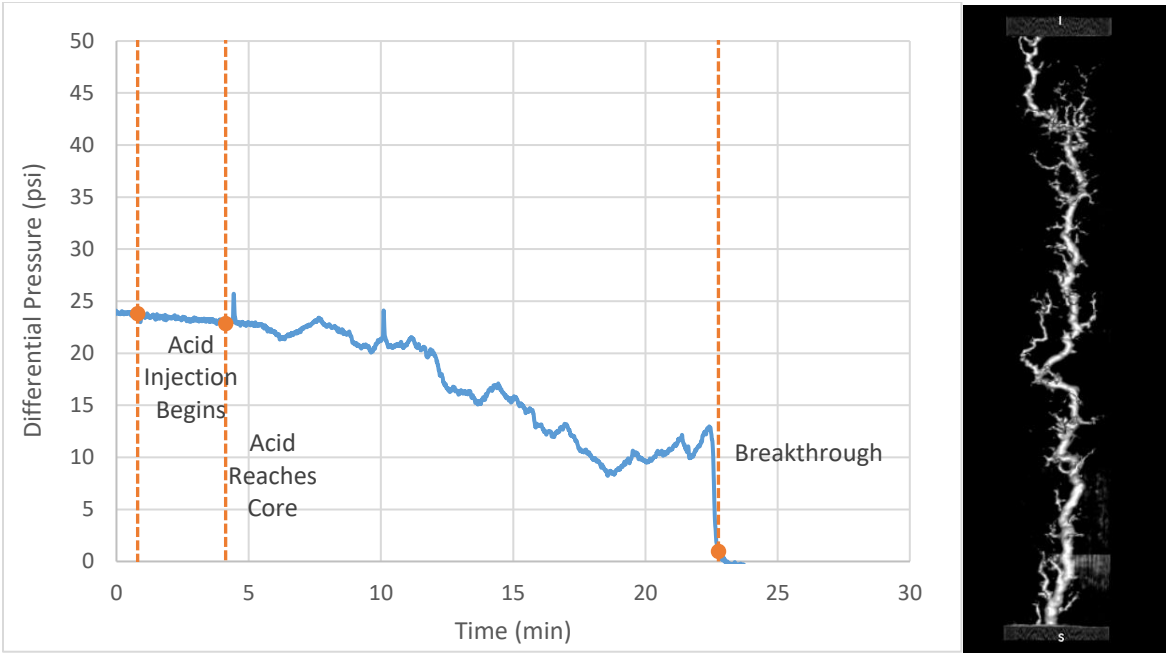

Figure 15 - Differential pressure during test and CT scan image for Core 6-125-4 (injection rate = 1 mL/min). Note that this test was run with an 8-in core.

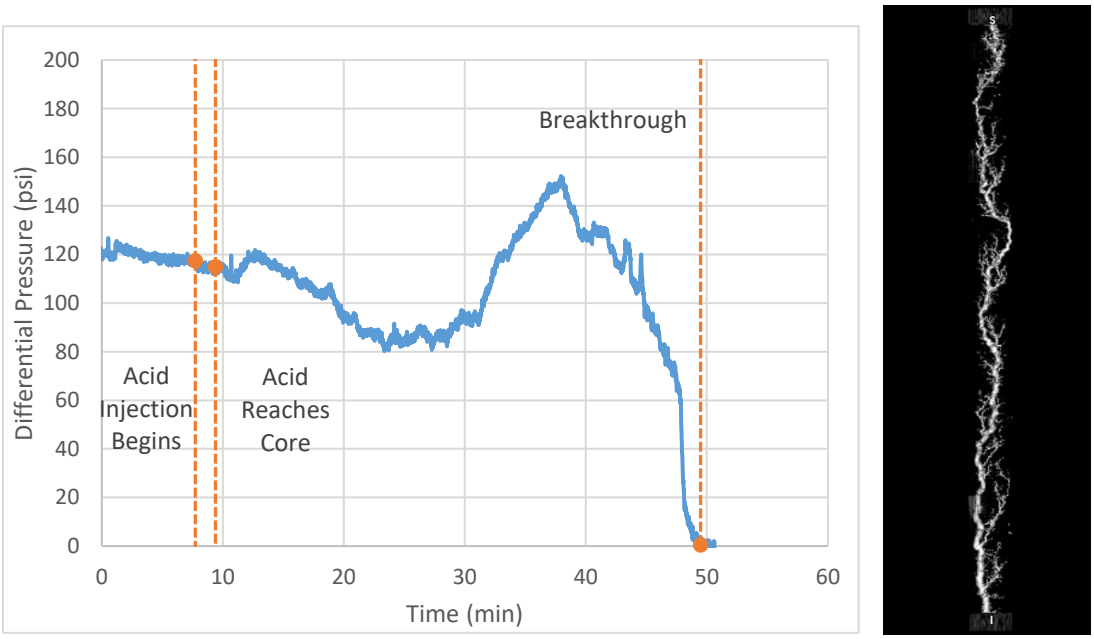

Figure 16 - Differential pressure during test and CT scan image for Core 6-125-2 (injection rate = 2 mL/min)

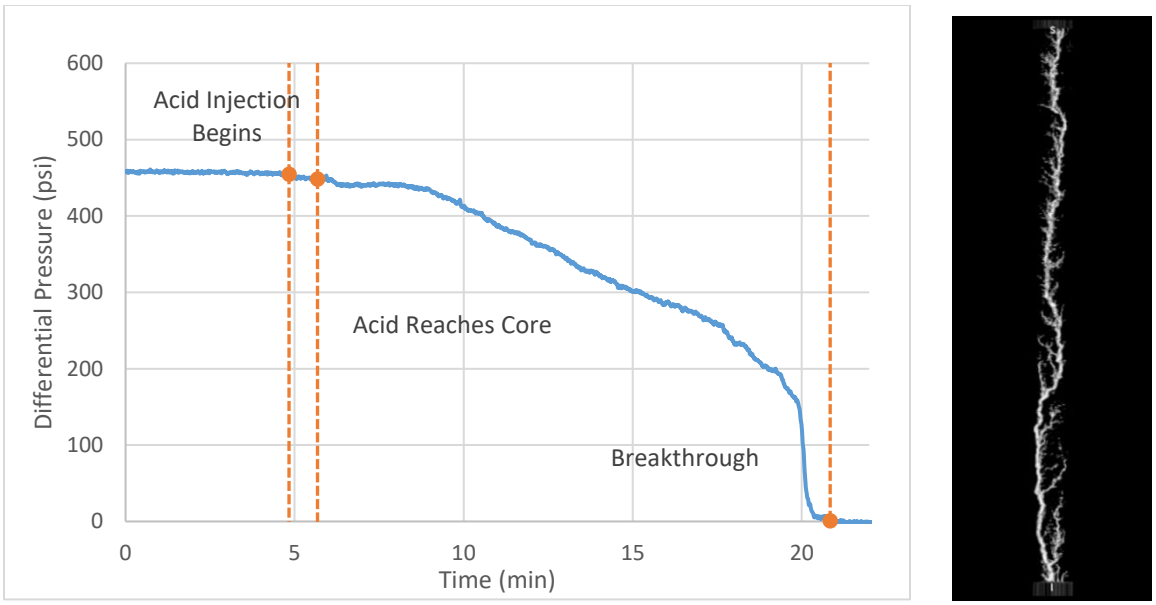

Figure 17 - Differential pressure during test and CT scan image for Core 6-125-1 (injection rate = 4 mL/min)

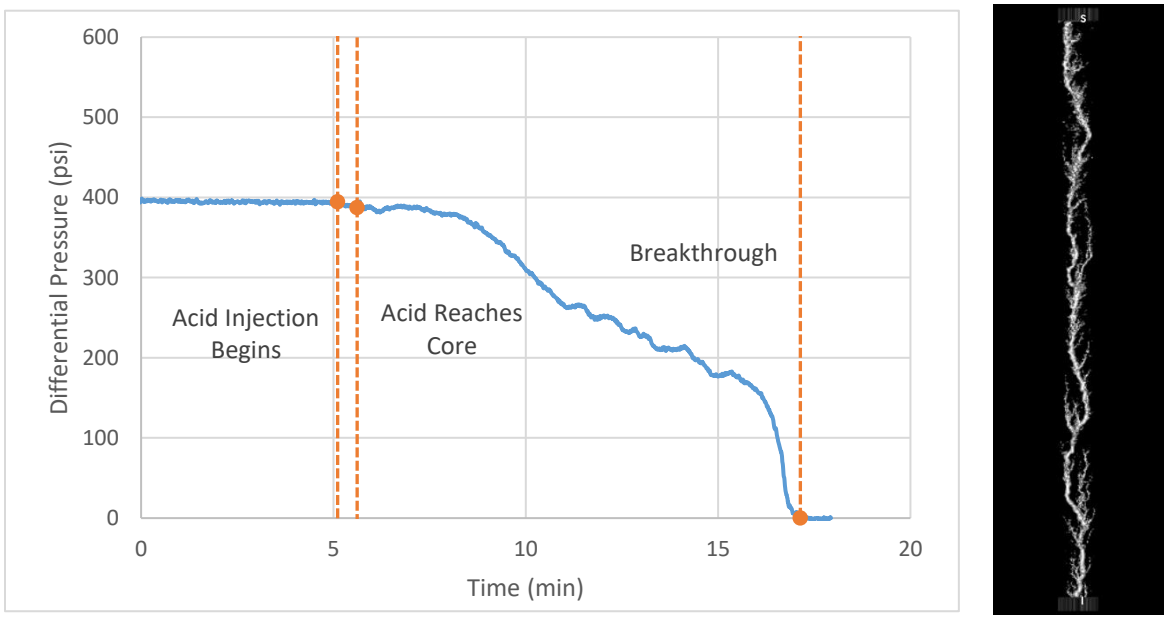

Figure 18 - Differential pressure during test and CT scan image for Core 6-125-3 (injection rate = 6.5 mL/min)

All wormhole images exhibit the ideal structure, a dominant wormhole with a controlled diameter. Figure 14 shows that PV_{BT} does not vary significantly at different interstitial velocities, showing a stable performance at a low injection rate, an advantage of using HCR-6000.

4.2.2 Core Flood Tests with HCR-6000 at 150°F

Three core flood tests have been conducted following the standard procedure at 150°F. The core properties are listed in **Table 4**. The calculated pore volumes to breakthrough value (PV_{BT}) corresponding to the acid injection rate and the interstitial velocity are listed in **Table 5**. The wormhole efficiency plot for these tests is shown in **Figure 19**. The wormhole behavior is as expected, with a typical efficiency curve shape.

Table 4 – Core properties for Tests Conducted at 150°F
(Reprinted from Gajipara et al., 2023)

Core #	Dry weight (g)	Saturated Weight (g)	Porosity (%)	Permeability (mD)
6-150-5	1267	1365	17	7
6-150-2	1264	1359	16	6
6-150-4	1256	1361	18	14

Table 5 – Experimental Results for Tests Conducted at 150°F
(Reprinted from Gajipara et al., 2023)

Core #	Acid injection rate (mL/min)	Interstitial Velocity (cm/min)	Pore volume to breakthrough
6-150-5	1	0.52	1.45
6-150-2	2	1.07	0.70
6-150-4	6	2.90	0.74

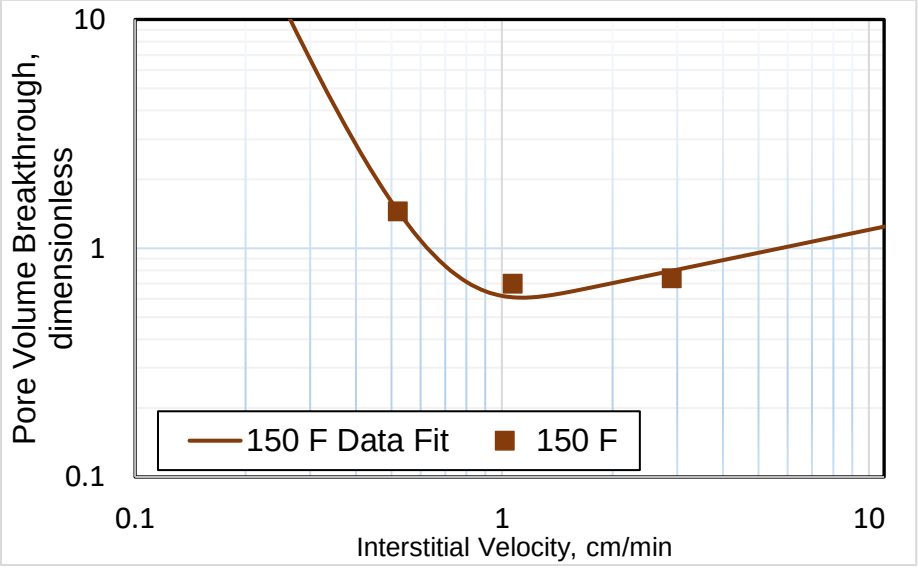

Figure 19 - Wormhole efficiency curve for 150°F tests
(Reprinted from Gajipara et al., 2023)

Figures 20-22 show pressure differential graphs for these tests, along with the CT images of the wormholes created. It is noted that the third experiment with core #6-150-5 was terminated after 130 minutes of acid injection due to a heating tape malfunction. The CT scan for that test showed good wormhole development. The wormhole length measured from the image (~85% to breakthrough) is extrapolated to calculate pore volume to breakthrough the entire core plug.

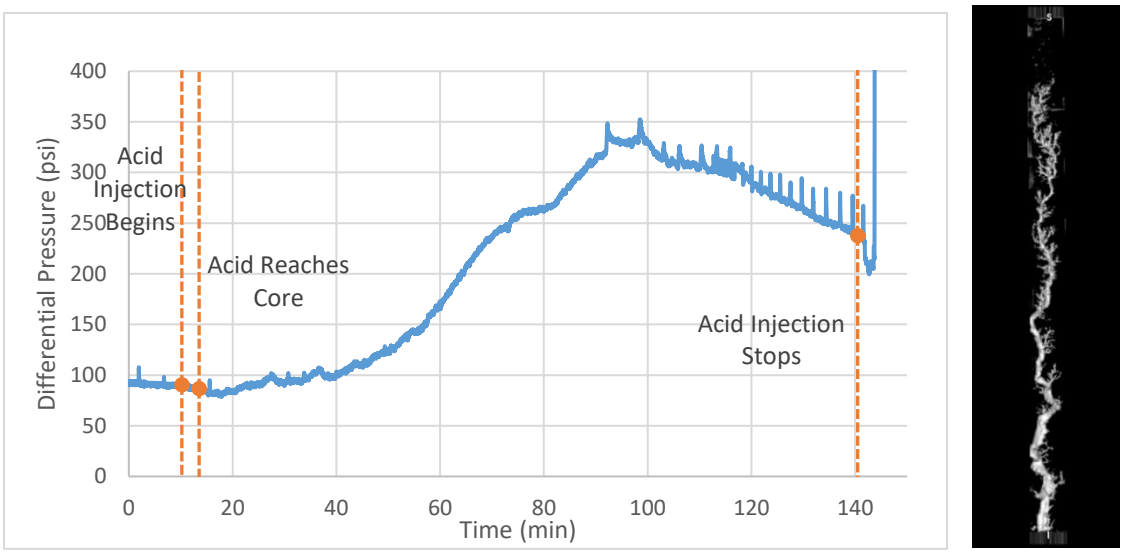

Figure 20 - Differential pressure during test and CT scan image for Core 6-150-5 (injection rate = 1 mL/min)

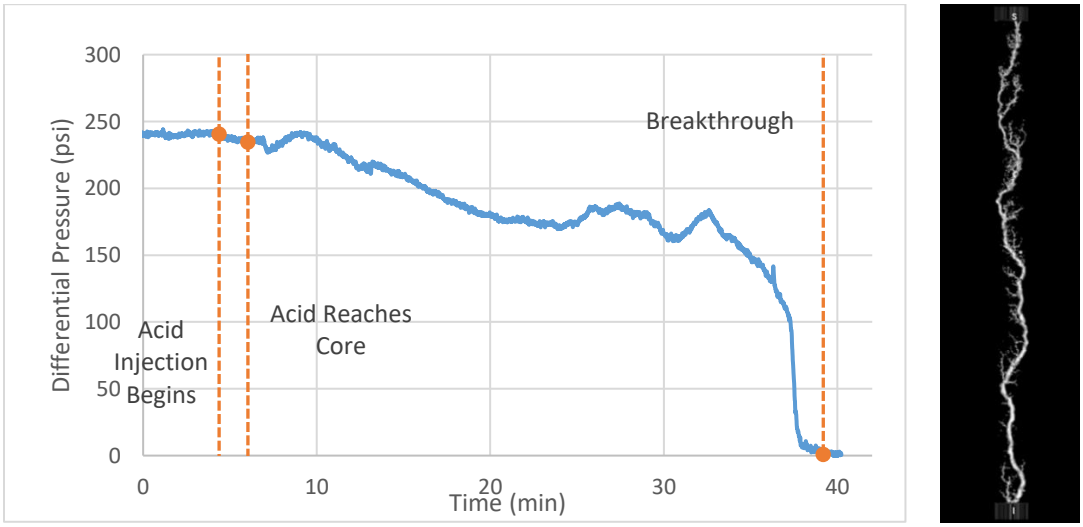

Figure 21 - Differential pressure during test and CT scan image for Core 6-150-2 (injection rate is 2 mL/min)

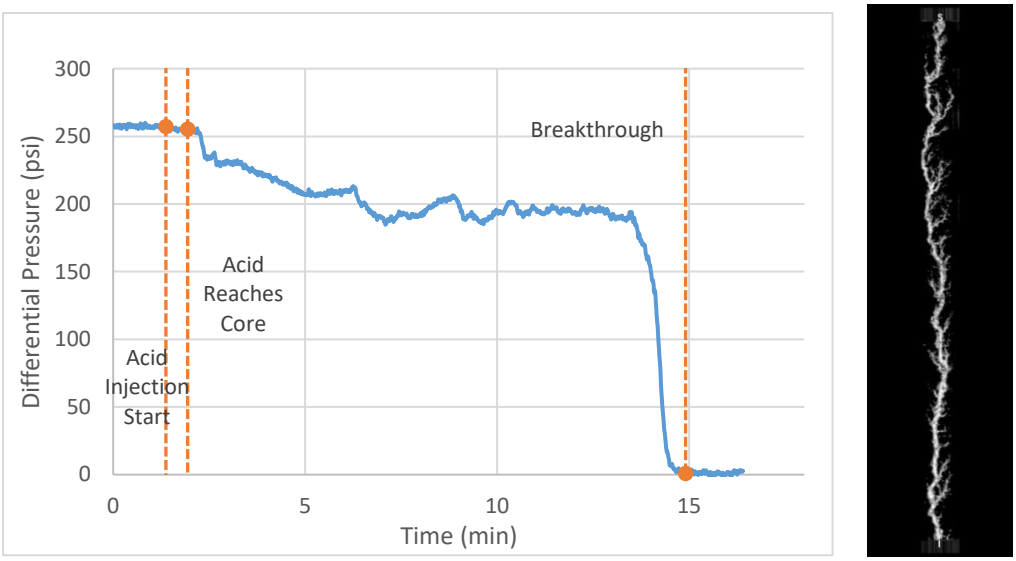

Figure 22 - Differential pressure during test and CT scan image for Core 6-150-4 (injection rate = 6 mL/min)

4.2.3 Core Flood Tests with HCR-6000 at 225°F

Five tests have been conducted at 225°F temperature. These tests utilized 90% HCR-6000 supplied by Fluid Energy Group with 0.3 vol% common commercial corrosion inhibitor. The core properties are listed in **Table 6**.

At 225°F test conditions, wormhole behavior changes significantly compared with the lower-temperature tests. It takes a longer time for the wormhole to propagate, and the stimulation efficiency declines. The pore volume to breakthrough is calculated for each test (PV_{BT}). **Table 7** summarizes the experimental conditions in terms of injection rate and interstitial velocity, and calculated PV_{BT} for each test. **Figure 23** shows the wormhole efficiency plot for the five tests at 225°F.

Table 6 - Core Properties for Tests Conducted at 225°F
(Reprinted from Gajipara et al., 2023)

Core #	Dry weight (g)	Saturated Weight (g)	Porosity (%)	Permeability (mD)
6-225-2	1245	1327	14	25
6-225-4	1246	1347	17	23
6-225-3	1241	1340	17	19
6-225-5	1224	1337	20	18
6-225-1	1236	1324	15	15

Table 7 - Experimental Results for Tests Conducted at 225°F
(Reprinted from Gajipara et al., 2023)

Core #	Acid injection rate (mL/min)	Interstitial Velocity (cm/min)	Pore volume to breakthrough
6-225-2	1.61	1	2.22
6-225-4	4	2.01	1.31
6-225-3	6	3.08	1.01
6-225-5	8	3.6	0.68
6-225-1	13	7.5	0.98

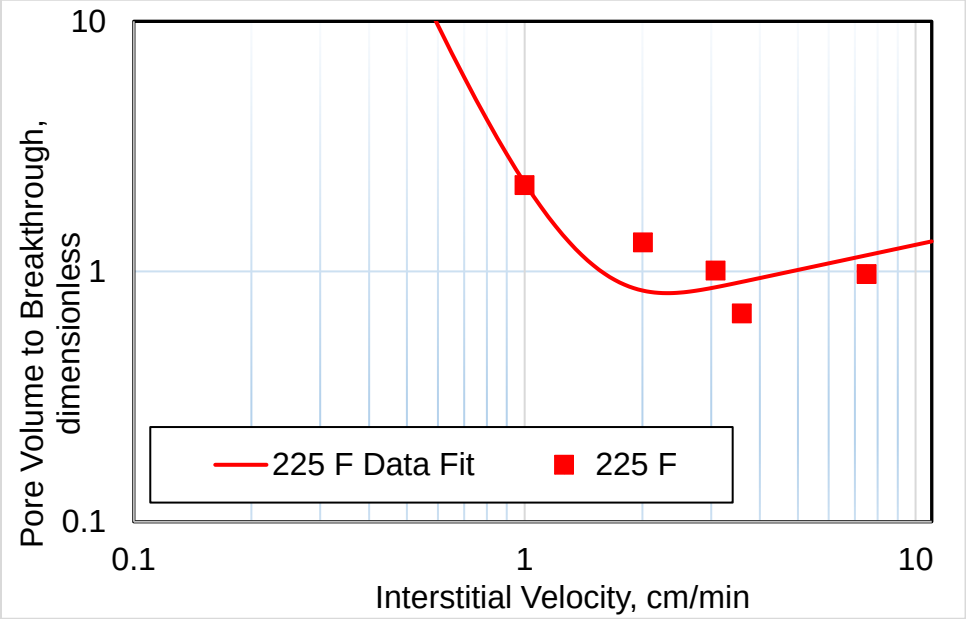

Figure 23 - Wormhole efficiency curve for 225°F tests
(Reprinted from Gajipara et al., 2023)

Other experimental results including pressure history during the injection and CT scan of wormhole structure are shown in **Figures 24-28.** The experiment with core #6-225-2 did not reach the breakthrough and the acid injection was stopped because of the unexpectedly long injection time (90 minutes). PV_{BT} was extrapolated based on wormhole growth relative to the length of the

core plug. After scanning, it is determined that the wormhole development process is normal, the long injection time is possibly caused by low interstitial velocity, thus in the following experiments, interstitial velocity is increased. The experiment with core #6-225-5 was terminated after 8.5 minutes of injection time due to a heating tape malfunction, and PV_{BT} was extrapolated as in the first test. Despite the issues during the experiments, all wormhole images show the optimum or preferred structure (one dominant wormhole with a controlled diameter). Even at a low injection rate, the diameter of the main wormhole did not enlarge significantly, indicating a reasonable pore volume of breakthrough and good efficiency (Figure 24).

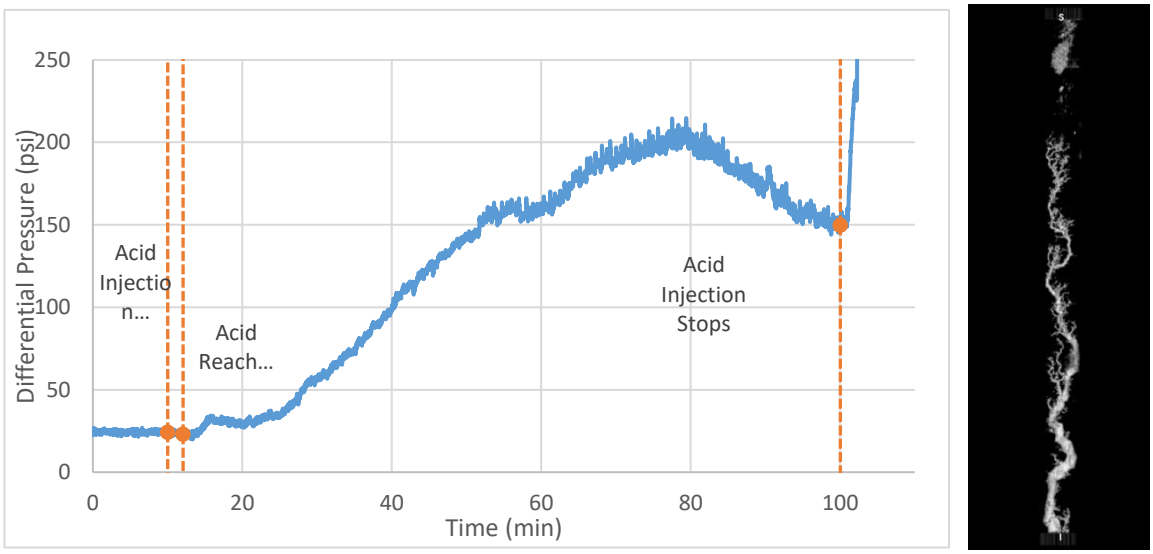

Figure 24 - Differential pressure during test and CT scan image for Core 6-225-2 (injection rate = 1.61 mL/min)

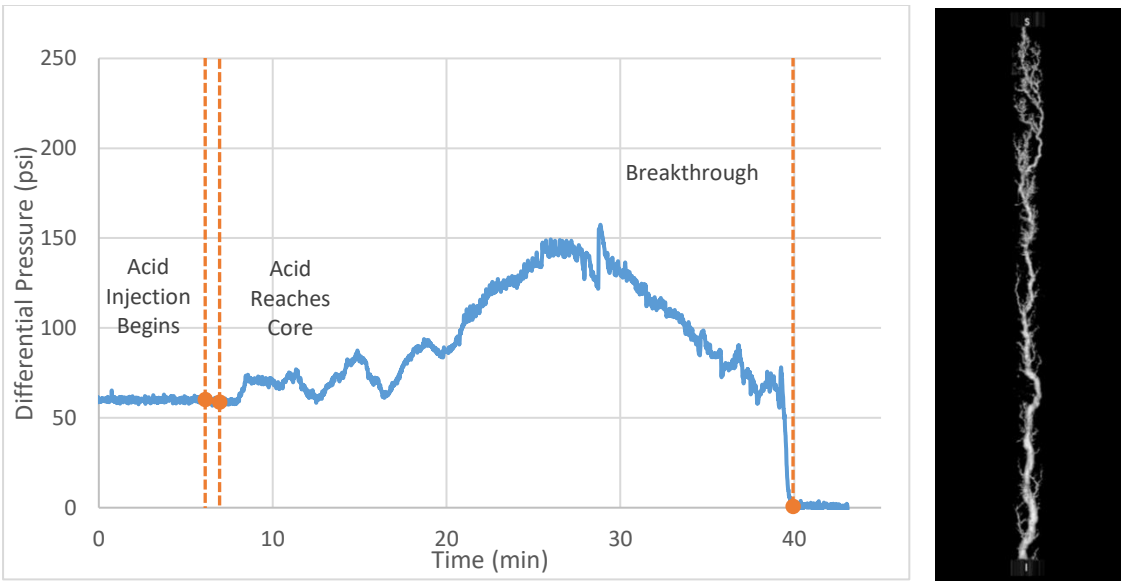

Figure 25 - Differential pressure during test and CT scan image for Core 6-225-4 (injection rate = 4 mL/min)

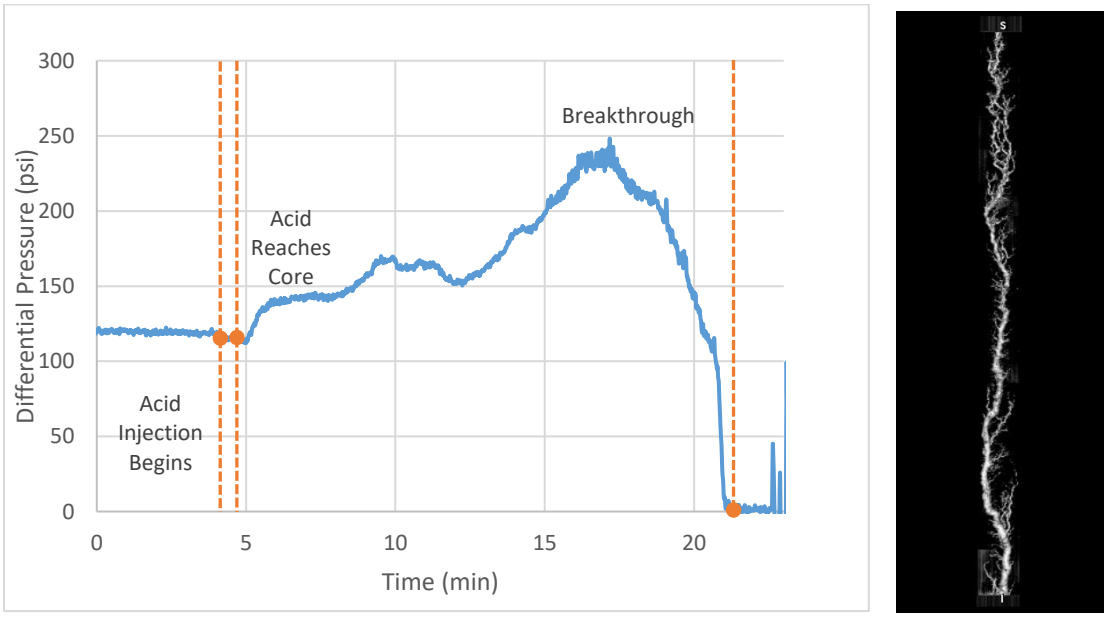

Figure 26 - Differential pressure during test and CT scan image for Core 6-225-3 (injection rate = 6 mL/min)

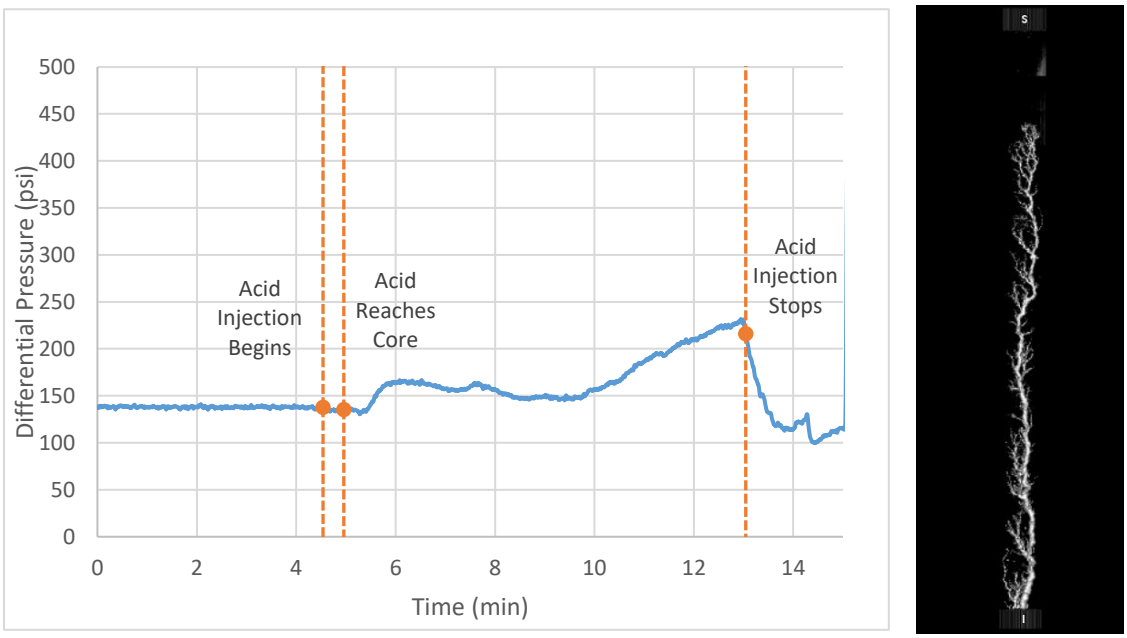

Figure 27 - Differential pressure during test and CT scan image for Core 6-225-5 (injection rate = 8 mL/min)

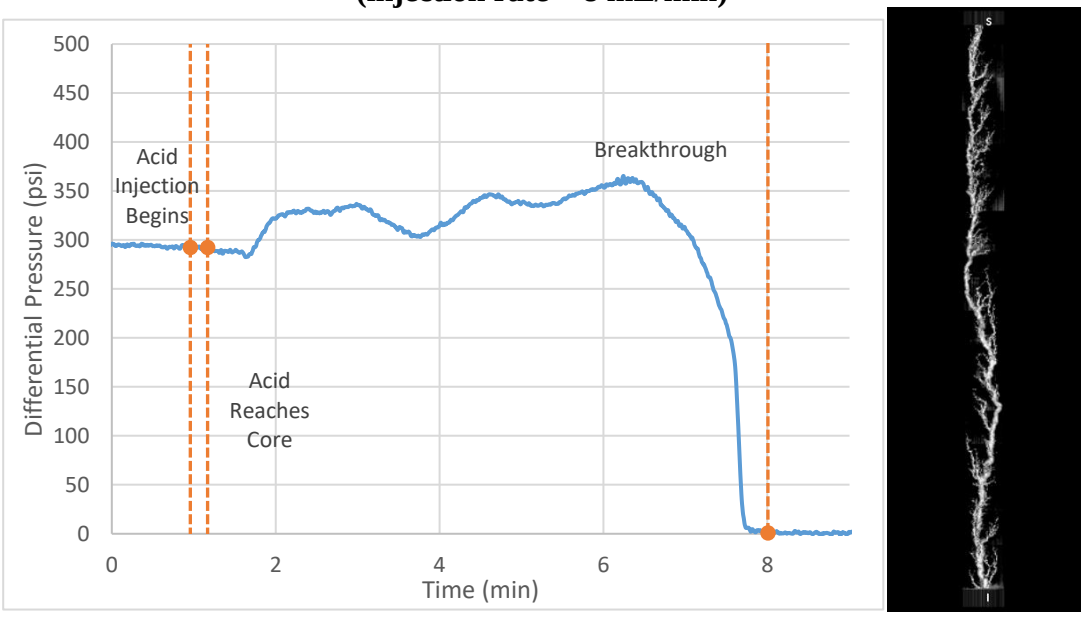

Figure 28 - Differential pressure during test and CT scan image for Core 6-225-1 (injection rate = 13 mL/min)

4.2.4 Core Flood Tests with HCR-6000 at 300°F

Five tests were run following the same procedure at 300°F. One test (core #6-300-6) was run with a 10-inch long core due to pressure limitations at a higher rate. The core properties are listed in **Table 8**. The calculated pore volumes to breakthrough value (PV_{BT}) corresponding to the acid injection rate and the interstitial velocity are shown in **Table 9**. The wormhole efficiency plot for these tests is shown in **Figure 29**, and the pressure history and CT scan images for the 5 tests are shown in **Figures 30-34**.

Table 8 - Core Properties for Tests Conducted at 300°F
(Reprinted from Gajipara et al., 2023)

Core #	Dry weight (g)	Saturated Weight (g)	Porosity (%)	Permeability (mD)
6-300-5	1260	1356	17	13
6-300-1	1252	1355	18	19
6-300-2	1242	1350	19	14
6-300-4	1242	1346	18	11
6-300-6	628	674	16	13

Table 9 - Experimental Results for Tests Conducted at 300°F
(Reprinted from Gajipara et al., 2023)

Core #	Acid injection rate (mL/min)	Interstitial Velocity (cm/min)	Pore volume to breakthrough
6-300-5	5.5	2.91	2.66
6-300-1	8	3.95	1.44
6-300-2	12	5.64	0.98
6-300-4	16	7.82	0.94
6-300-6	19	10.49	0.93

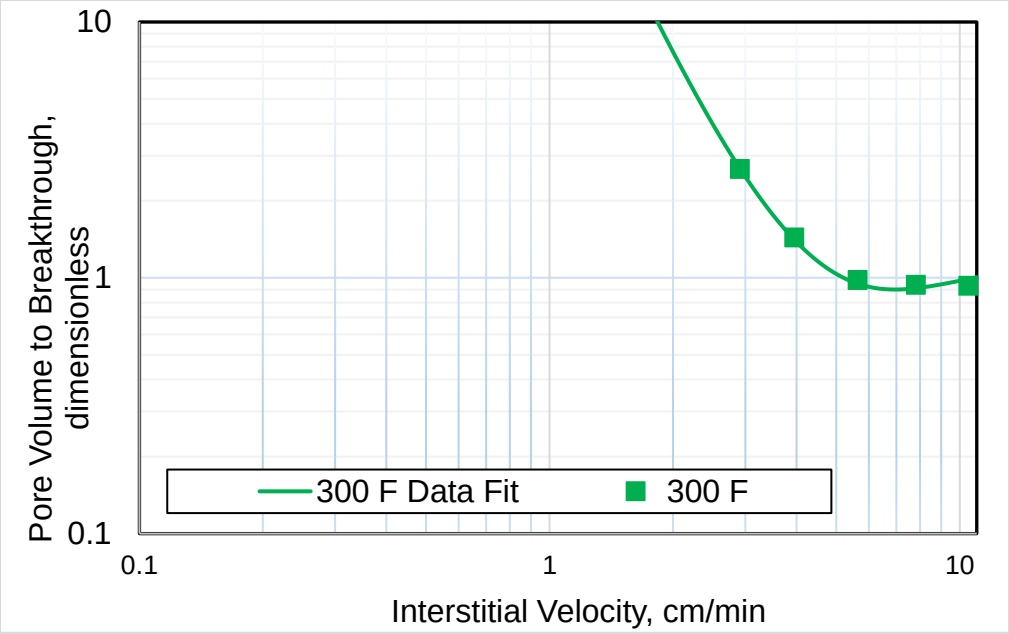

Figure 29 - Wormhole efficiency curve for 300°F tests (Reprinted from Gajipara et al., 2023)

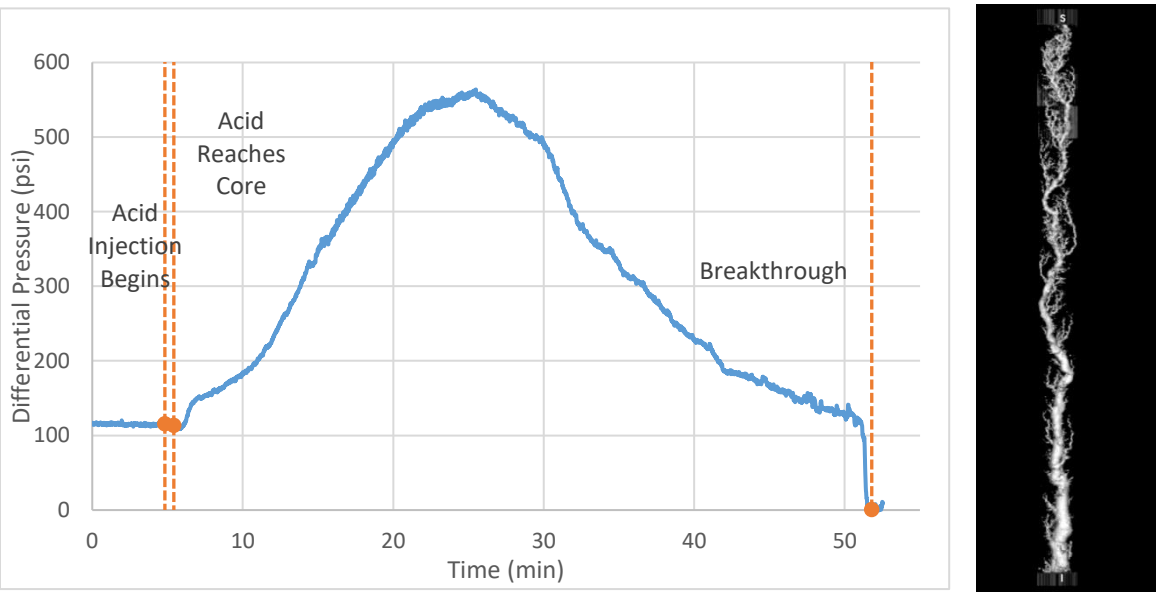

Figure 30 - Differential pressure during test and CT scan image for Core 6-300-5 (injection rate =5.5 mL/min)

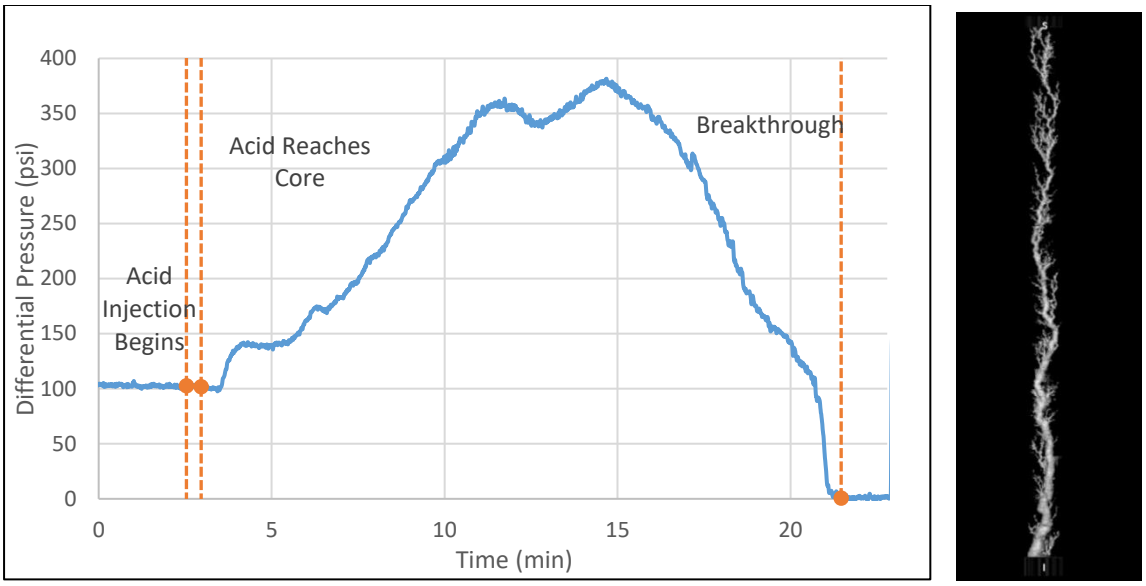

Figure 31 - Differential pressure during test and CT scan image for Core 6-300-1 (injection rate =8 mL/min)

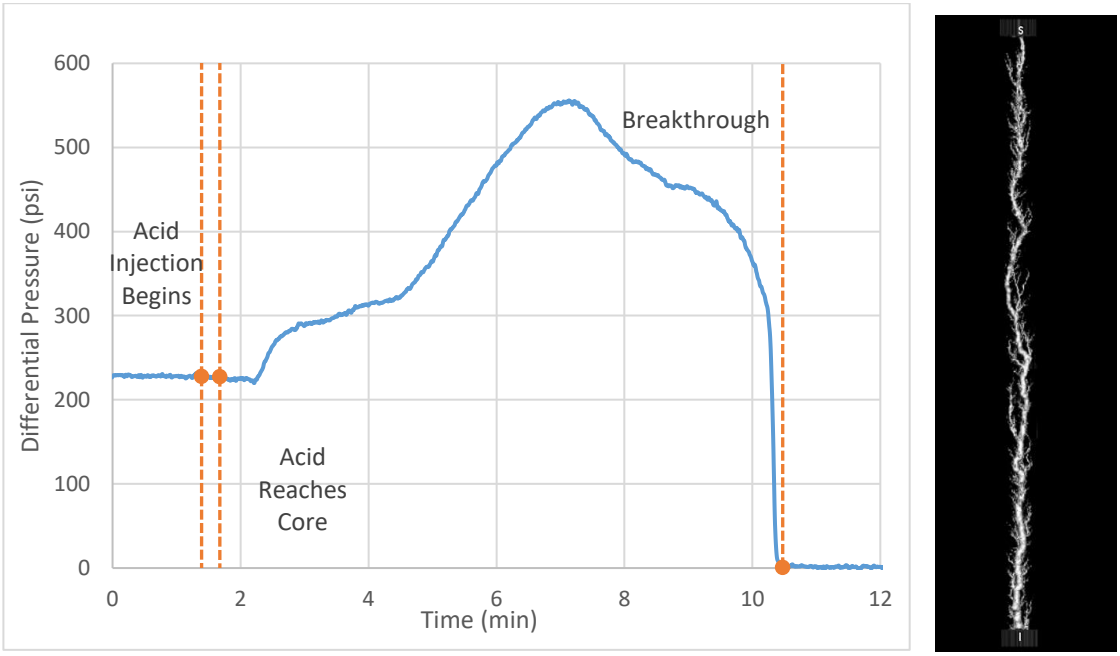

Figure 32 - Differential pressure during test and CT scan image for Core 6-300-2 (injection rate =12 mL/min)

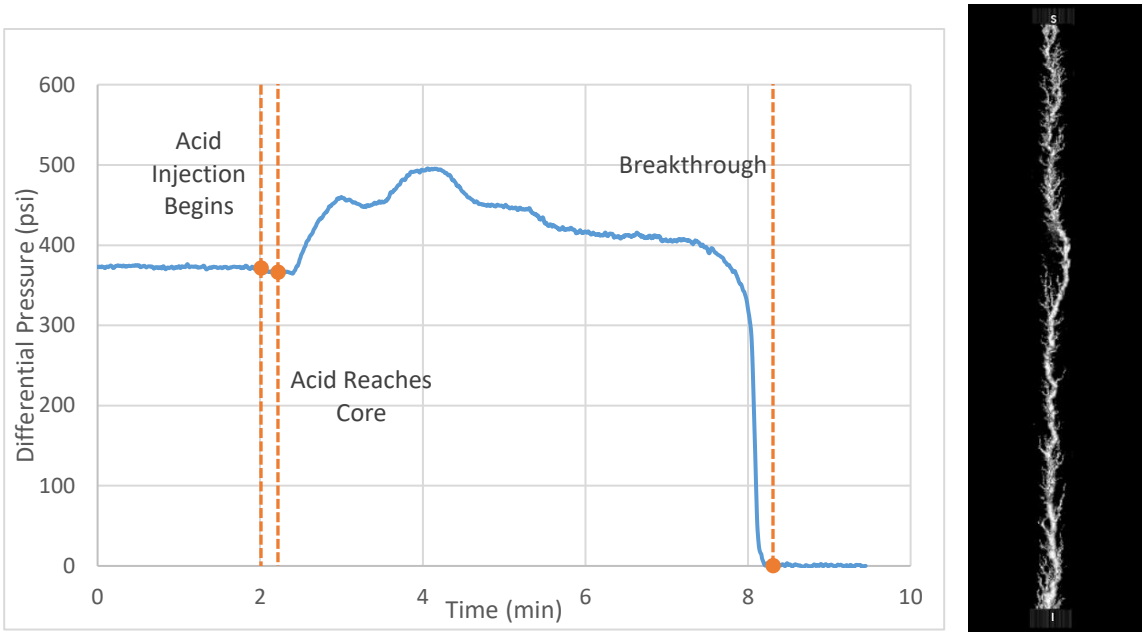

Figure 33 - Differential pressure during test and CT scan image for Core 6-300-4 (injection rate =16 mL/min)

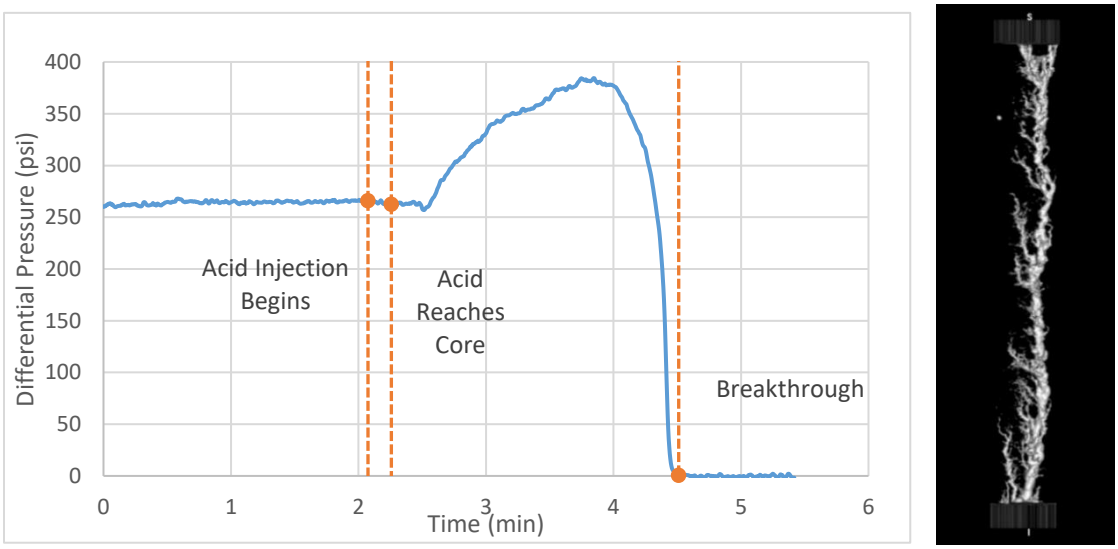

Figure 34 - Differential pressure during test and CT scan image for Core 6-300-6 (injection rate =19 mL/min). Note that this test was run with a 10-in core

There are few if any, test data for 300°F in published literature. This is the hardest set of tests in this study. The safety concern limits acid testing at high temperatures in general. At high temperatures, wormhole diameter generally increases. Confining sleeves can be damaged when the wormhole diameter grows too large. Core samples can collapse. This is the reason an HCl test

comparison could not be done. However, the HCR-6000 tests for the designed injection rates were successfully completed.

The Buijse and Glasbergen (2005) model was used to curve-fit the experimental data to identify the optimal conditions at different temperatures. The final result of all wormhole efficiency curves is presented in **Figure 35**. The symbols on the figure are lab-measured results, and the lines are curve-fitted results based on Buijse and Glasbergen (2005) correlation. The squares are for data points for HCR-6000 tests. The optimal conditions with HCR-6000 for all temperatures are listed in **Table 10**. It clearly shows that as temperature increases, both optimal interstitial velocity and optimal breakthrough pore volume increase. This indicates that if the reservoir temperature is high, acid stimulation faces more challenges to maintain efficiency.

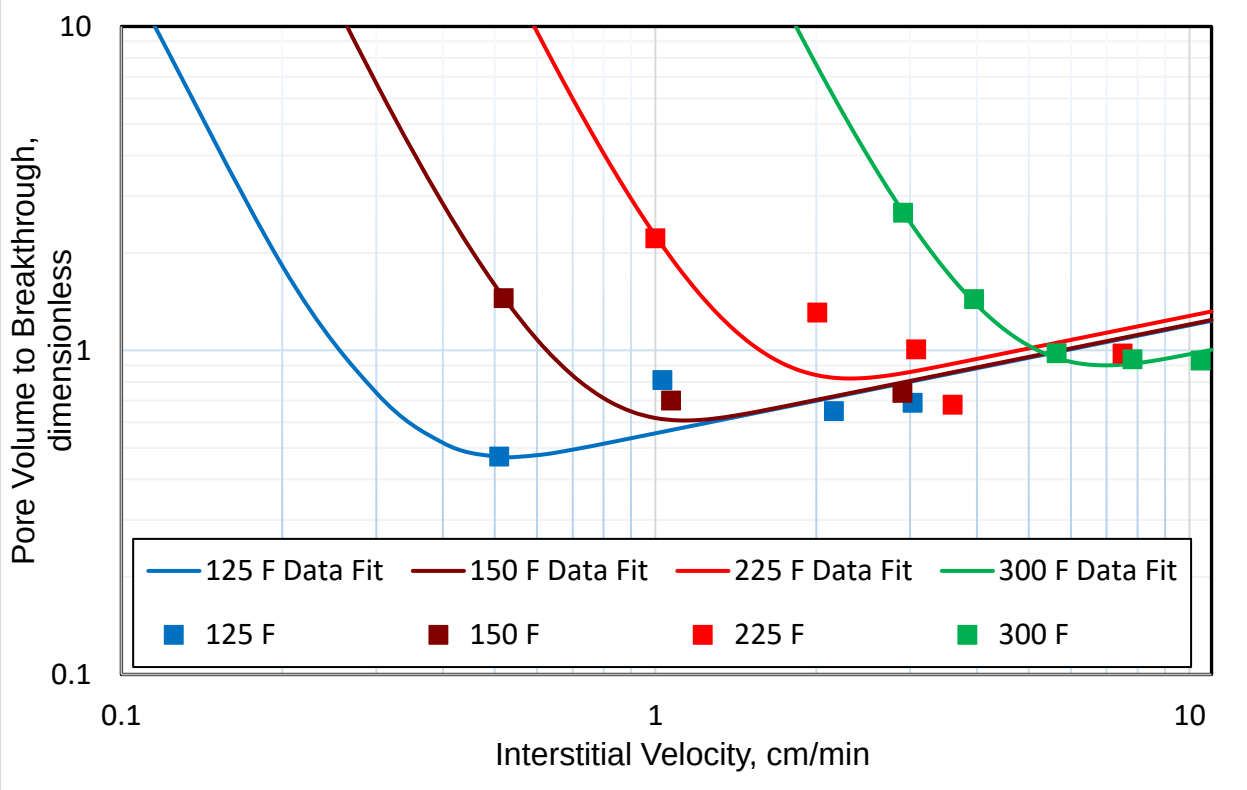

Figure 35 – Experimental results are plotted at 125°F, 150°F, 225°F, and 300°F while running HCR-6000. The results are curve-fitted using Buijse and Glasbergen (2005) model to generate wormhole efficiency curves. (Adapted from Gajipara et al., 2023)

Table 10 - Optimal Condition Identified by Buijse-Glasbergen Curve-fit (Reprinted from Gajipara et al., 2023)

Temperature (°F)	125	150	225	300
Optimal Pore Volume to Breakthrough	0.47	0.61	0.82	0.9
Optimal Interstitial Velocity (cm/min)	0.5	1.1	2.3	7

The following observations are concluded from this set of tests. 1) Higher PV_{BT} values are observed as the temperature reaches 300°F compared to HCR-6000 at lower temperatures. 2) It is noticed that the optimal interstitial velocity is higher compared with the tests at lower temperatures, and the wormhole efficiency curve shifted toward the right on the graph (Figure 35). 3) With the lowest injection rate (vi=2.9 cm/min, Figure 30), the wormhole diameter is slightly larger than the ones at optimal conditions. (4) Similar tests with HCl are not possible as HCl does not form viable wormholes at the temperature at the targeted injection rates.

4.2.5 Core Flood Tests with 15% HCl

To compare HCR-6000 performance with HCl, three core flood tests have been conducted utilizing 15wt% HCl at 125°F, 150°F, and 225°F. Indiana Limestone cores of 1.5-inch diameter and 10-inch length were used for these tests. These tests were run at the optimal interstitial velocity interpreted from the tests with HCR-6000 at each temperature (see Table 10). As HCl has a much higher reaction power, we did not conduct the test with HCl at 300°F for safety concerns. The core properties are listed in **Table 11**. The calculated pore volumes to breakthrough value (PV_{BT}) corresponding to the acid injection rate and the interstitial velocity are listed in **Table 12**. The results of the HCl tests are shown in **Figure 36**.

Table 11 - Core Properties for Tests Conducted with 15% HCl (Reprinted from Gajipara et al., 2023)

Core #	Temperature (°F)	Dry weight (g)	Saturated Weight (g)	Porosity (%)	Permeability (mD)
H-125-1	125	617	665	17	21
H-150-1	150	627	669	15	15
H-225-2	225	616	664	17	27

Table 12 - Experimental Results for Tests Conducted with 15% HCl (Reprinted from Gajipara et al., 2023)

Core #	Temperature (°F)	Acid injection rate (mL/min)	Interstitial Velocity (cm/min)	Pore volume to breakthrough
H-125-1	125	3	1.58	0.47
H-150-1	150	2	1.21	3.05
H-225-2	225	4.5	2.37	3.76

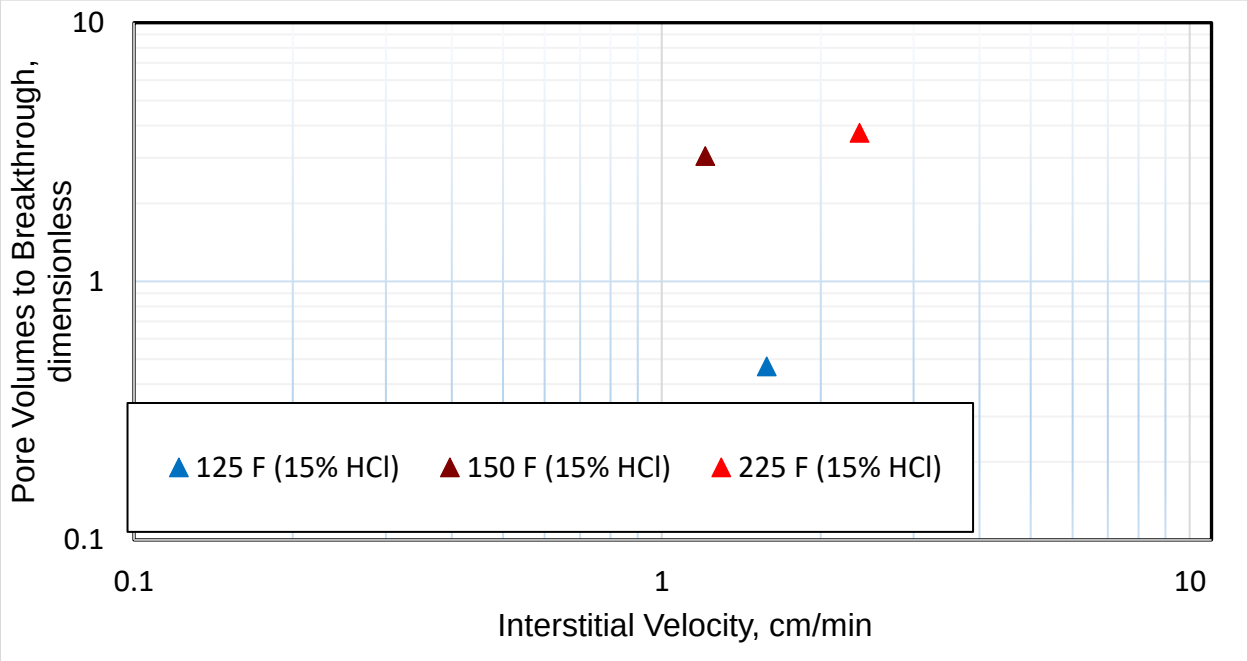

Figure 36 – Experimental results for 15% HCl tests (Adapted from Gajipara et al., 2023)

Figures 37-39 show the differential pressure history during the tests and the CT images for these tests. The experiment at 150 °F (test H-150-1, Figure 38) did not reach the breakthrough. Injection was stopped because of the unexpectedly long injection time (60 minutes). The CT scan

of the core showed sufficient wormhole development, and wormhole pore volume of breakthrough is calculated from the CT image.

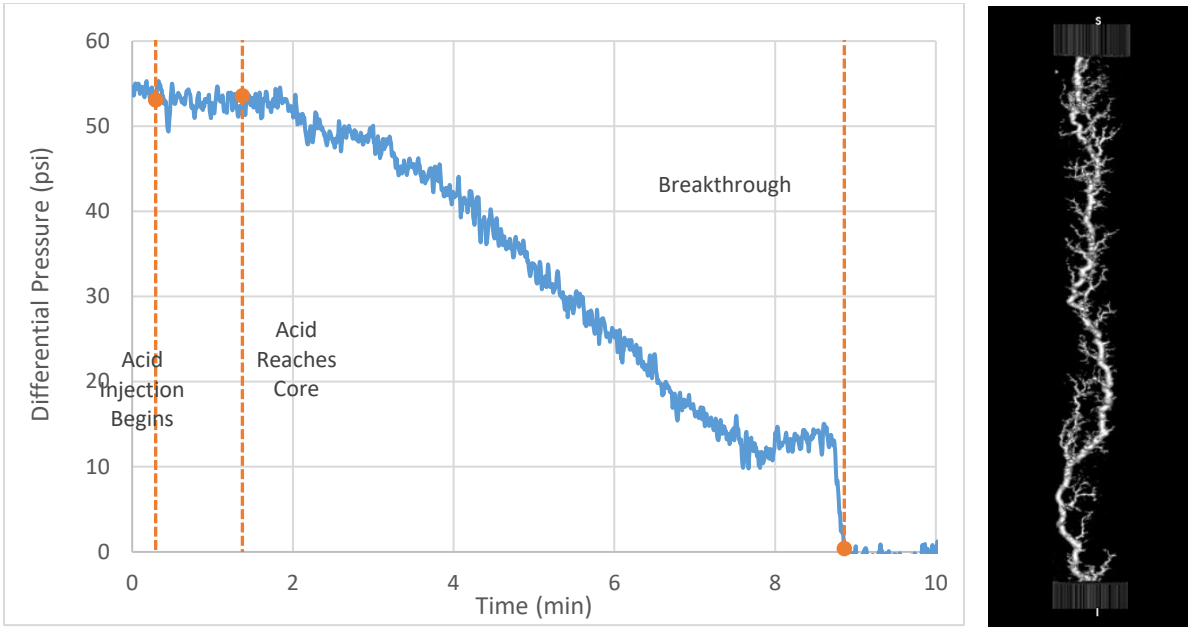

Figure 37 – Differential pressure during test and CT scan image for Core H-125-1 at the temperature of 125°F

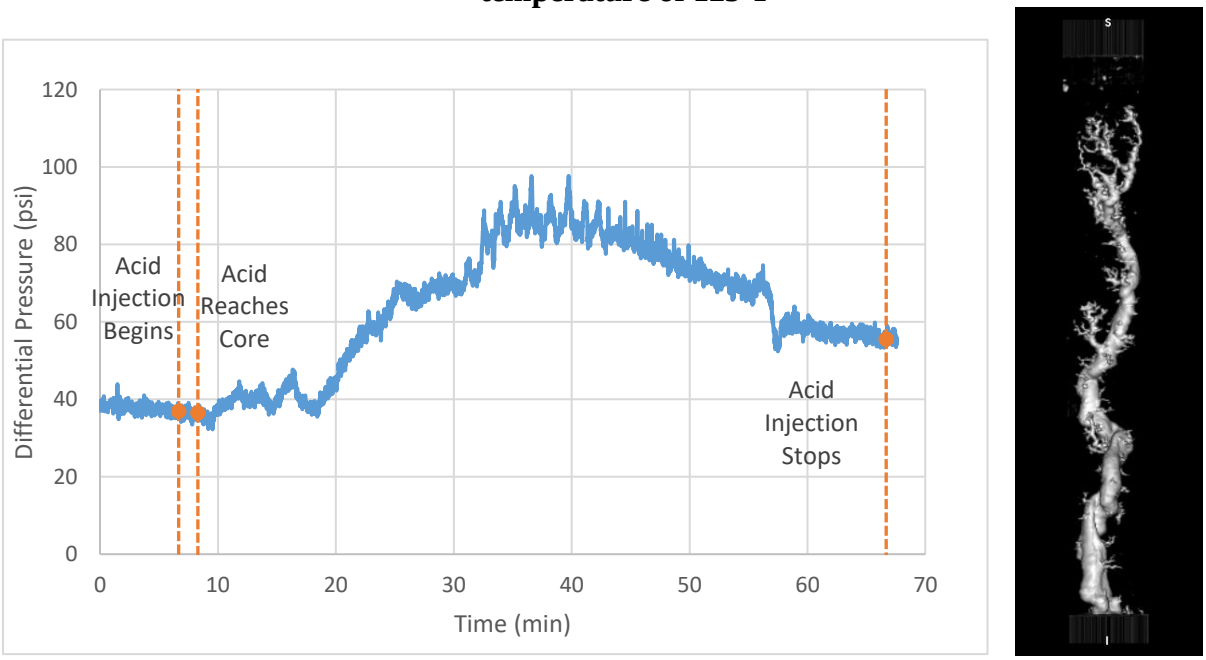

Figure 38 – Differential pressure during test and CT scan image for Core H-150-1 at the temperature of 150°F

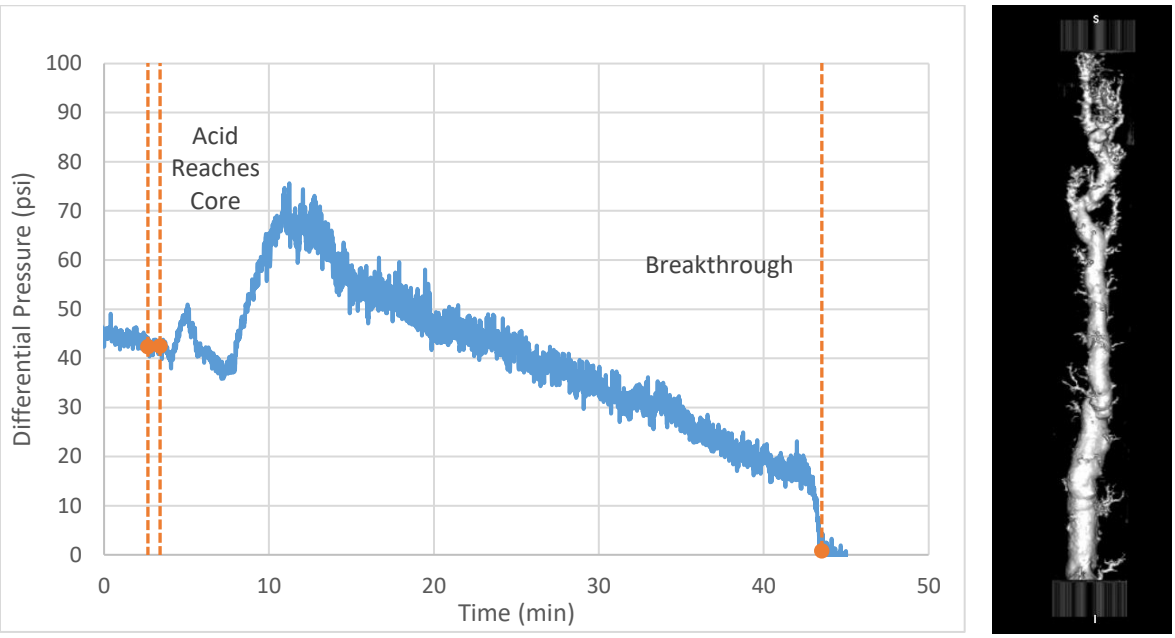

Figure 39 - Differential pressure during test and CT scan image for Core H-225-2 at the temperature of 225°F

It is observed from Figures 37-39 that as temperature increases, wormhole diameter quickly enlarged (Figures 38 and 39). The larger diameter of the wormhole means lower wormhole efficiency and should be minimized in acid treatments.

The comparison of the HCR-6000 and HCl test results are shown in **Figure 40**. The HCl tests are represented with the triangle symbols, and the arrows show the optimal interstitial velocity for HCR-6000 at each temperature (Table 10). Of the three tests, PV_{BT} for 15% HCl is comparable at higher interstitial velocity to the one for HCR-6000 at 125°F, indicating that at this condition, HCR-6000 has a similar efficiency to 15% HCl. It is noticed that at lower interstitial velocity, HCR-6000 maintains high efficiency with decreasing PV_{BT}, which leads to the conclusion that this acid system (HCR-6000) is advantageous when the injection rate is limited by operating conditions. For higher temperatures (150°F and 225°F), at the tested conditions, HCR-6000 expresses much higher efficiency (significantly lower pore volume to breakthrough) compared

with 15% HCl. As mentioned before, the HCl test at 300°F was not completed because of the concern about safety and damage to the confining sleeves.

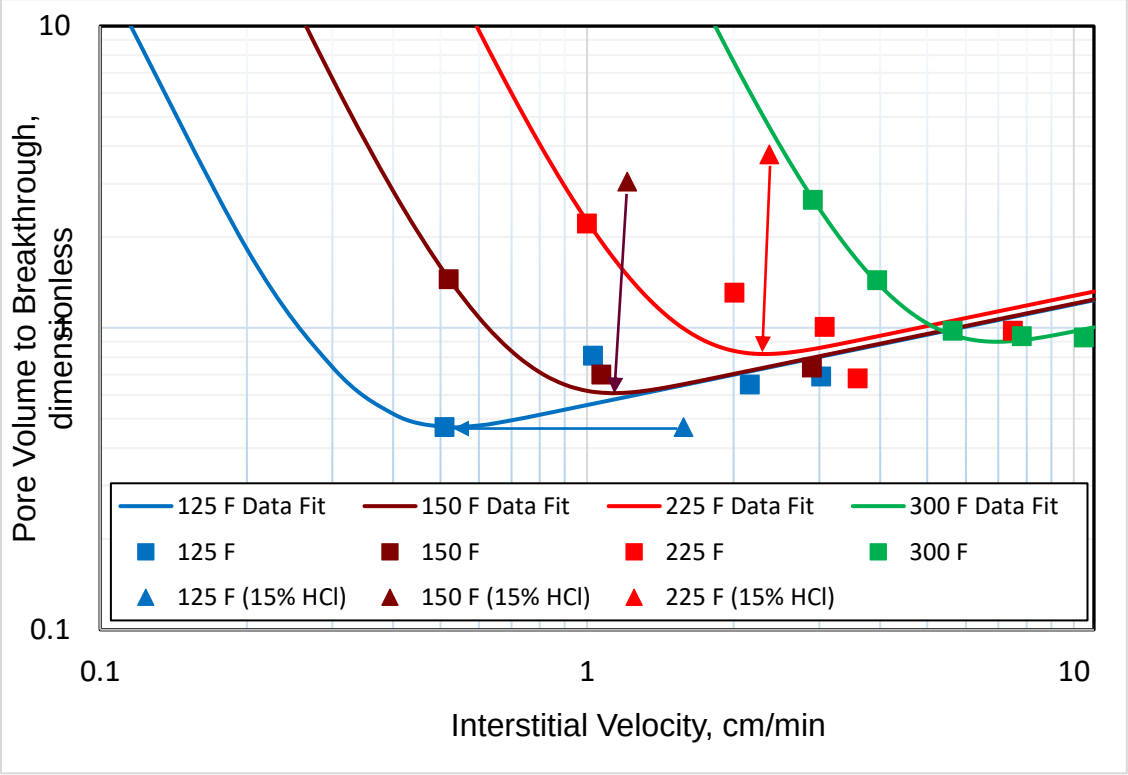

Figure 40 – Comparison of HCR-6000 and 15% HCl tests. The arrows show the optimal interstitial velocity derived from HCR-6000 tests at that temperature. (Adapted from Gajipara et al., 2023)

4.2.6 Temperature Effect on Wormhole Behavior

The optimal conditions with HCR-6000 for all the temperatures tested are listed in Table 10. This table is generated based on the data presented in Figure 35. From Figure 35 and Table 10, it is clearly observed that as temperature increases, both the optimal interstitial velocity and optimal pore volumes to breakthrough increase. This results in the wormhole efficiency plot shifting towards the right in Figure 35 as temperature increases from 125°F to 300°F. A higher injection rate is required to keep the injection at the optimal condition, and more acid volume is

required to treat the same drainage volume at elevated temperatures. This is an indication of decreased stimulation efficiency.

Table 10 shows that the optimal interstitial velocity increases 14 times from 0.5 cm/min to 7 cm/min when temperature increases from 125°F to 300°F. Keeping injection at the optimal condition requires a much higher injection rate, and therefore much higher surface injection pressure. The pressure increase is caused by two reasons, the downhole injection pressure is linearly proportional to the injection rate, and the wellbore frictional pressure drop is related to the injection rate to the second power. Achieving the optimal injection condition is more challenging at higher temperatures, and sometimes can be limited by the injection equipment. On the other hand, the optimal pore volume to breakthrough is only doubled when the temperature increases from 125°F to 300°F, from 0.47 to 0.9 (Table 10). Twice the volume of acid is required to propagate wormholes into the formation for the same coverage (wormhole length).

Consistent with the observations from this study, it has been reported historically by other researchers that temperature has a negative effect on wormhole efficiency. With increasing temperatures, the optimal interstitial velocity and optimal pore volume to breakthrough increase. **Figure 41** (Bazin 2001) shows a study of 7% HCl with Lavoux limestone, and **Figure 42** (Fredd and Fogler 1999) shows an experimental study of Indiana limestone with HCl. Even though the temperature only reached 176°F in both studies, the increasing trend of optimal conditions is clear from Figures 41 and 42. The optimal interstitial flux has been shown to depend on a Damkohler number, the ratio of reaction rate to convection rate (Fredd and Fogler 1999). So, as the reaction rate increases with temperature, the corresponding optimal flux increases. The mass transfer rate of acid to the wormhole walls also increases with temperature, leading to more dissolution at the wormhole walls, thus increasing wormhole diameter and pore volumes to breakthrough.

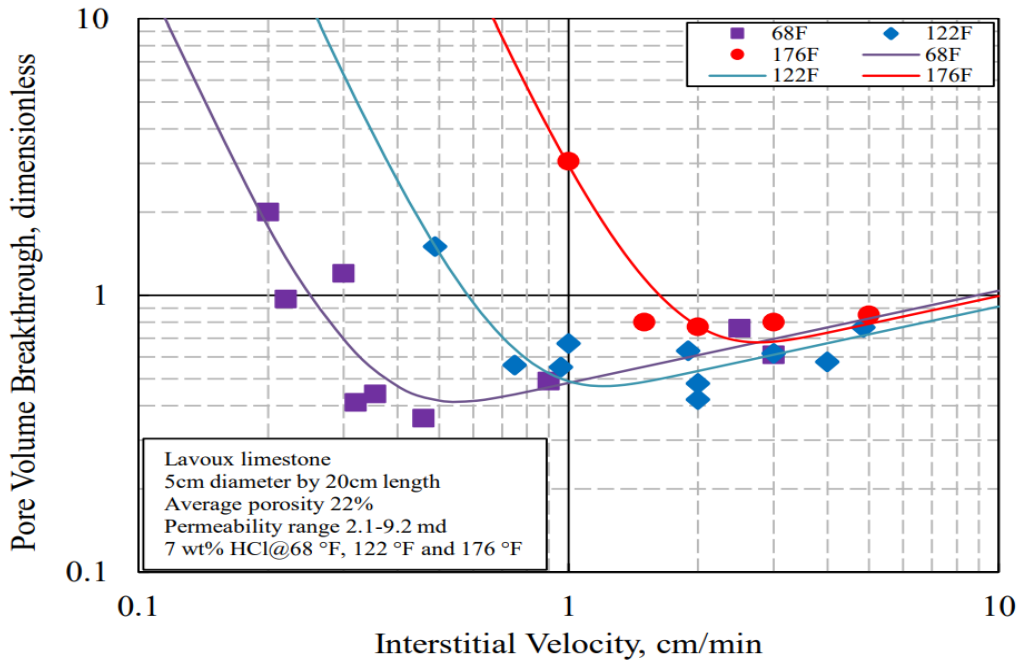

Figure 41 - Wormhole efficiency relationships reported by Bazin (2001)

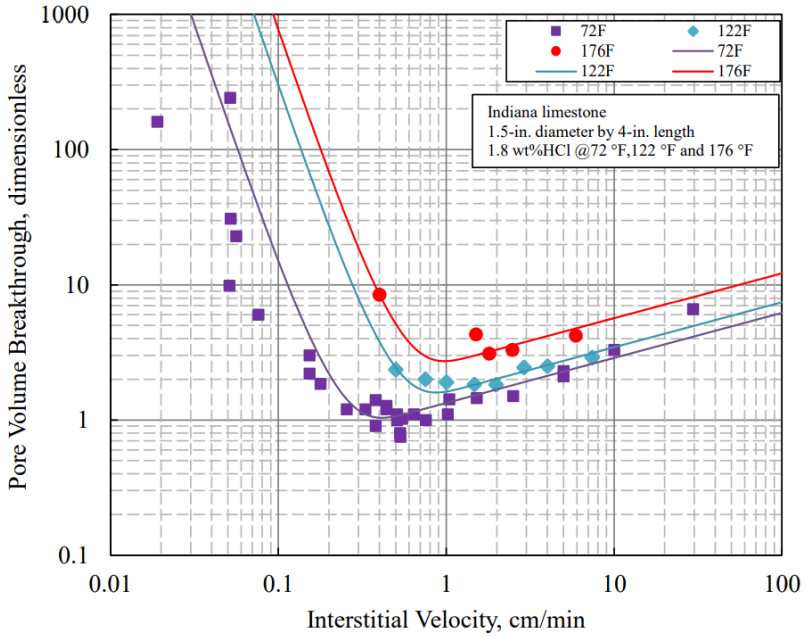

Figure 42 - Wormhole efficiency relationships reported by Fredd and Fogler (1999)

On a typical wormhole efficiency curve, the slope of the curve on the left side of the optimal point (interstitial velocity is below the optimal) is much steeper than the slope of the curve on the right side of the optimal point (interstitial velocity is higher than the optimal). It is well-understood

that if the injection condition cannot be kept at the optimal condition, then injecting at higher rate yields better efficiency than injecting at a lower rate. Using the 176°F test in Figure 41 as an example, when the interstitial velocity decreases from 2 cm/min (the optimal) to 1 cm/min, pore volume to breakthrough increases from 0.8 to 3. However, the pore volume to breakthrough is almost the same when the interstitial velocity increases from 2 cm/min to 3 cm/min. This leads to one of the advantages of HCR-6000. **Figure 43** plots $PV_{BT,opt}$ and $v_{i,opt}$ as functions of temperature. The curve for $PV_{BT,opt}$ is flat, and it is less sensitive to temperature. At low interstitial velocity or elevated temperature, the wormholes created by HCR-6000 all have this structure with a controlled diameter. This can be observed by comparing wormhole images for HCR-6000 to that for the HCl tests. At 225°F, the wormhole diameter is significantly enlarged when 15% HCl is used, resulting in very low efficiency of wormholing.

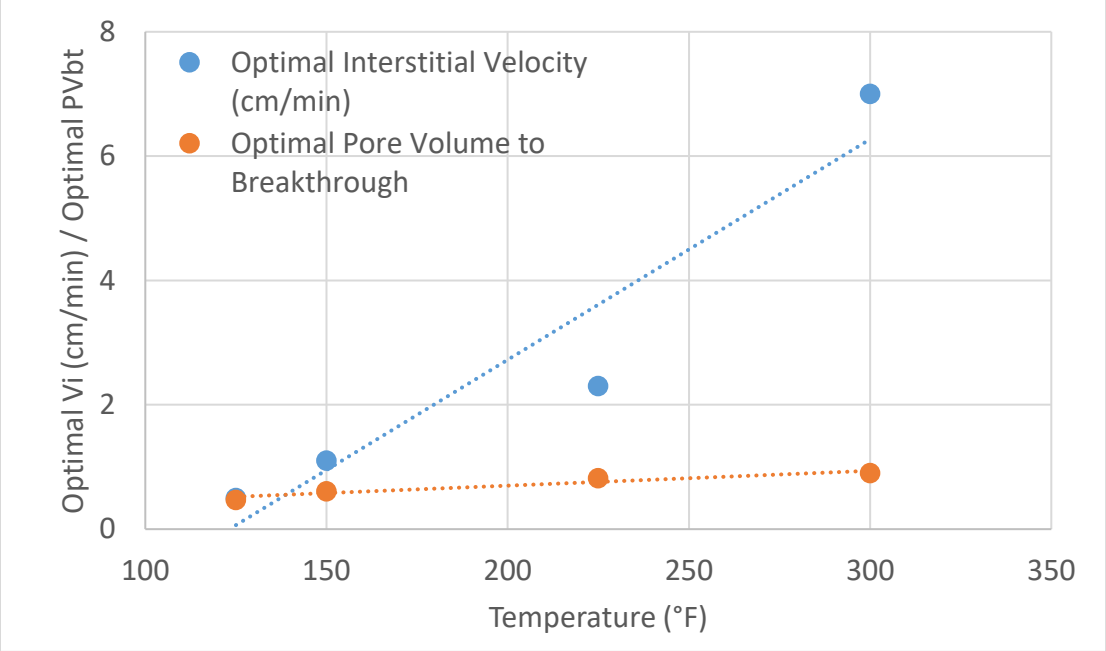

Figure 43 - Experimental observation of optimal condition as a function of temperature for HCR-6000 (Adapted from Gajipara et al., 2023)

4.3 Core Flood Experiments with HCR-6000-MTX

Four core flood tests have been conducted using HCR-6000-MTX alternative acid (Purdy et al., 2019) at 180°F temperature. Indiana Limestone cores of 1.5-inch diameter and 8 inches in length were used for the tests. The core properties, such as permeability and porosity, are listed in **Table 13**. The pore volume to breakthrough is calculated for each test (PV_{BT}). **Table 14** summarizes the experimental conditions in terms of injection rate and interstitial velocity, and calculated PV_{BT} for each test.

Table 13 - Core Properties for Tests Conducted with HCR-6000-MTX

Core #	Dry weight (g)	Saturated Weight (g)	Porosity (%)	Permeability (mD)
6-180-1	503	541	16	13
6-180-2	504	545	18	12
6-180-3	498	531	14	14
6-180-4	504	542	16	12

Table 14 - Experimental Results for Tests Conducted with HCR-6000-MTX

Core #	Acid injection rate (mL/min)	Interstitial Velocity (cm/min)	Pore volume to breakthrough
6-180-1	2	1.08	0.39
6-180-2	1	0.5	0.48
6-180-3	6	3.71	0.55
6-180-4	4	2.15	0.43

The experimental results are presented in **Figure 44**. Buijse and Glasbergen (2005) model was used to generate the wormhole efficiency relationship by fitting the experimental data. The results from Sohn (2018) study done using HCR-6000 alternative acid and 15% HCl are also plotted in Figure 44 for comparison. The optimal conditions for HCR-6000-MTX, as well as HCR-6000 and 15% HCl (Sohn, 2018), are listed in **Table 15**. It was noticed that the optimal PV_{BT} for HCR-6000-MTX is lower than that of HCR-6000 and 15% HCl. However, the optimal interstitial velocity with HCR-6000-MTX is higher than HCR-6000 but lower than 15% HCl. It also

important to note that HCR-6000-MTX shows better efficiency at higher injection rates compared to HCR-6000.

Table 15 - Optimal Condition Obtained from Experimental Results

	HCR-6000-MTX	HCR-6000	15% HCl
Optimal Pore Volume to Breakthrough	0.34	0.42	0.45
Optimal Interstitial Velocity (cm/min)	0.8	0.5	2

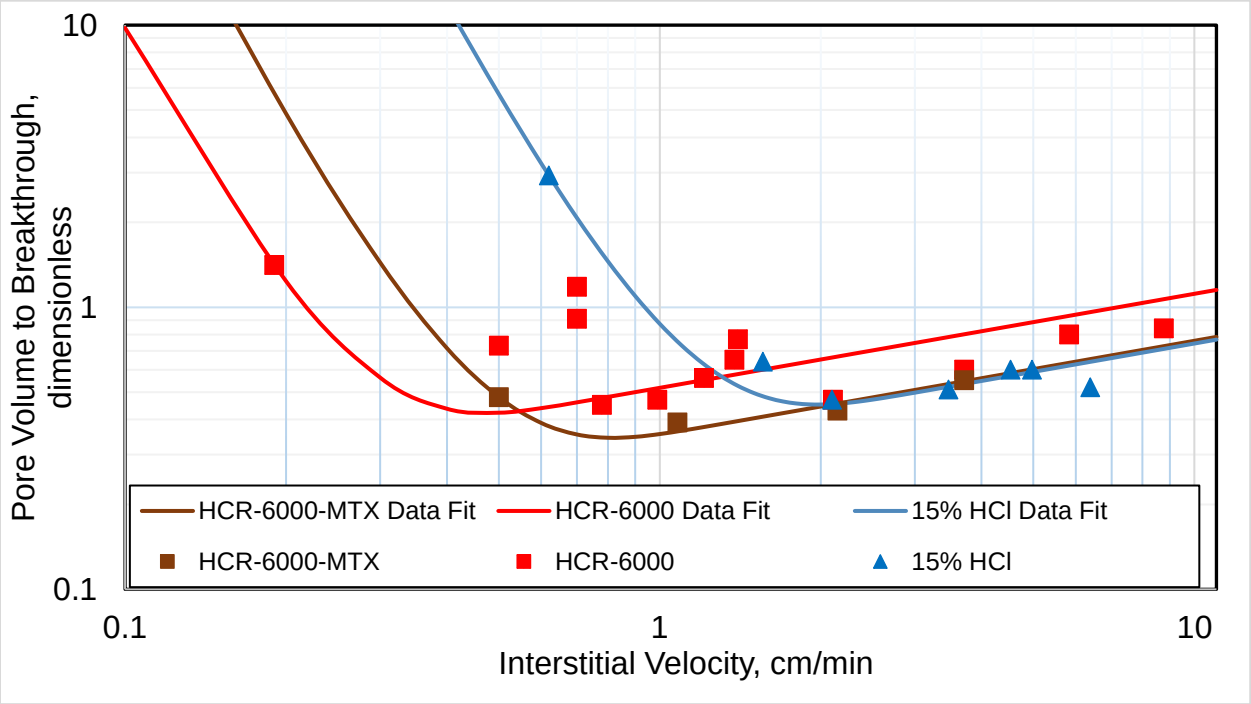

Figure 44 – Wormhole Efficiency Plot for each test with HCR-6000-MTX, HCR-6000 (Sohn, 2018), and 15% HCl (Sohn, 2018)

The differential pressure history during the test along and the CT scan image of the wormhole are shown in **Figures 45-48**.

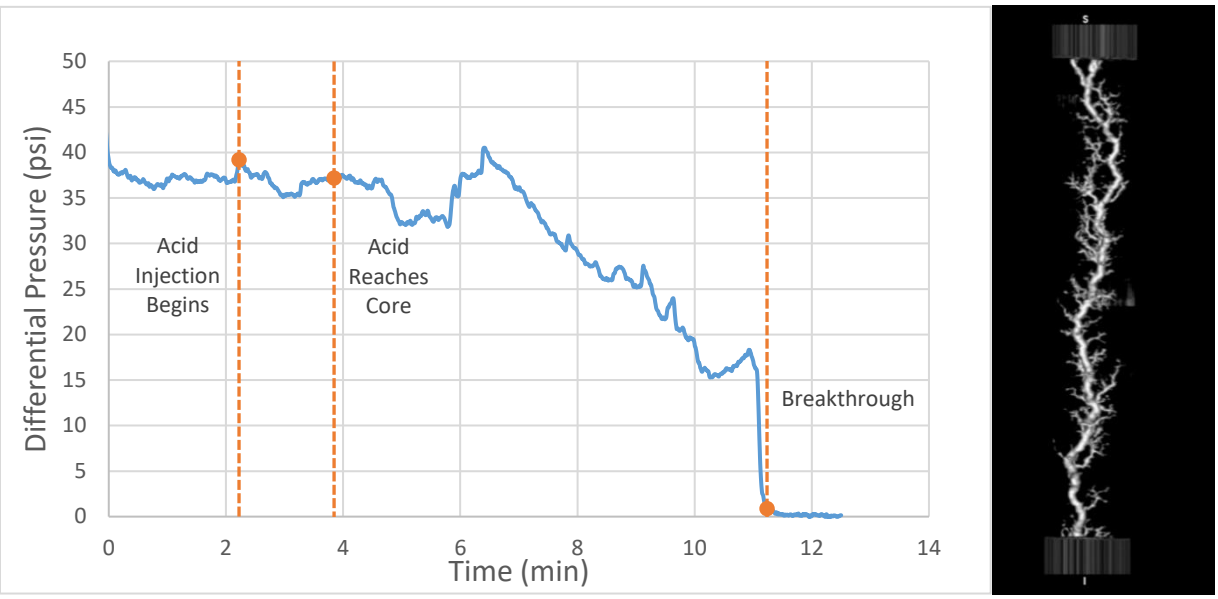

Figure 45 - Differential pressure during test and CT scan image for Core 6-180-1 (injection rate = 2 mL/min)

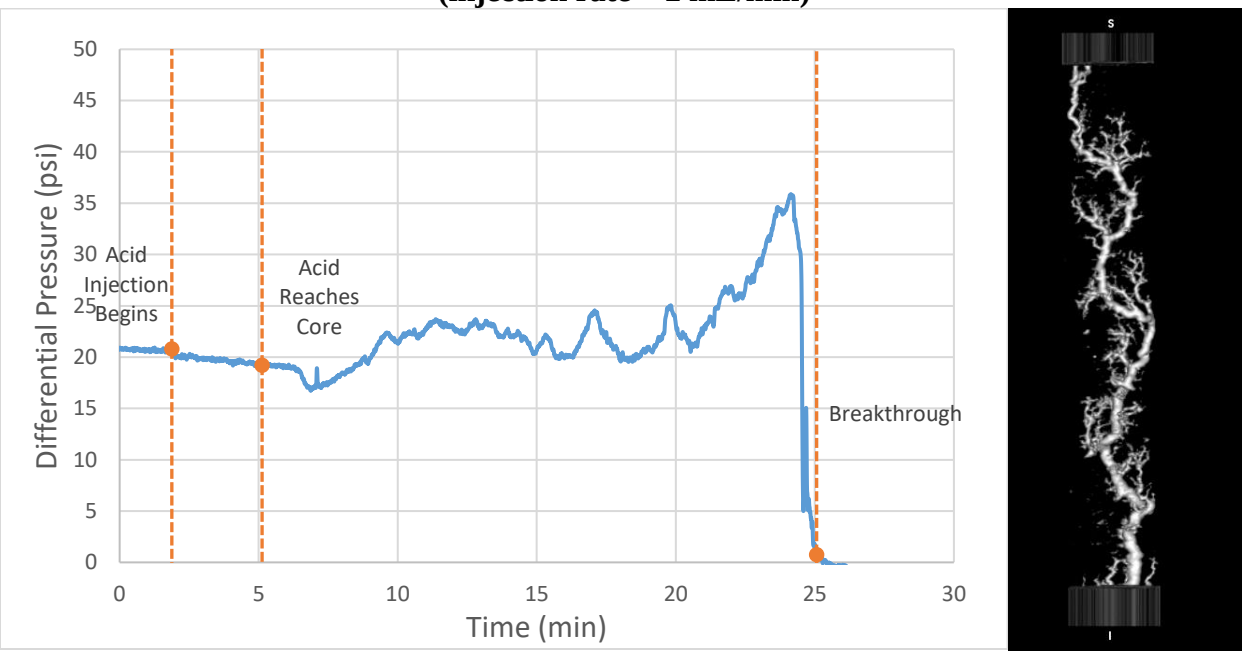

Figure 46 - Differential pressure during test and CT scan image for Core 6-180-2 (injection rate = 1 mL/min)

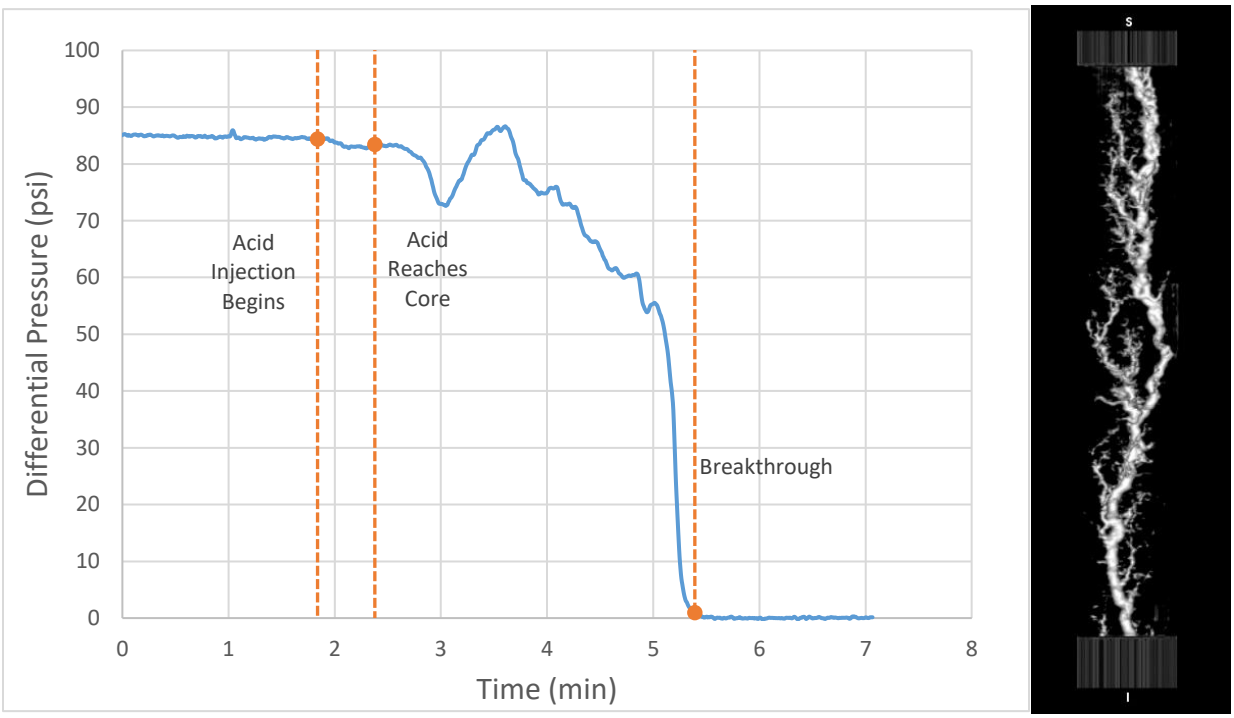

Figure 47 - Differential pressure during test and CT scan image for Core 6-180-3 (injection rate = 6 mL/min)

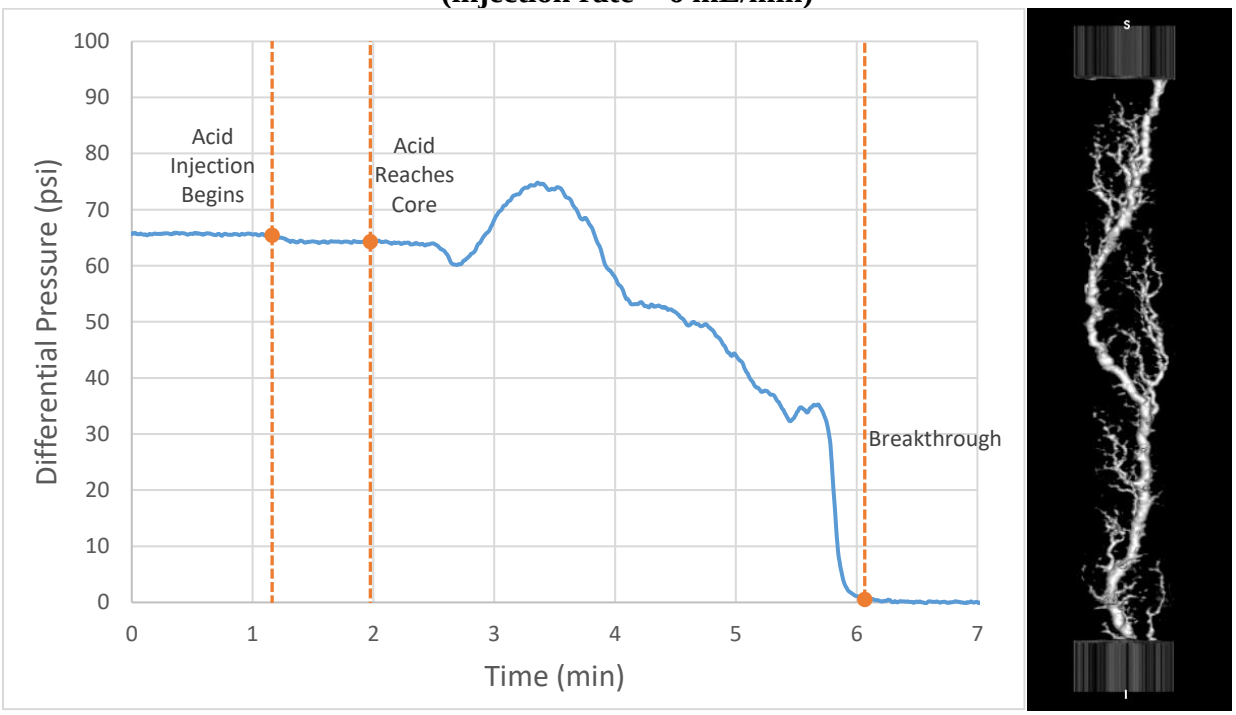

Figure 48 - Differential pressure during test and CT scan image for Core 6-180-4 (injection rate = 4 mL/min)

A comparison of resulting wormhole structures at similar interstitial velocity with all three acids is shown in **Figure 49** at higher interstitial velocity and in **Figure 50** at lower interstitial velocity.

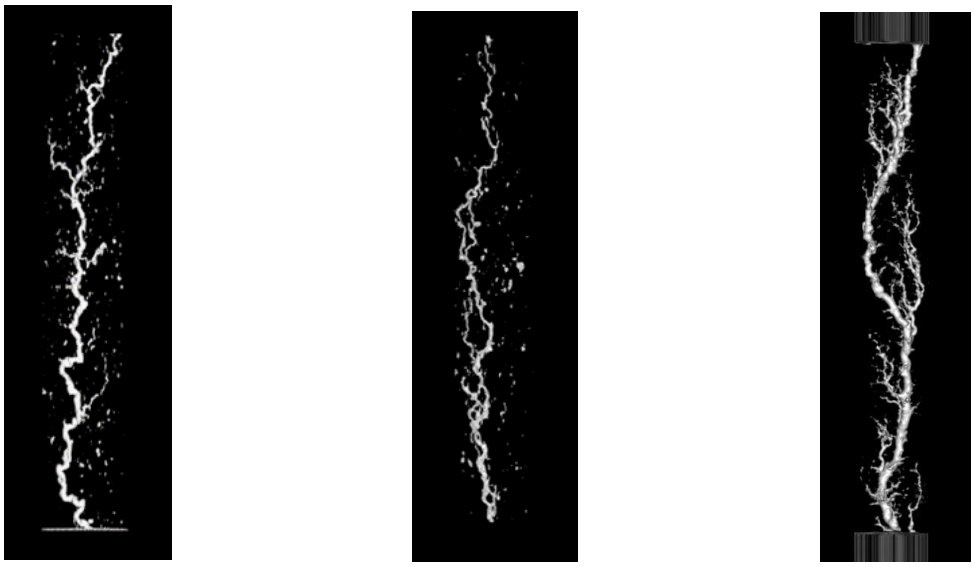

1. 15% HCl — Vi = 2.1 cm/min

2. HCR-6000 — Vi = 2.11 cm/min

3. HCR-6000-MTX — Vi = 2.15 cm/min

Figure 49 – Wormhole structures created using 15% HCl, HCR-6000 (Sohn, 2018), and HCR-6000-MTX acids at a higher interstitial velocity

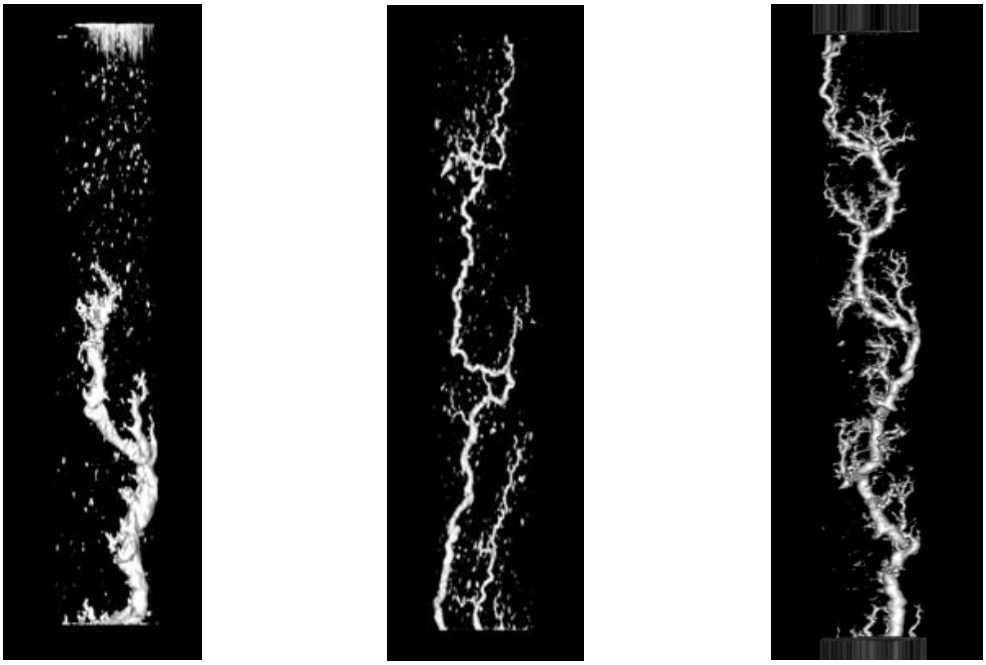

1. 15% HCl Vi = 0.62 cm/min

2. HCR-6000 Vi = 0.5 cm/min

3. HCR-6000-MTX Vi = 0.5 cm/min

Figure 50 – Wormhole structures created using 15% HCl, HCR-6000 (Sohn, 2018), and HCR-6000-MTX acids at a lower interstitial velocity

At around 2.1 cm/min interstitial velocity, the wormhole generated with HCR-6000 shows a skinnier diameter as compared to the other two acids (Figure 49). The wormhole diameters generated with 15% HCl and HCR-6000-MTX are similar in size. Note that these results are at the optimal interstitial velocity of 15% HCl. But at around 0.5 cm/min interstitial velocity, the generated wormhole diameter with 15% HCl is significantly larger than two HCR acids (Figure 50). So at lower injection rates, the stimulation treatment using 15% HCl requires more amount of acid (higher PV_{BT}) resulting in very low efficiency.

4.4 Dolomite Core Flood Experiments with HCR-9000

An experimental study has been carried out to systematically evaluate HCR-9000 alternative acid (Purdy et al., 2019) for high-temperature dolomite formation. Two versions of

HCR-9000, Ver-1 and Ver-2, were used in this study. The temperature was set in the experiments as 230°F. All experiments were run using Silurian Dolomite cores of 1.5 in diameter and 8 in length.

One test was conducted using 90% HCR-9000-Ver-1 acid, which is equivalent to 15% HCl. The core properties, such as permeability and porosity, are listed in **Table 16**. The experimental conditions in terms of injection rate and interstitial velocity, and calculated PV_{BT} for each test are summarized in **Table 17**. The experimental result from this test is plotted in **Figure 51** with a red marker.

Table 16 - Core Properties for Test Conducted with HCR-9000-Ver-1

Core #	Acid	Dry weight (g)	Saturated Weight (g)	Porosity (%)	Permeability (mD)
D3	HCR-9000-Ver-1	525	557	14	432

Table 17 - Experimental Result for Test Conducted with HCR-9000-Ver-1

Core #	Acid	Acid injection rate (mL/min)	Interstitial Velocity (cm/min)	Pore volume to breakthrough
D3	HCR-9000-Ver-1	8	5.08	2.35

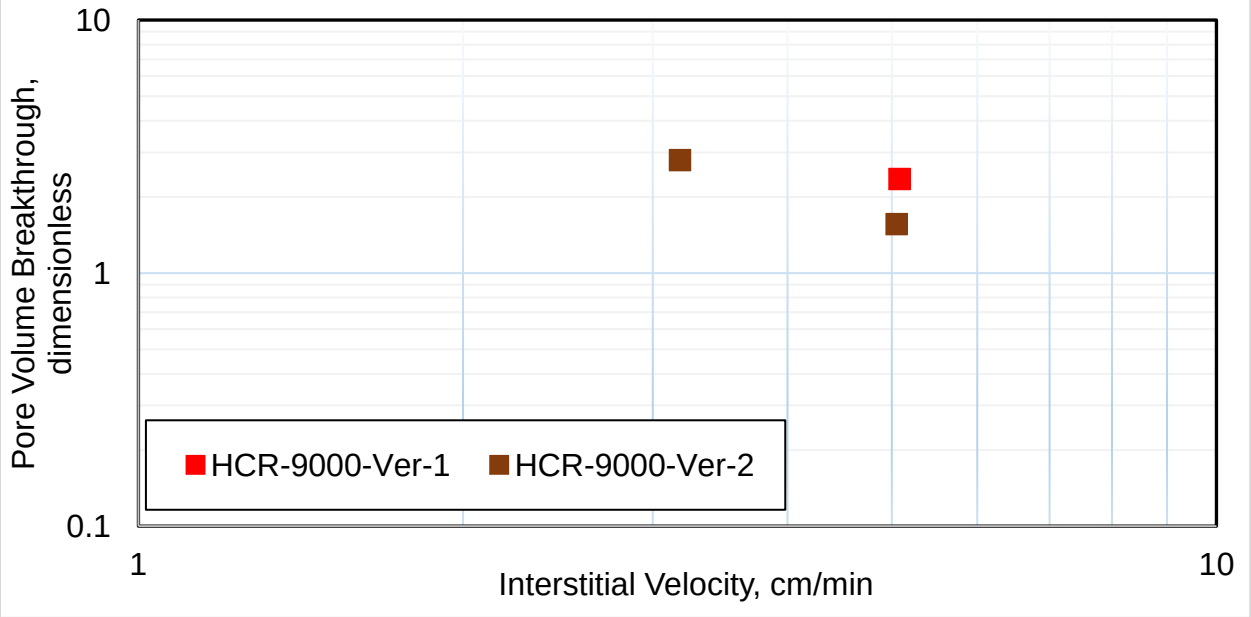

Figure 51 – Experimental result for each test conducted with HCR-9000 alternative acid

The pressure history during the test and the CT scan image of the wormhole are shown in **Figure 52**. This experiment did not reach a breakthrough. The acid injection was stopped due to the increasing differential pressure for safety concerns. The pore volume to breakthrough was calculated using the wormhole length from the CT scan image. It is noticed from Figure 52 that Ver-1 of HCR-9000 did not lead to efficient wormholing, and a wormhole with a large diameter was generated requiring high acid volume. Only one test was conducted with this version of acid because the test conducted with HCR-9000-Ver-2 at similar conditions showed better result with lower PV_{BT} (Figure 51).

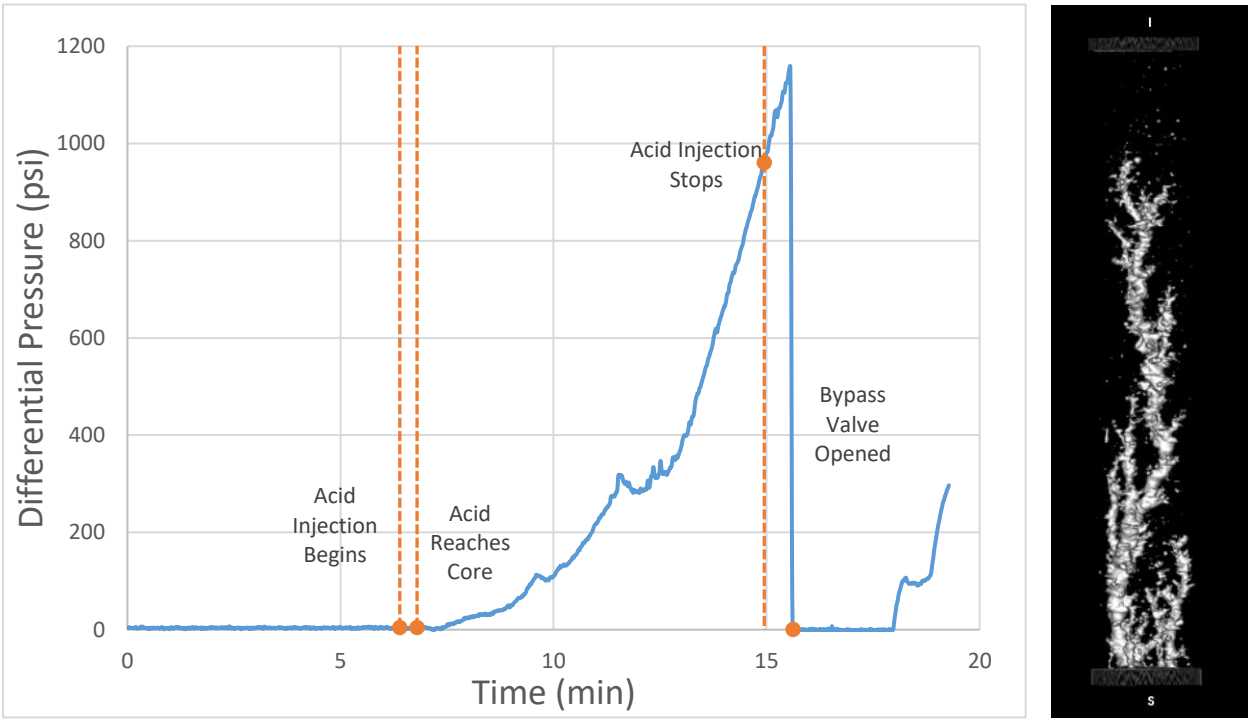

Figure 52 - Differential pressure during test and CT scan image for Core D3 (injection rate = 8 mL/min)

Two core flood tests were conducted using 90% HCR-9000-Ver-2 acid, which is equivalent to 15% HCl. The core properties, such as permeability and porosity, are listed in **Table 18**. The

pore volume to breakthrough is calculated for each test (PV_{BT}). **Table 19** summarizes the experimental conditions in terms of injection rate and interstitial velocity, and calculated PV_{BT} for each test. The experimental results from these tests are plotted in Figure 51 with a brown marker.

Table 18 - Core Properties for Tests Conducted with HCR-9000-Ver-2

Core #	Acid	Dry weight (g)	Saturated Weight (g)	Porosity (%)	Permeability (mD)
D4	HCR-9000-Ver-2	530	562	14	364
D2	HCR-9000-Ver-2	530	569	17	220

Table 19 - Experimental Results for Tests Conducted with HCR-9000-Ver-2

Core #	Acid	Acid injection rate (mL/min)	Interstitial Velocity (cm/min)	Pore volume to breakthrough
D4	HCR-9000-Ver-2	5	3.18	2.79
D2	HCR-9000-Ver-2	9.7	5.05	1.56

The pressure history during these tests and the CT scan images of the wormholes are shown in **Figure 53** and **Figure 54**. Notice that the differential pressure for all HCR-9000 tests increases rapidly with acid injection. This can be due to a possibility of precipitation of effluent after acid's reaction with rock, or a possible increase in apparent viscosity after the reaction. This set of tests was trouble-less and a breakthrough was reached in each test. The wormhole generated at lower interstitial velocity (core D4) has a slightly larger diameter as compared to the test with higher interstitial velocity (core D2). Comparing the two tests for HCR-9000-Ver-2, at higher interstitial velocity, the pore volume to breakthrough is lower (1.56) than the one at the lower interstitial velocity (2.79). It shows better wormhole efficiency at higher interstitial velocity (Figure 54 and Table 19). Logically another test with a higher interstitial velocity than 5.05 cm/min should be conducted. The possible differential pressure was estimated to reach 700 psi at higher rates of 15 mL/min. This causes the injection pressure and confining pressure to exceed the system's pressure

limit. A test at an injection rate below 15 mL/min is not beneficial to run, because it will not result in a comparable difference in interstitial velocity. The temperature of heating tape was estimated to be kept at higher than 450°F to maintain the desired fluid temperature at such higher rates, which causes safety concerns. Thus, a test at a higher rate was not conducted.

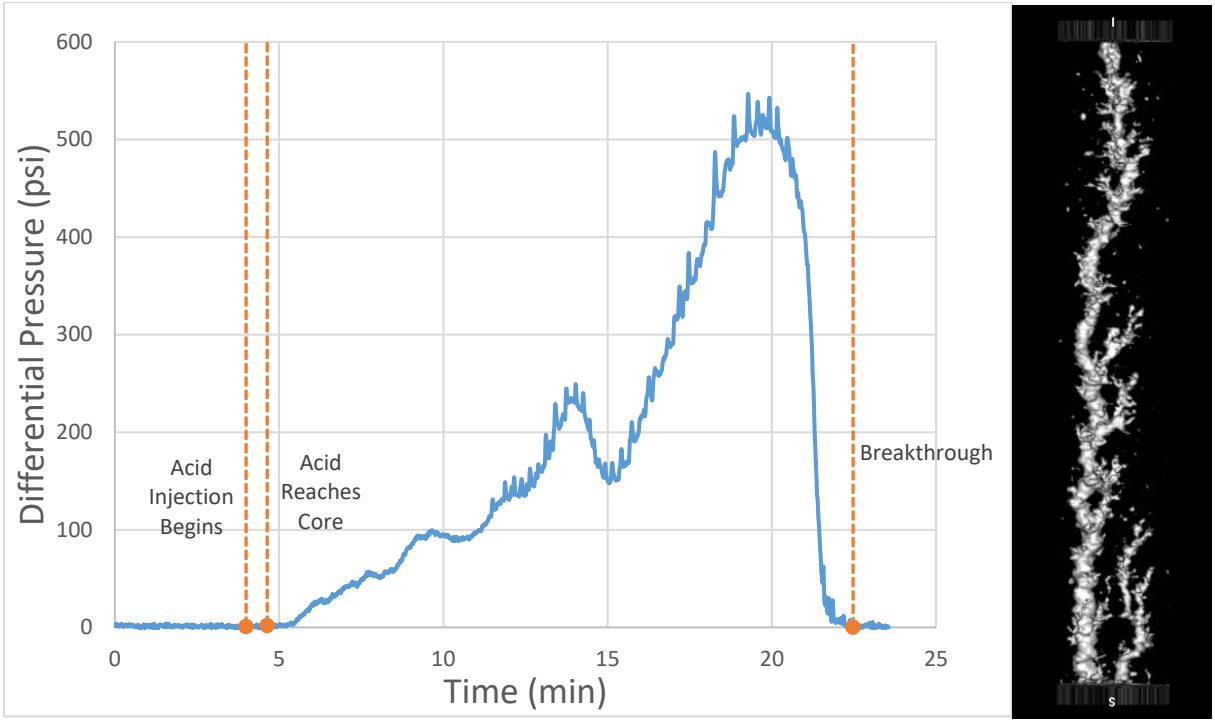

Figure 53 - Differential pressure during test and CT scan image for D4 (injection rate = 5 mL/min)

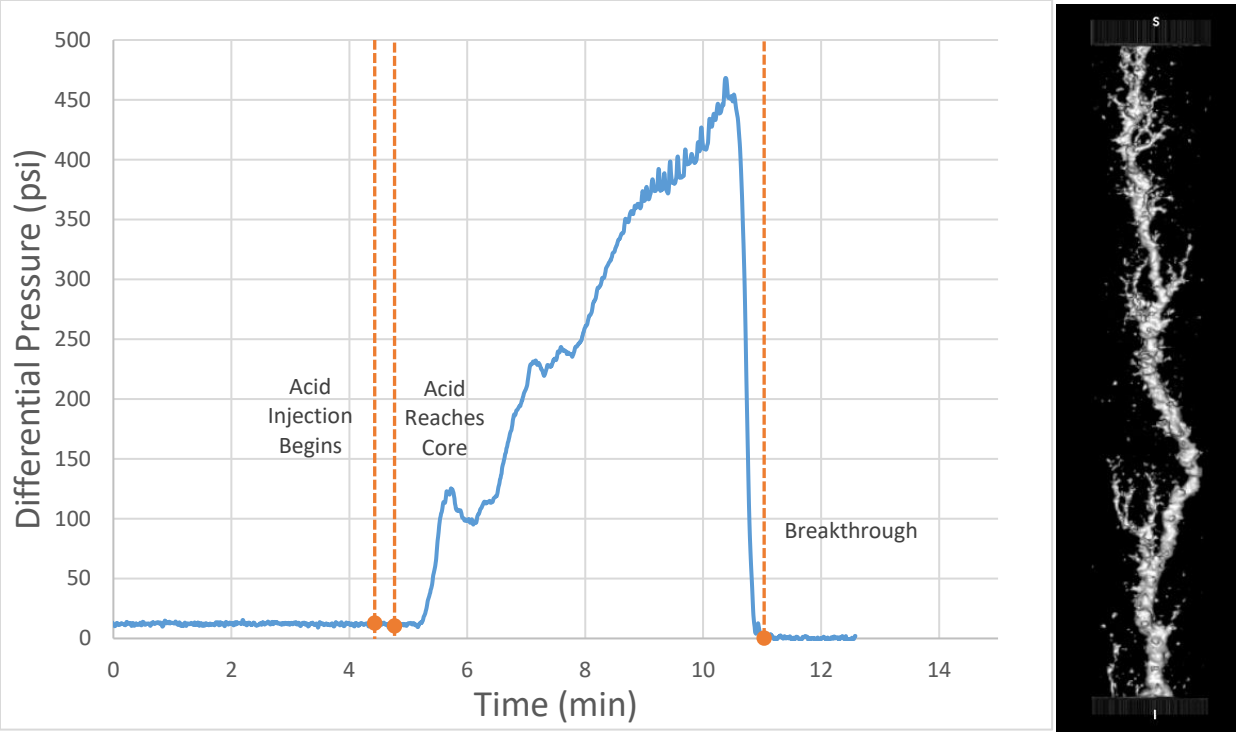

Figure 54 - Differential pressure during test and CT scan image for D2 (injection rate = 9.7 mL/min)

Dong (2015) studied the effect of temperature in dolomite acidizing using 15% HCl. **Figure 55** shows core-flooding experimental from that study. It showed that HCl efficiency for dolomite depends on the temperature, with optimal temperature being around 185°F. **Figure 56** shows show the wormhole comparison of 15% HCl (Dong, 2015) and HCR-9000- Ver-2 acid with Silurian Dolomite cores. The wormhole diameters from both the tests are nearly same. Note that these tests are not at exactly the same conditions. However, the wormhole structure with HCR-9000 does not show any significant improvement over 15% HCl.

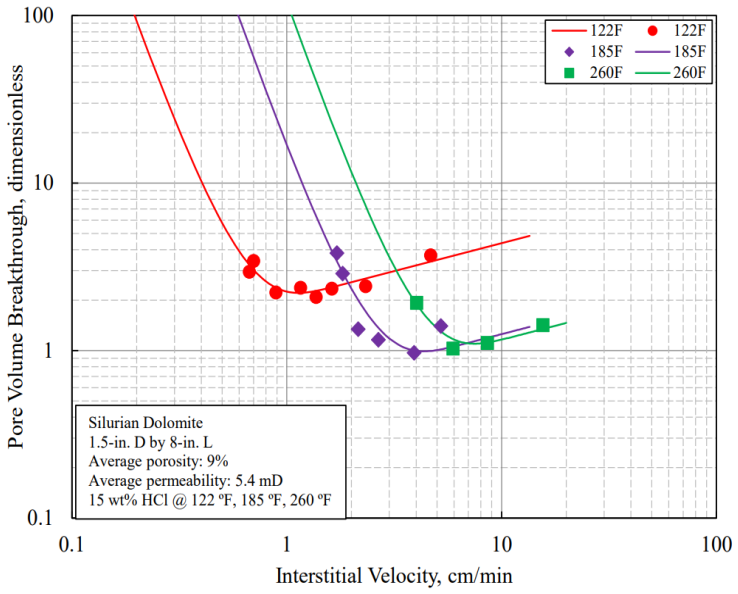

Figure 55 - Effect of temperature on wormhole behavior of dolomite cores with 15% HCl (Dong, 2015)

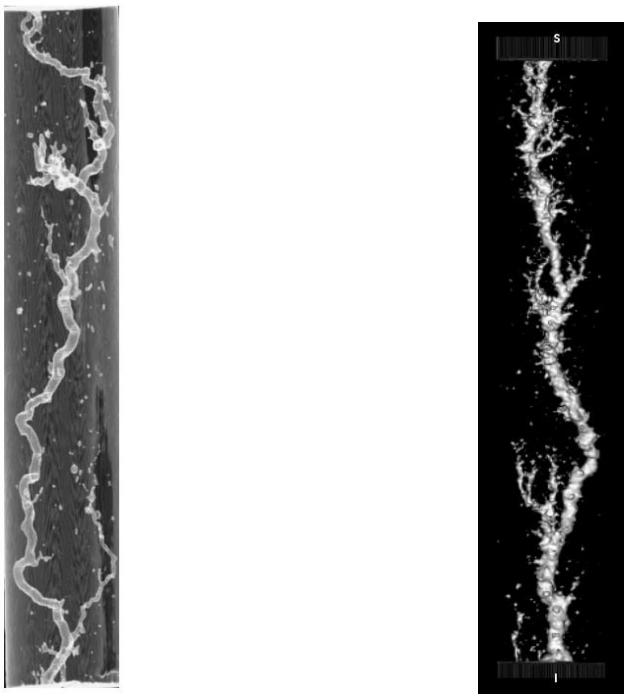

15% HCl	HCR-9000-Ver-2
vi = 5.94 cm/min	vi = 5.05 cm/min
T = 260°F	T = 260°F

Figure 56 – Wormhole structures created using 15% HCl (Dong, 2015) and HCR-9000 acids with Silurian Dolomite cores

5. CONCLUSIONS AND RECOMMENDATIONS

This research studied the performance of three alternative acid systems, as well as 15% HCl under different conditions. Coreflood acidizing experiments were conducted to understand the wormhole behavior of each acid system at a particular temperature. The experimental results were plotted on a log-log plot of interstitial velocity (v_i) and pore volume to breakthrough (PV_{BT}). These experimental results were curve fitted using the Buijse-Glasbergen model to analyze the wormhole efficiency behavior and optimal conditions. Structures of generated wormholes were analyzed from the CT scan images. The following conclusions can be made based on the experimental results:

1. At elevated temperatures, optimal interstitial velocity and pore volume to breakthrough increase, and the wormhole efficiency curves move towards the right on the efficiency plot, indicating lower efficiency as temperature increases. Elevated temperature poses a challenge to matrix acid stimulation.
2. HCR-6000 alternative acid performs better than 15% HCl at the same condition. At all conditions tested, the wormhole structure created by the alternative acid has a controlled diameter, and pore volume to breakthrough does not vary significantly. This advantage is more pronounced at higher temperatures.
3. Both HCR-6000 and HCR-6000-MTX alternative acid systems show better wormhole efficiency compared to 15% HCl, especially at lower interstitial velocities.
4. Ver-2 of HCR-9000 acid shows better wormhole efficiency compared to Ver-1 at similar experimental conditions. But the wormhole efficiency does not show any significant advantage over 15% HCl.

Future work can be performed to better understand the effect of temperature on wormhole efficiency for all alternative acid systems. Generating wormhole efficiency curves for HCl at all tested temperatures by conducting experiments can be insightful for better comparison of stimulation efficiency. Chemical analysis can also be done for alternative acid systems to understand the chemical dynamics and behavior at the molecular level. This would also help in upscaling the lab experimental results for field applications. Different types of alternative systems can be compared with the acids analyzed in this study with regard to wormhole performance and stimulation efficiency. Finally, different rock types like chalk, dolomite, and sandstone could also be tested with these alternative acid systems for a wide range of applications.

REFERENCES

Bazin, B. (2001). From Matrix Acidizing to Acid Fracturing: A Laboratory Evaluation of Acid/Rock Interactions. SPE Production & Facilities 16 (1): 22-29. doi: https://doi.org/10.2118/66566-PA

Bettencourt, G.S. (2022). Experimental Evaluation of Lactic Acid for Matrix Acidizing of Carbonates, Master of Science Thesis, Texas A&M University

Buijse, M. A., & Glasbergen, G. (2005). A semi-empirical model to calculate wormhole growth in carbonate acidizing. SPE Annual Technical Conference. https://doi.org/10.2118/96892-ms

Dong, K. (2015). Theoretical and Experimental Study on Optimal Condition in Carbonate Acidizing, Ph.D. Dissertation, Texas A&M University

Economides, M.J., Hill, A. D., Economides, C., & Zhu, D. (2013). Petroleum Production Systems (second ed.). Upper Saddle River, NJ: Prentice Hall

Fredd, C.N. and Fogler, H.S. (1999). Optimum Conditions for Wormhole Formation in Carbonate Porous Media: Influence of Transport and Reaction. SPE Journal 4 (3): 196-205. doi: 10.2118/56995-pa

Furui, K., Burton, R.C., Burkhead, D.W. et al. 2010. A Comprehensive Model of High-Rate Matrix Acid Stimulation for Long Horizontal Wells in Carbonate Reservoirs. Paper presented at the SPE Annual Technical Conference and Exhibition, Florence, Italy. SPE-134265-MS. DOI: 10.2118/134265-ms

Gajipara, R.P., Hill, A.D., Zhu, D. et al. (2023). Systematic Evaluation of Alternative Acid System for High-Temperature Carbonate Formation. Paper presented at the SPE Western Regional Meeting, Anchorage, Alaska, USA. doi: https://doi.org/10.2118/213006-MS

Grabski, E.R. (2012). Matrix Acidizing Core Flooding Apparatus: Equipment and Procedure Description. Master of Science Thesis, Texas A&M University

Hoefner, M.L. and Fogler, H.S. (1987). Role of Acid Diffusion in Matrix Acidizing of Carbonates. SPE Journal of Petroleum Technology 39 (2): 203-208. doi: 10.2118/13564-pa

Hoefner, M.L., and Fogler, H.S. (1989, February 1). Fluid-Velocity and Reaction-Rate Effects During Carbonate Acidizing: Application of Network Model. Society of Petroleum Engineers. doi: 10.2118/15573-PA

Knox, J.A., Pollock, R.W., & Beecroft, W.H. (1965, January 1). The Chemical Retardation of Acid and How it can be Utilized. Journal of Canadian Petroleum Technology 4 (01): 5-12. doi: 10.2118/65-01-02

McDuff, D.R., Shuchart, C.E., Jackson, S.K., Postl, D., and Brown, J.S. (2010). Understanding Wormholes in Carbonates: Unprecedented Experimental Scale and 3-D Visualization. Paper presented at the SPE Annual Technical Conference and Exhibition, Florence, Italy. doi: https://doi.org/10.2118/134379-MS

Purdy, C., Weissenberger, M., Jamieson, A.D., (2019). Using Synthetic Acid Compositions as Alternatives to Conventional Acids in the Oil and Gas Industry. Canadian Patent 2974757.

Sohn, Y.S. (2018). Experimental and Simulated Investigation on the Effect of Chemically Retarded Acid Systems in Carbonates, Master of Science Thesis, Texas A&M University

Wang, Y., Hill, A.D., and Schechter, R.S. (1993). The Optimal Injection Rate for Matrix Acidizing of Carbonate Formations. Paper presented at the SPE Annual Technical Conference and Exhibition, Houston, Texas. SPE 26578. DOI: 10.2118/26578-ms

Zhu, D., Hill. D., Ugursal, A. et al. (2022). A Modified Acid System to Enhance Carbonate Matrix Acid Stimulation – An Experimental Study. The Canadian Journal of Chemical Engineering 100(6), 1187. https://doi.org/10.1002/cjce.24251

APPENDIX A

Core face pictures before and after the test

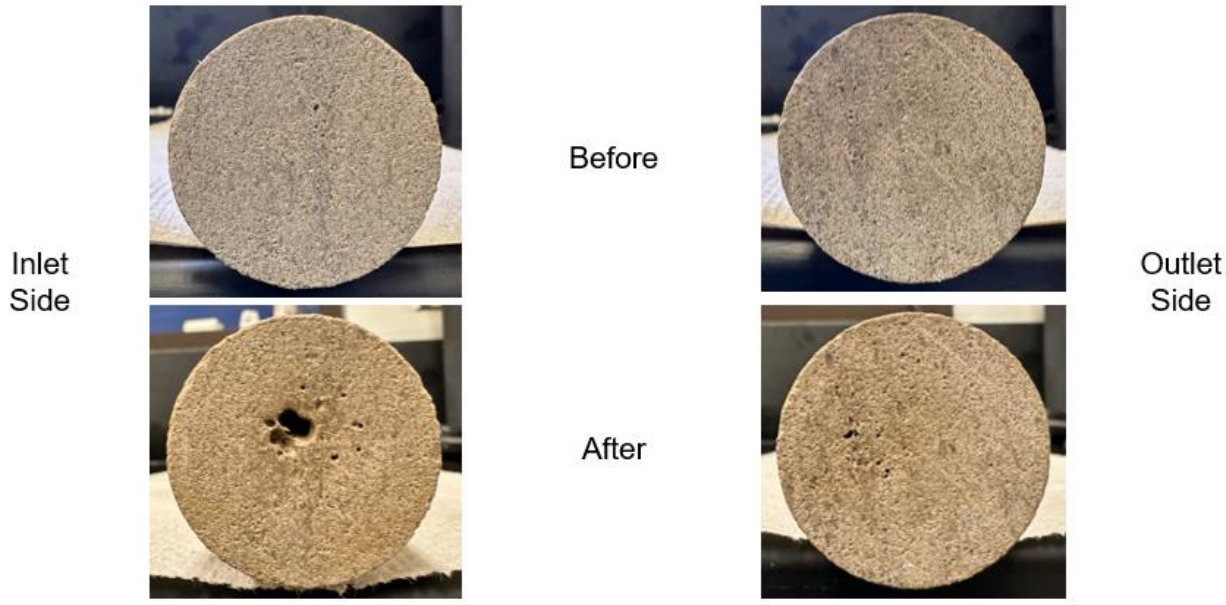

Figure A1 – Core 6-125-1 (Injection rate = 4 mL/min at 125°F)

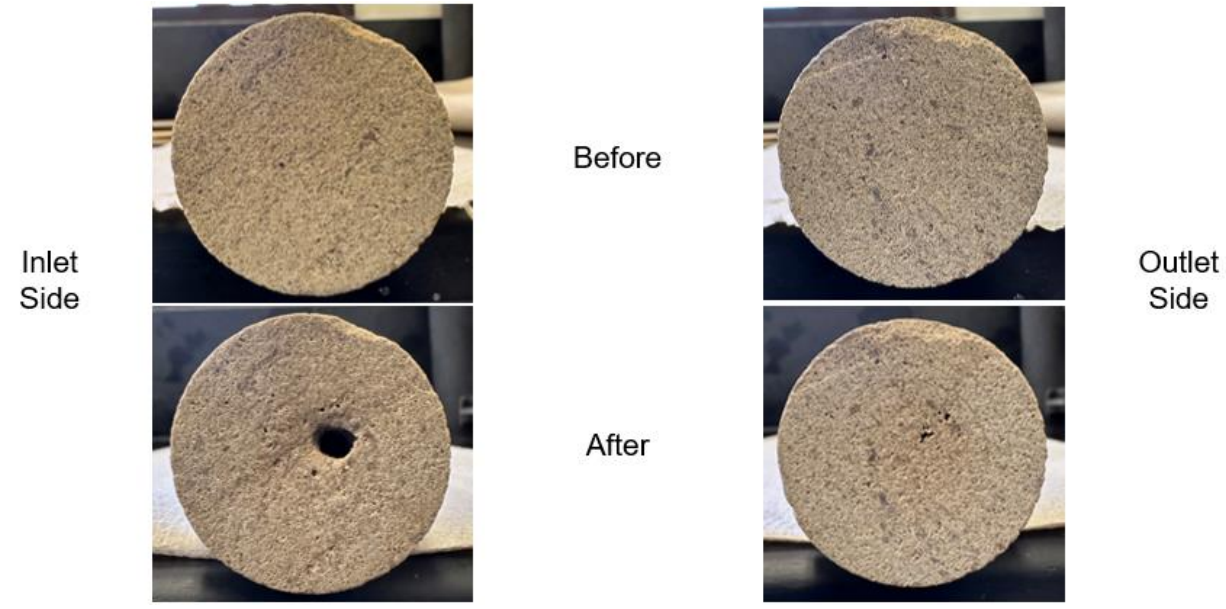

Figure A2 – Core 6-125-2 (Injection rate = 2 mL/min at 125°F)

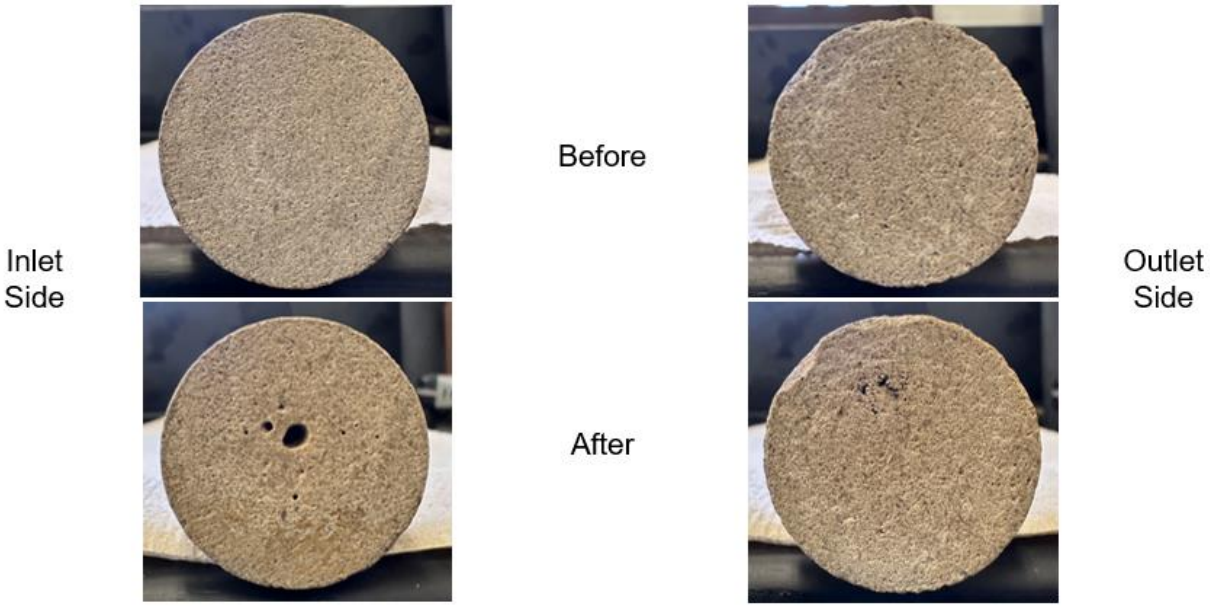

Figure A3 – Core 6-125-3 (Injection rate = 6.5 mL/min at 125°F)

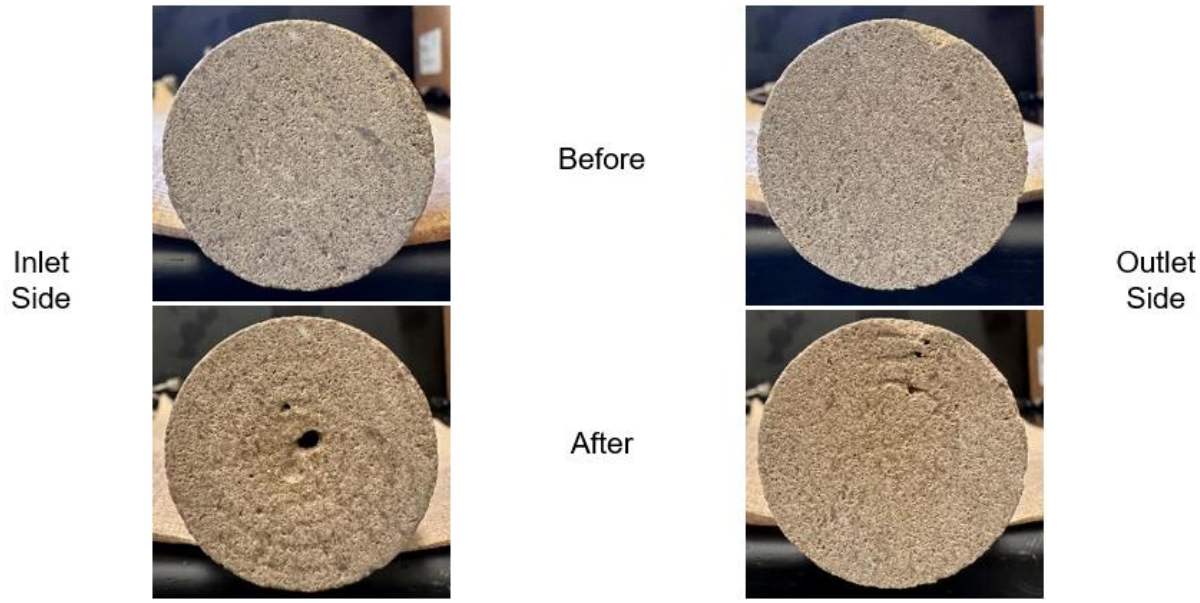

Figure A4 – Core 6-125-4 (Injection rate = 1 mL/min at 125°F)

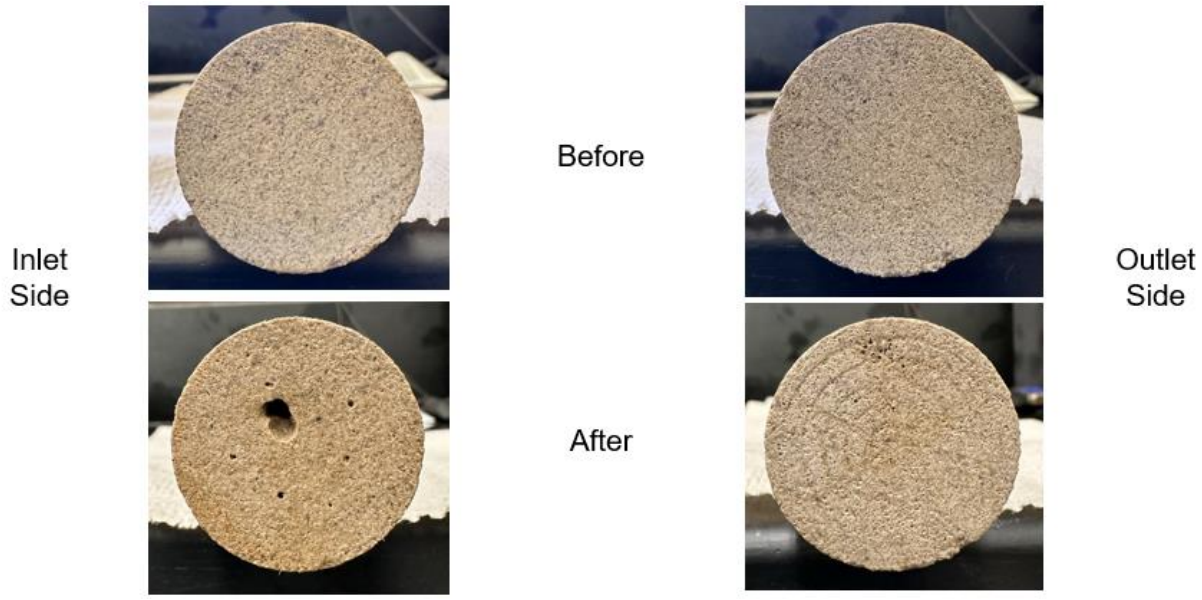

Figure A5 – Core 6-150-4 (Injection rate = 6 mL/min at 150°F)

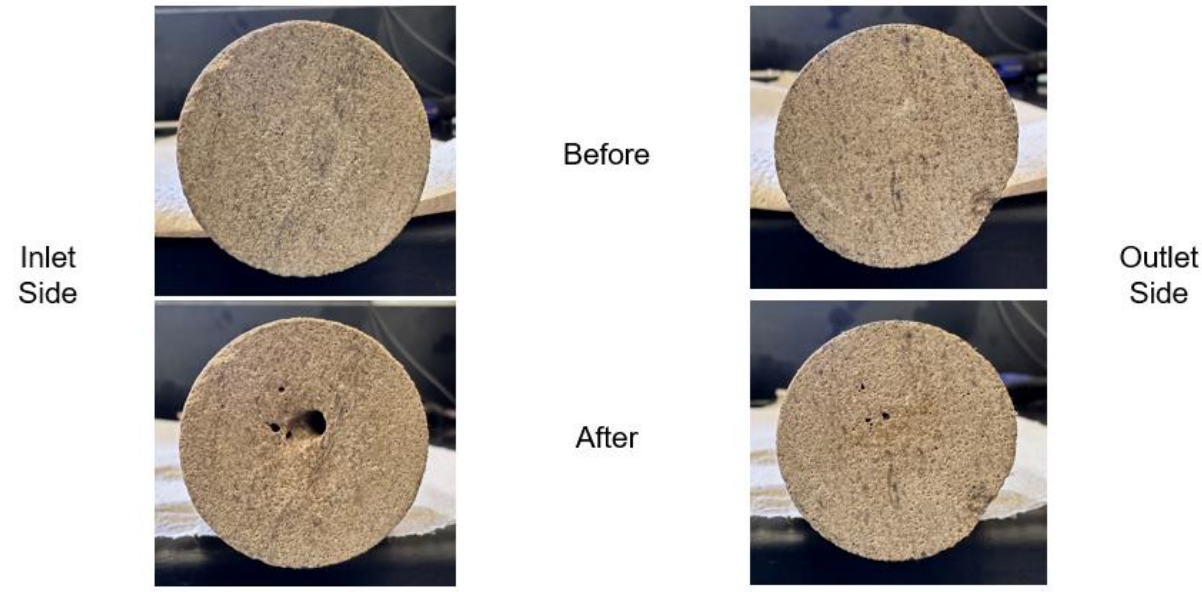

Figure A6 – Core 6-150-2 (Injection rate = 2 mL/min at 150°F)

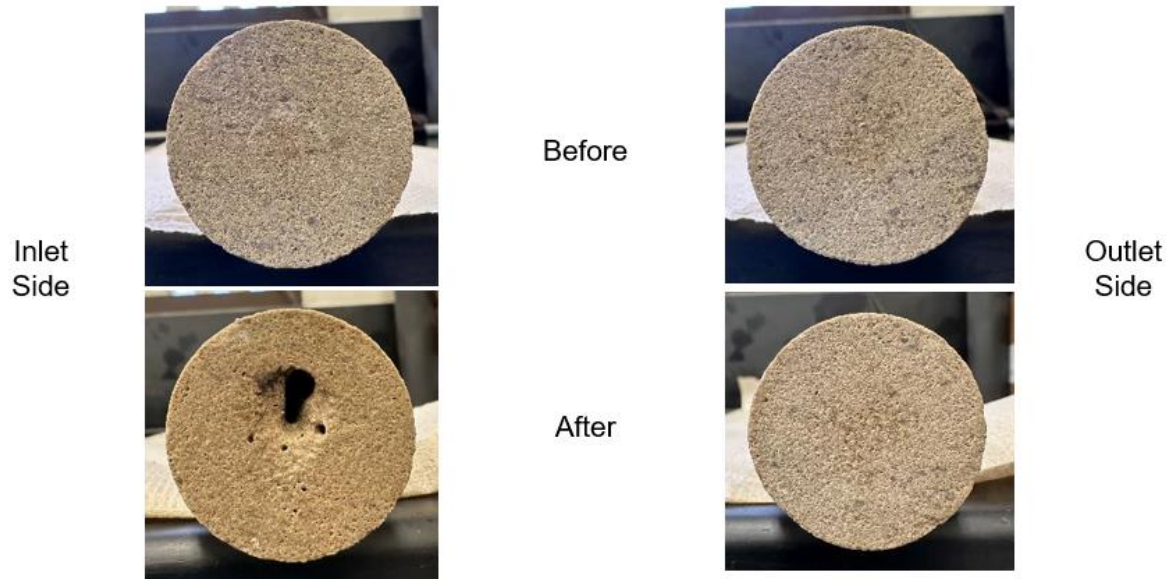

Figure A7 – Core 6-150-5 (Injection rate = 1 mL/min at 150°F)

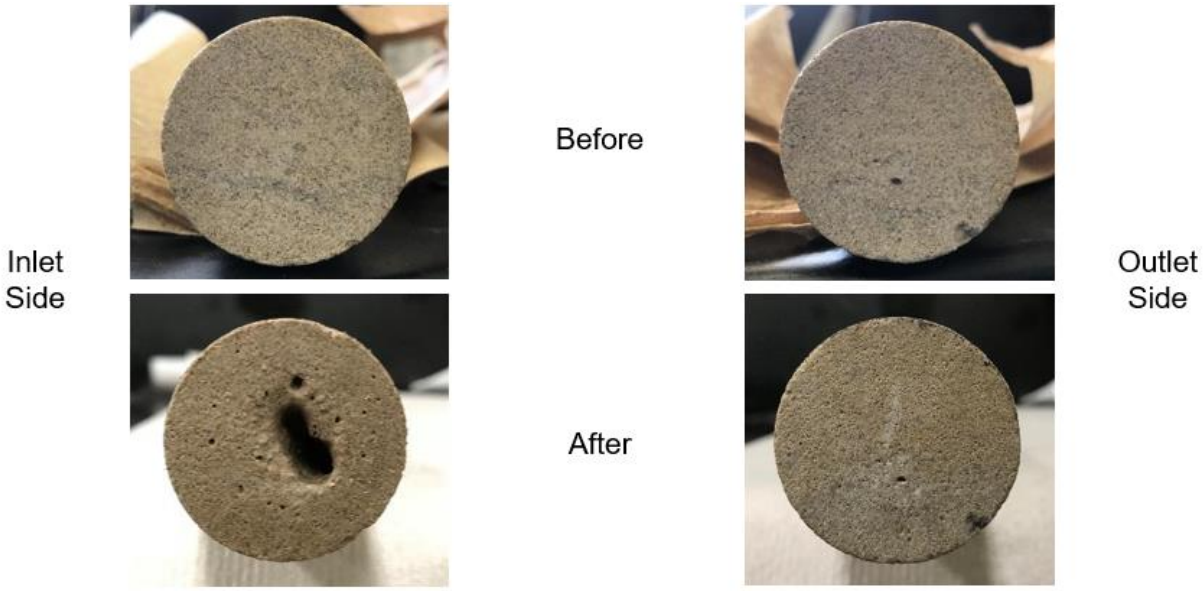

Figure A8 – Core 6-225-2 (Injection rate = 1.61 mL/min at 225°F)

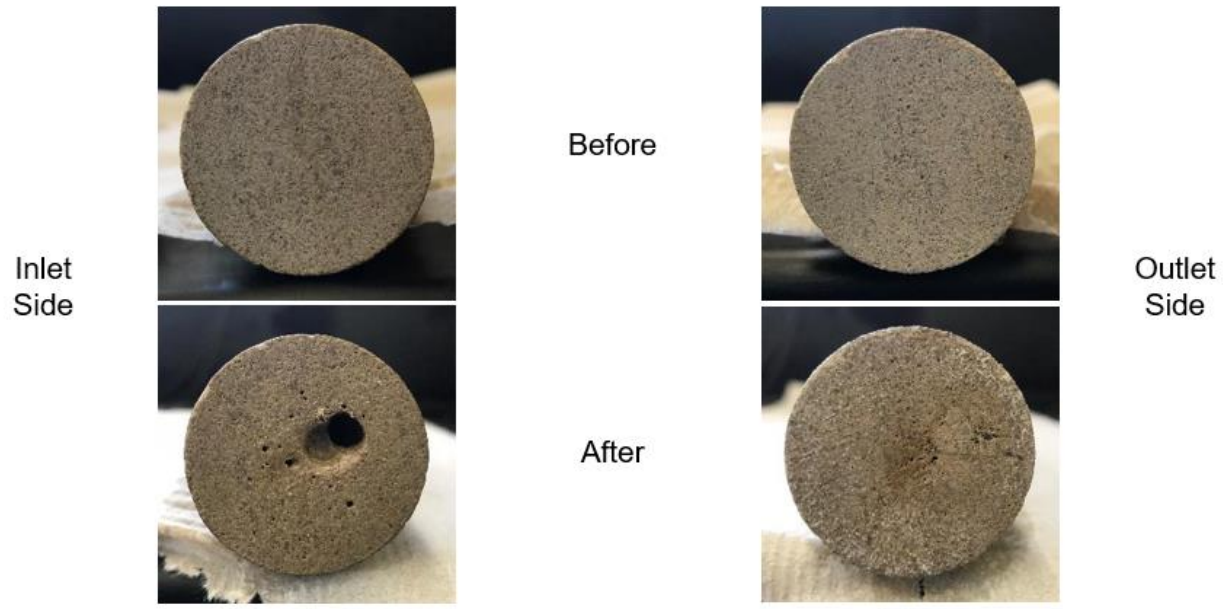

Figure A9 – Core 6-225-3 (Injection rate = 6 mL/min at 225°F)

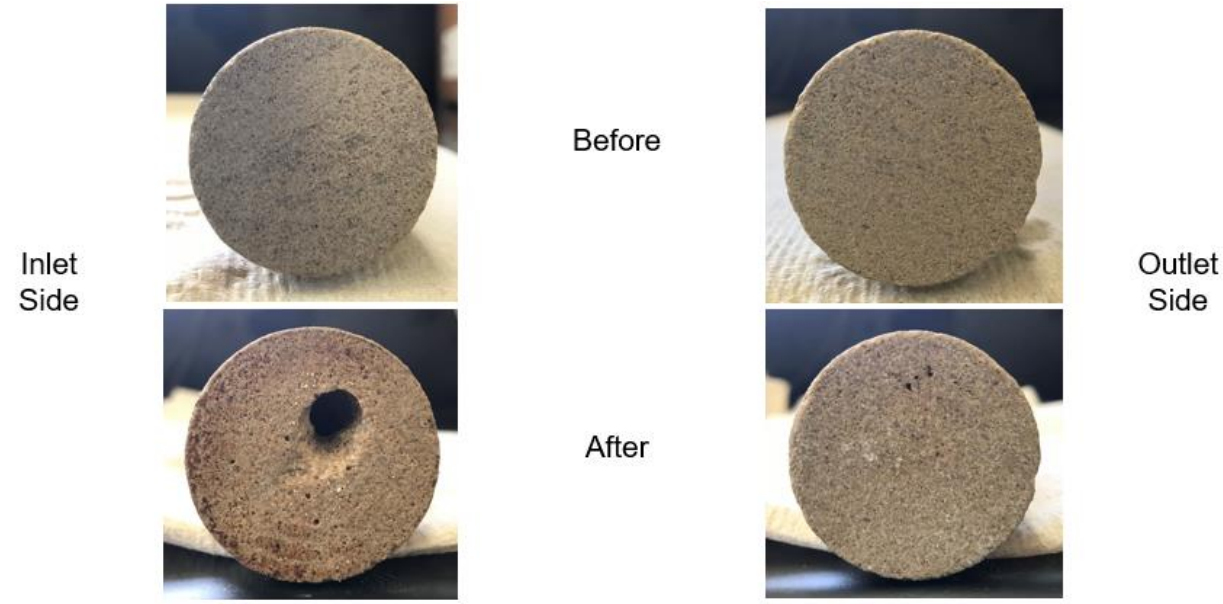

Figure A10 – Core 6-225-4 (Injection rate = 4 mL/min at 225°F)

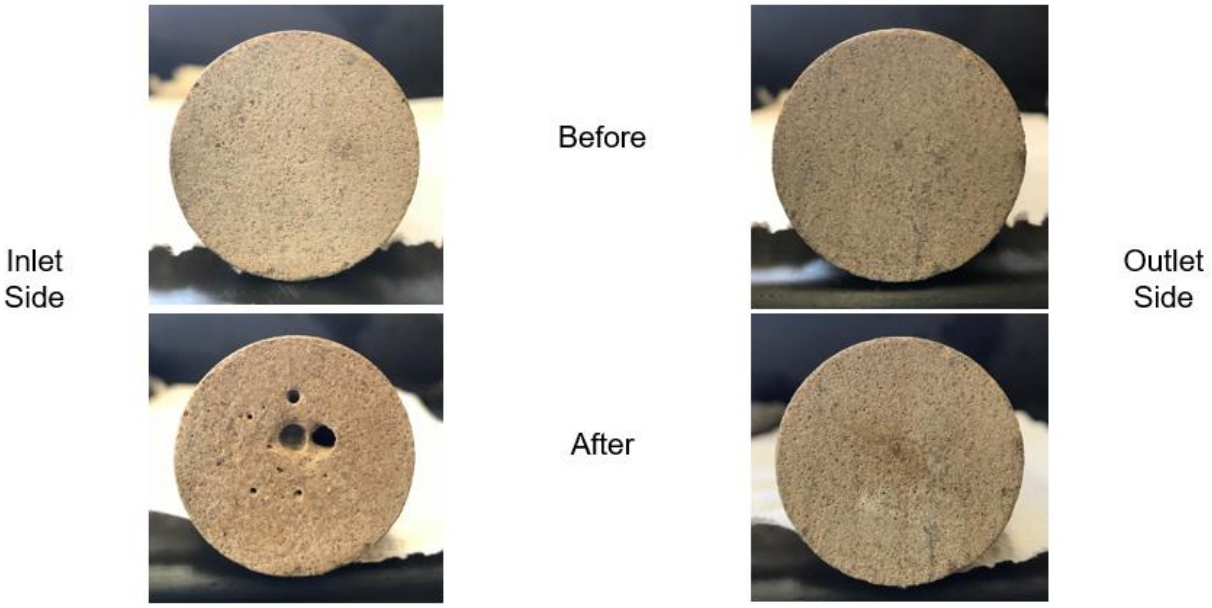

Figure A11 – Core 6-225-5 (Injection rate = 8 mL/min at 225°F)

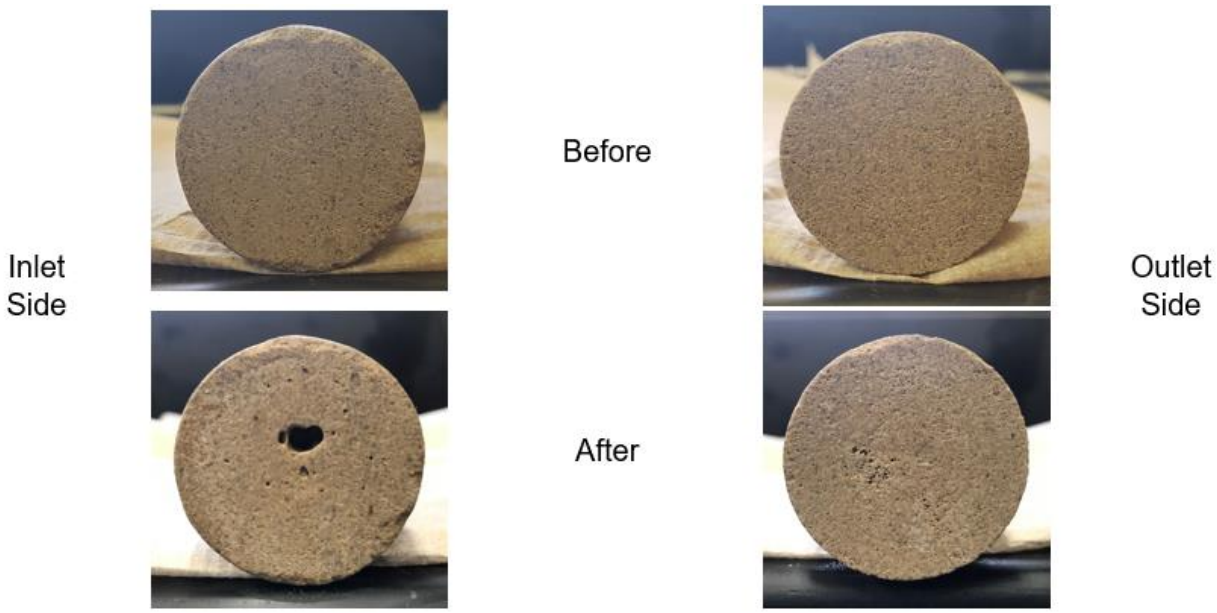

Figure A12 – Core 6-225-1 (Injection rate = 13 mL/min at 225°F)

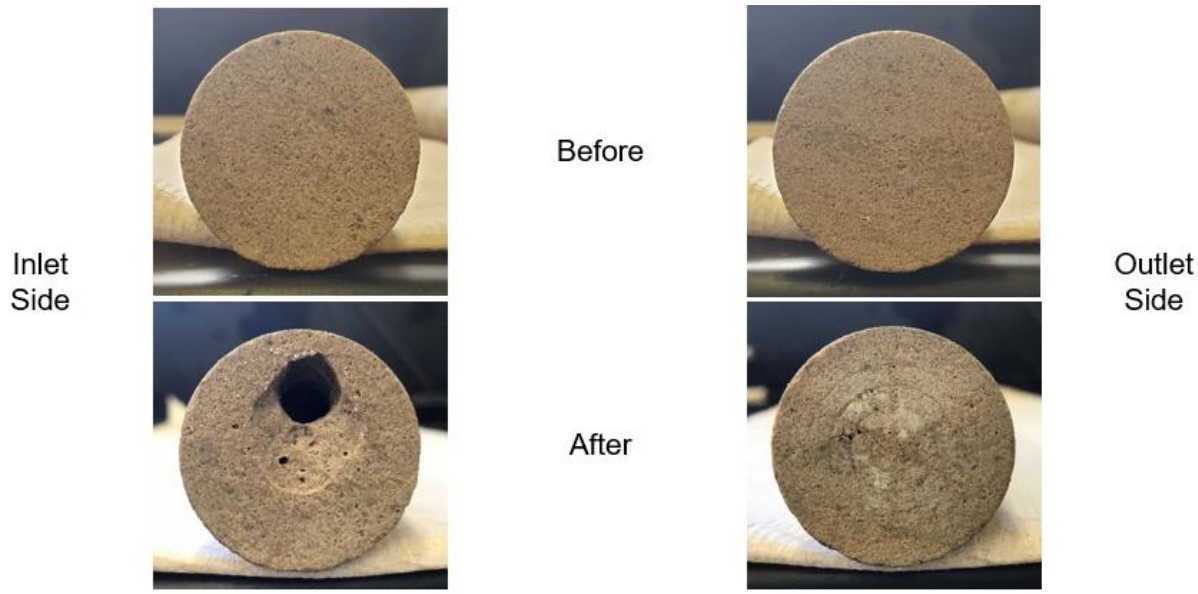

Figure A13 – Core 6-300-1 (Injection rate = 8 mL/min at 300°F)

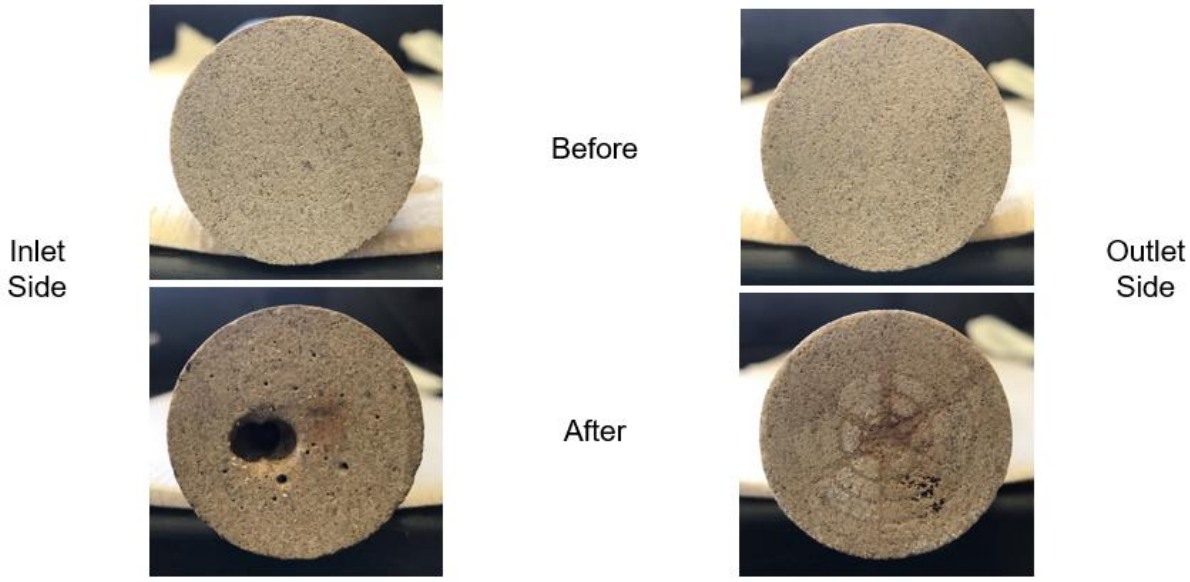

Figure A14 – Core 6-300-2 (Injection rate = 12 mL/min at 300°F)

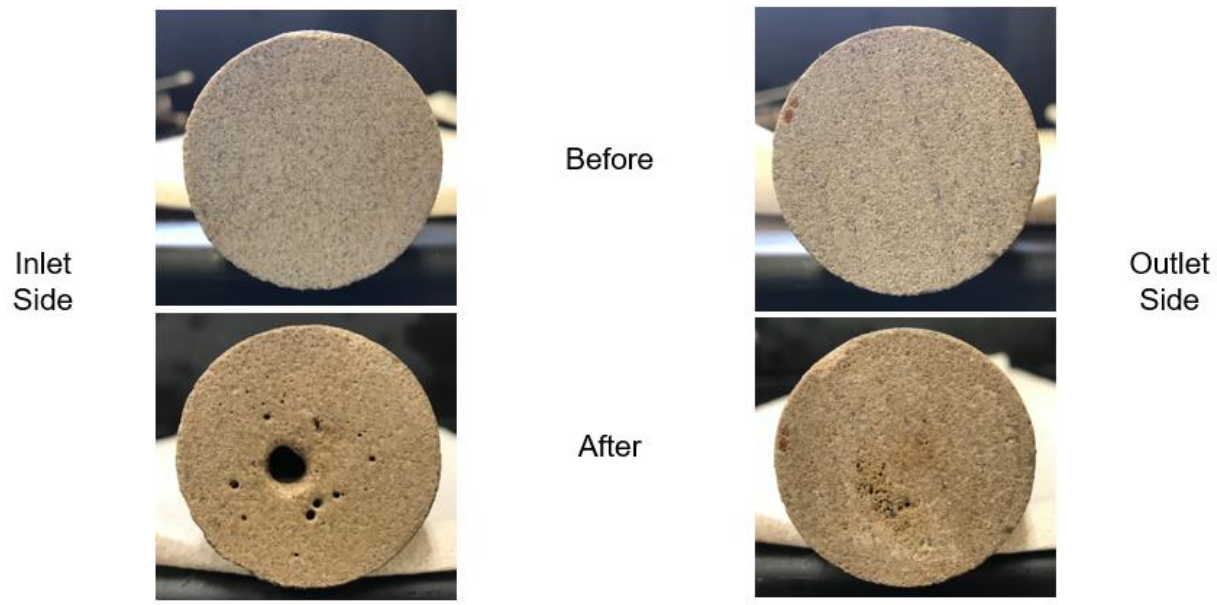

Figure A15 – Core 6-300-4 (Injection rate = 16 mL/min at 300°F)

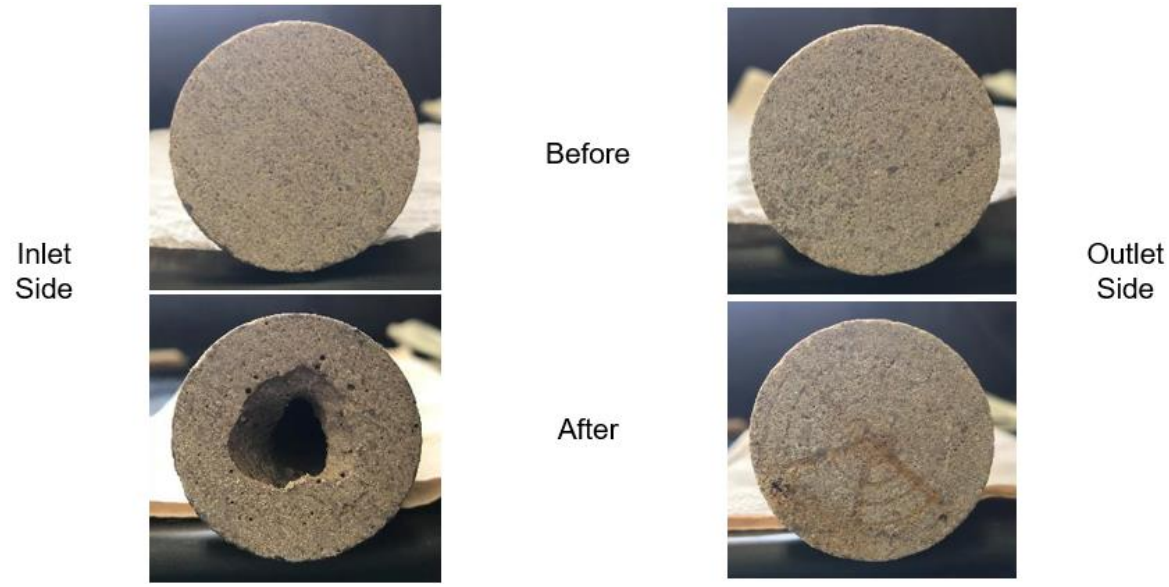

Figure A16 – Core 6-300-5 (Injection rate = 5.5 mL/min at 300°F)

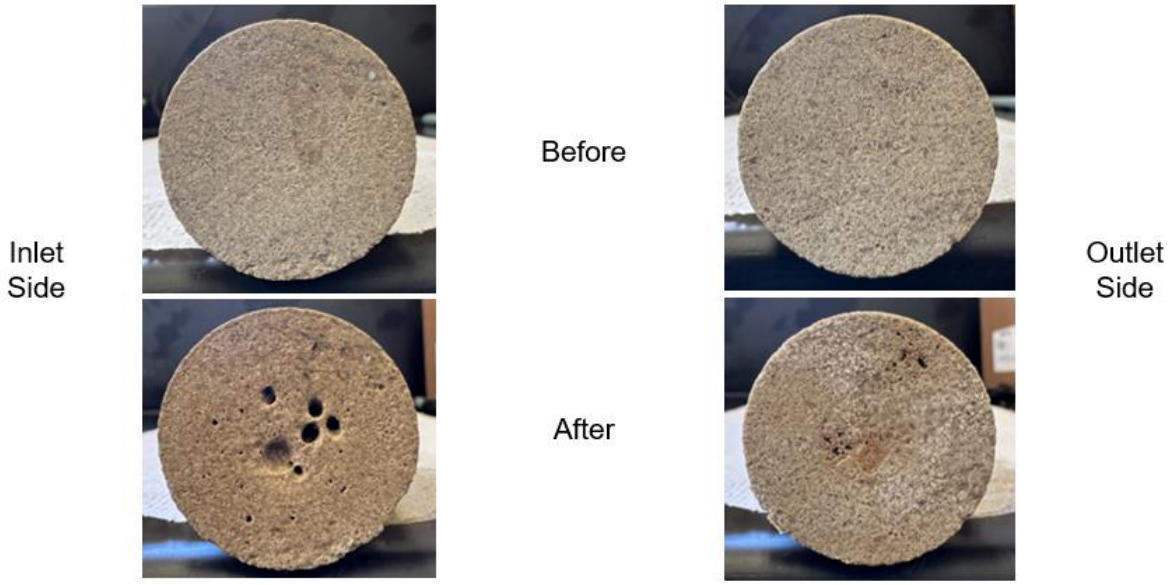

Figure A17 – Core 6-300-6 (Injection rate = 19 mL/min at 300°F)

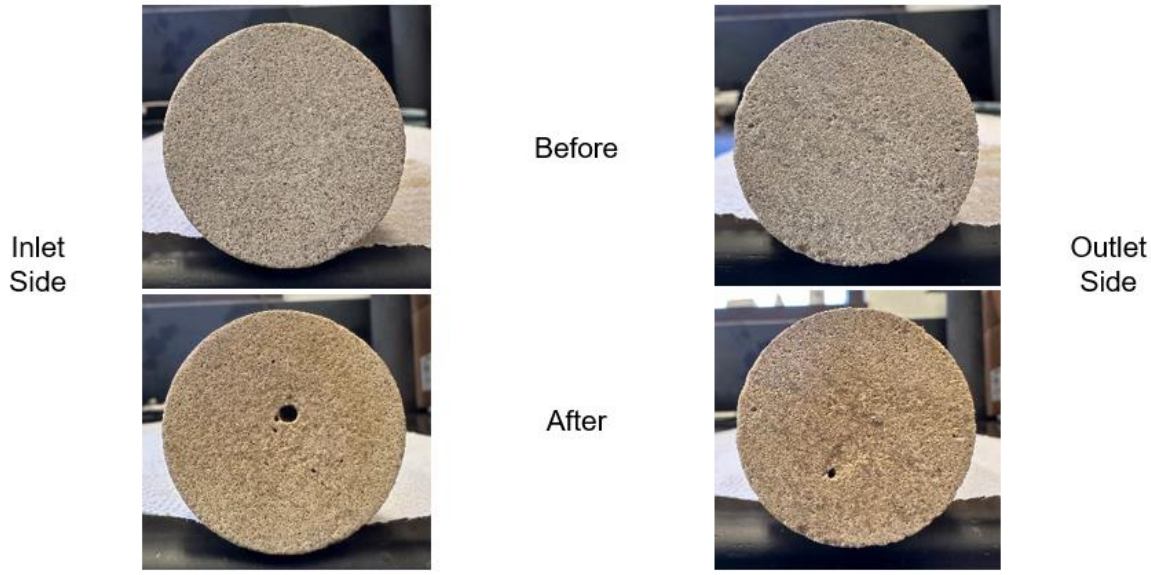

Figure A18 – Core H-125-1 (Injection rate = 3 mL/min at 125°F)

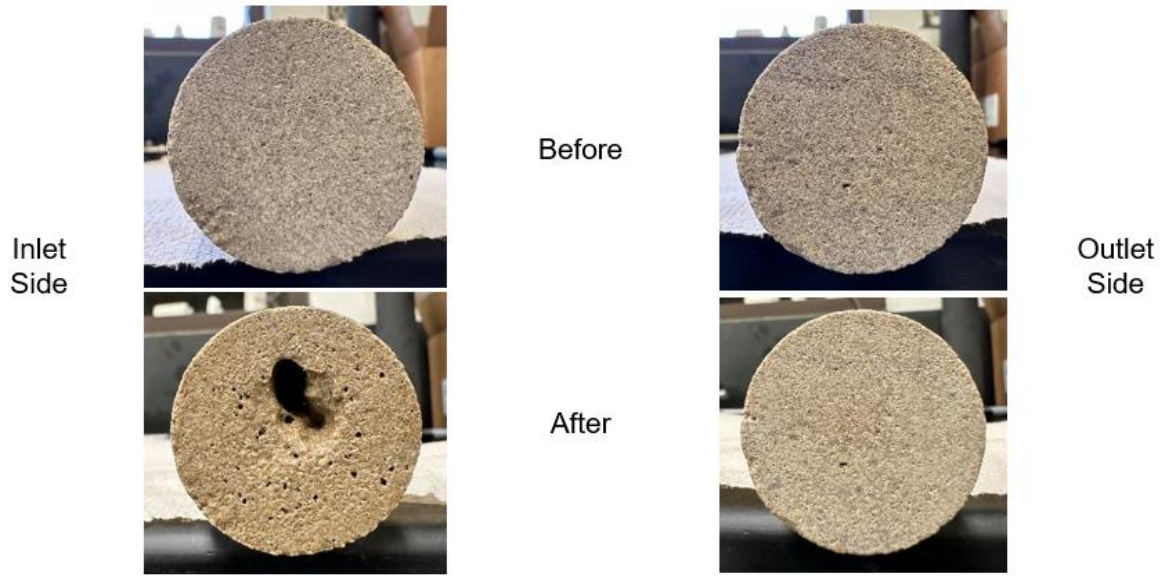

Figure A19 – Core H-150-1 (Injection rate = 2 mL/min at 150°F)

Figure A20 – Core H-225-2 (Injection rate = 4.5 mL/min at 225°F)

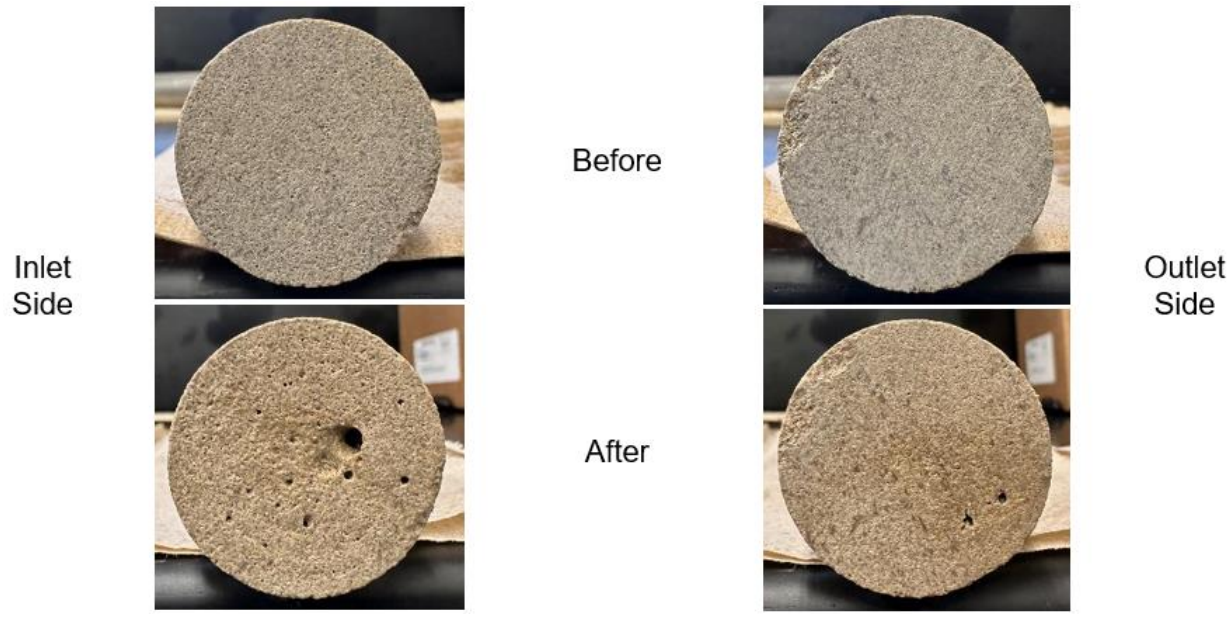

Figure A22 – Core 6-180-2 (Injection rate = 1 mL/min at 180°F)

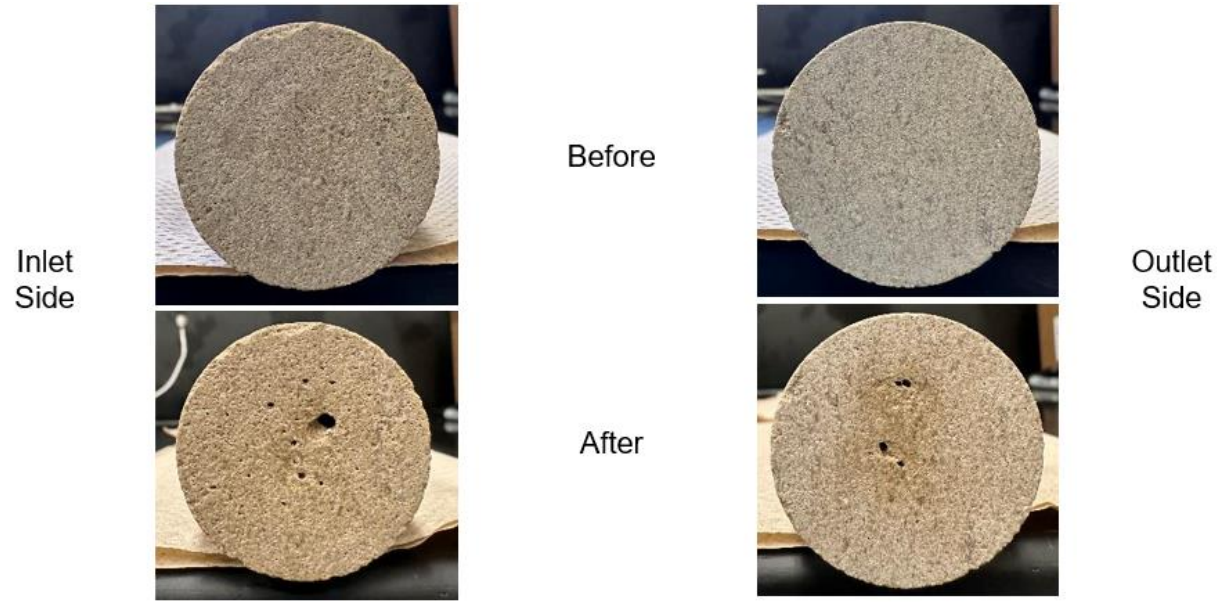

Figure A22 – Core 6-180-1 (Injection rate = 2 mL/min at 180°F)

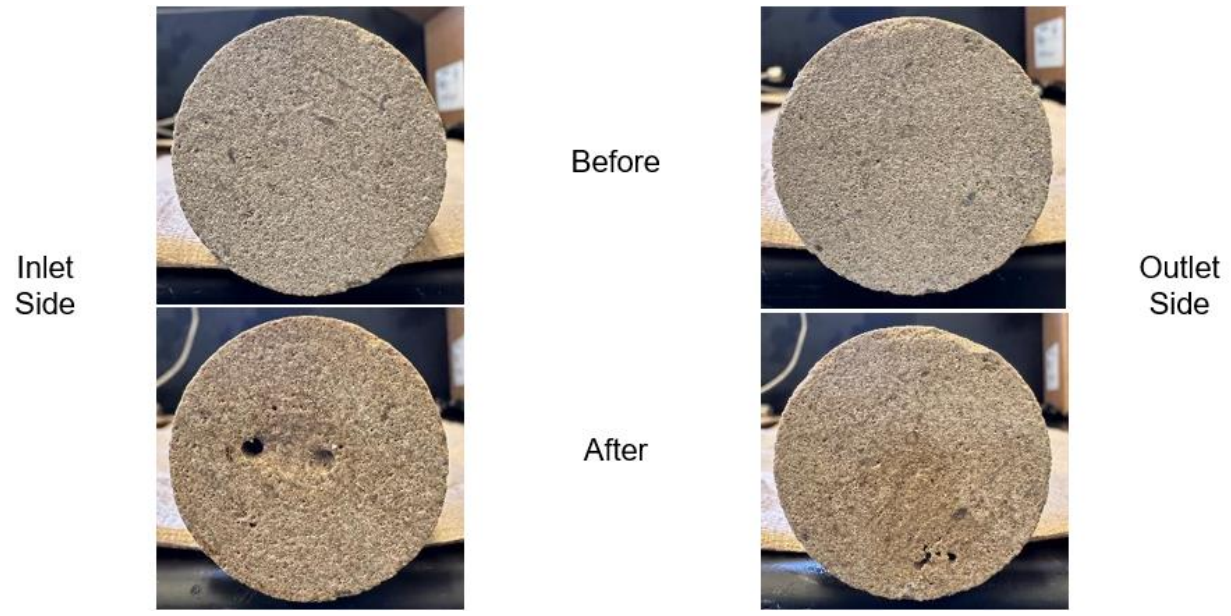

Figure A23 – Core 6-180-4 (Injection rate = 4 mL/min at 180°F)

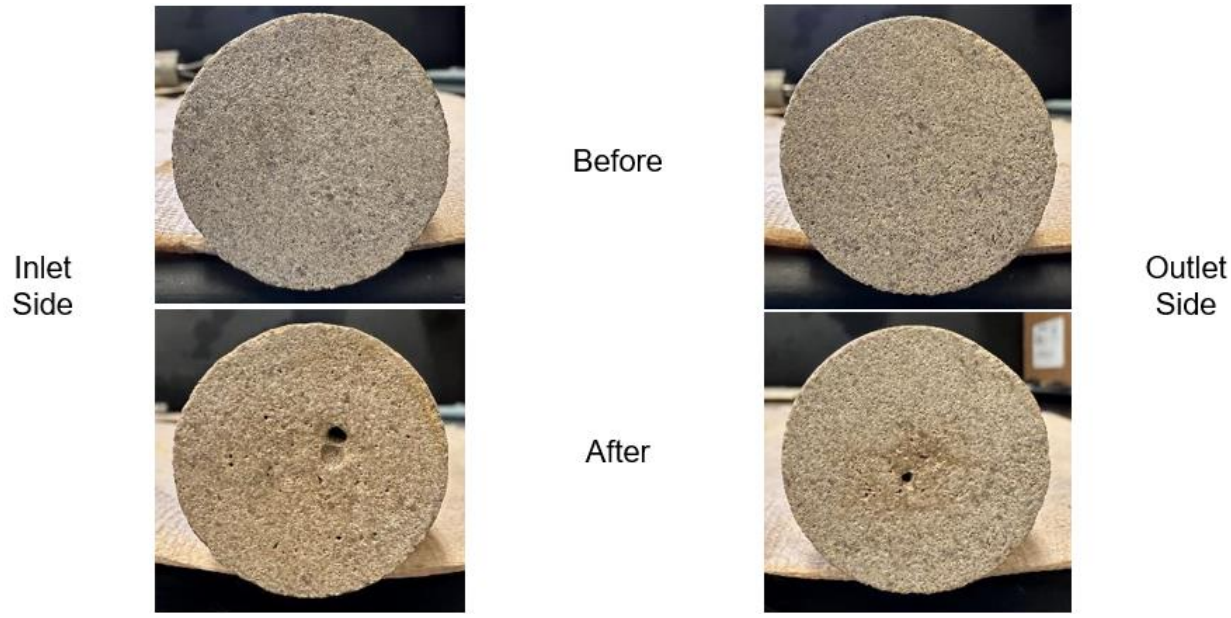

Figure A24 – Core 6-180-3 (Injection rate = 6 mL/min at 180°F)

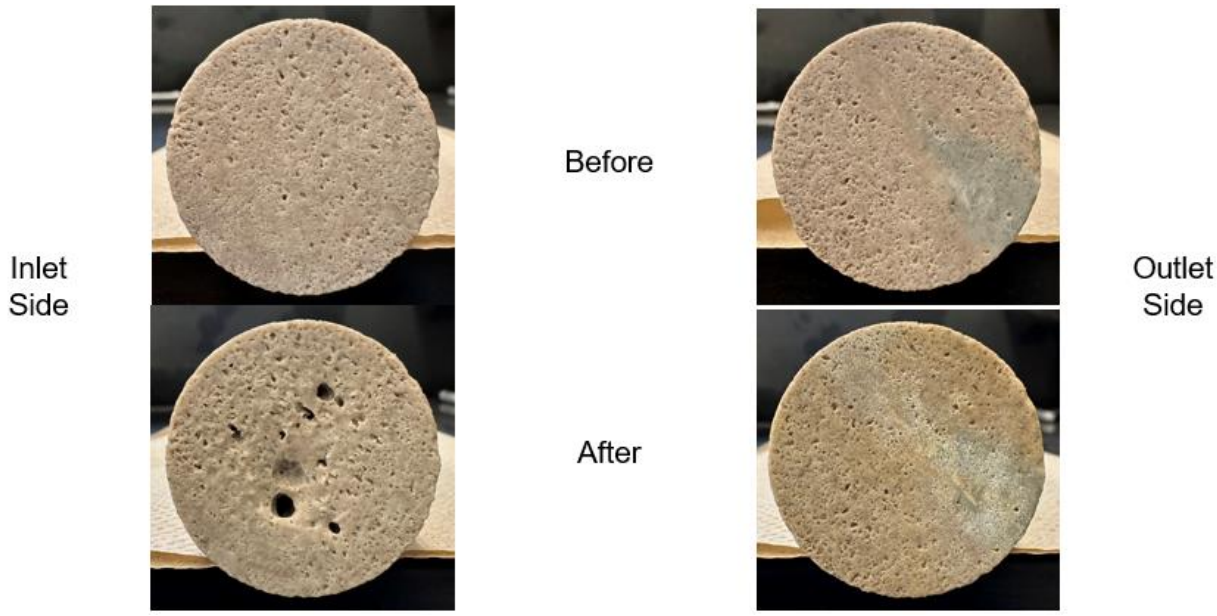

Figure A25 – Core D3 (Injection rate = 8 mL/min at 230°F)

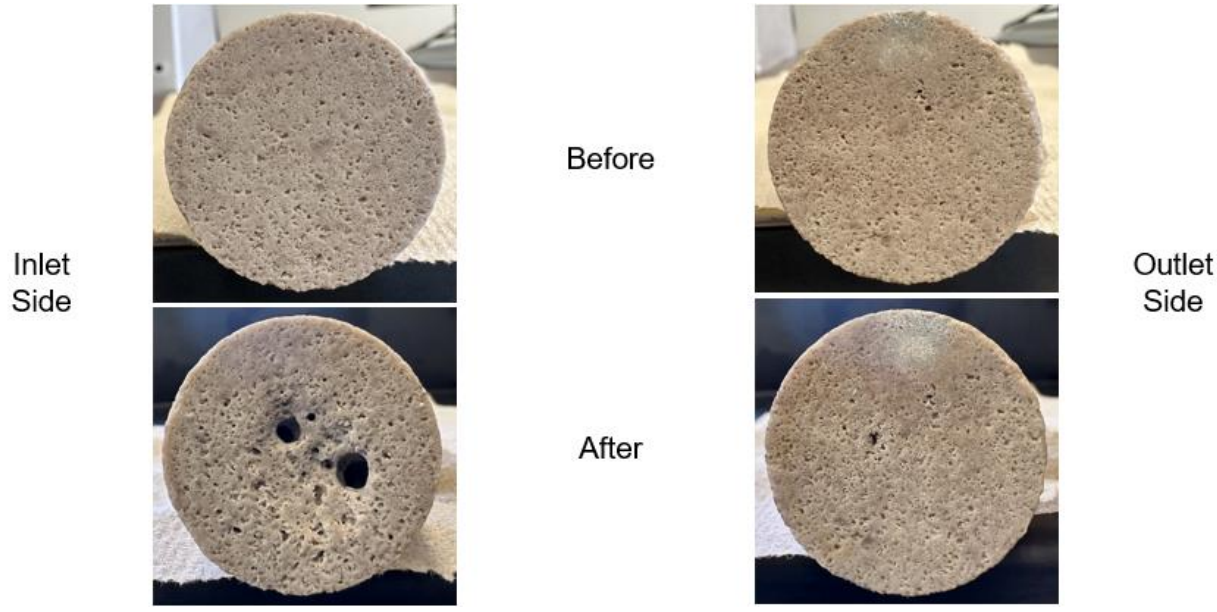

Figure A26 – Core D4 (Injection rate = 5 mL/min at 230°F)

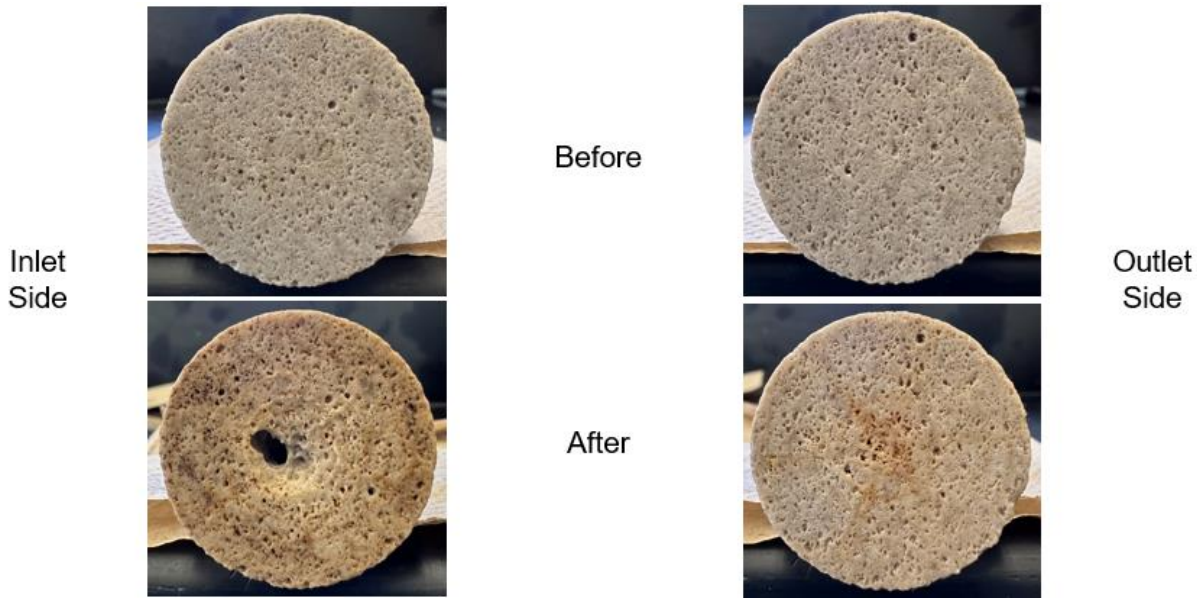

Figure A27 – Core D2 (Injection rate = 9.7 mL/min at 230°F)